JAERI - M
89-227

EVALUATION REPORT ON CCTF CORE-II REFLOOD TEST C2-AA2 (RUN 58)

— INVESTIGATION OF DOWNCOMER INJECTION EFFECTS —

January 1990

Tsutomu OKUBO, Tadashi IGUCHI, Jun SUGIMOTO
Hajime AKIMOTO and Yoshio MURAO

日 本 原 子 力 研 究 所
Japan Atomic Energy Research Institute

JAERI-Mレポートは，日本原子力研究所が不定期に公刊している研究報告書です。
入手の問合わせは，日本原子力研究所技術情報部情報資料課（〒319-11茨城県那珂郡東海村）あて，お申しこしください。なお，このほかに財団法人原子力弘済会資料センター（〒319-11 茨城県那珂郡東海村日本原子力研究所内）で複写による実費頒布をおこなっております。

JAERI-M reports are issued irregularly.
Inquiries about availability of the reports should be addressed to Information Division, Department of Technical Information, Japan Atomic Energy Research Institute, Tokai-mura, Naka-gun, Ibaraki-ken 319-11, Japan.

編集兼発行　日本原子力研究所
印　　刷　㈱原子力資料サービス

JAERI-M 89-227

Evaluation Report on CCTF Core-II Reflood Test C2-AA2 (Run 58) - Investigation of downcomer injection effects -

Tsutomu OKUBO, Tadashi IGUCHI, Jun SUGIMOTO+
Hajime AKIMOTO and Yoshio MURAO

Department of Reactor Engineering
Tokai Research Establishment
Japan Atomic Energy Research Institute
Tokai-mura, Naka-gun, Ibaraki-ken

(Received December 21, 1989)

This report is an evaluation report of the CCTF Core-II test C2-AA2 (Run 58). In this test the ECC water was injected into the downcomer as well as into the intact cold legs in order to investigate characteristics of thermo-hydrodynamic behavior in a downcomer injection test. For this purpose, the test conditions were determined to be the same as those for the base case test (Test C2-4 (Run 62)) except for the ECC water injection locations. The ECC water injection location in the base case test was only the cold leg.

Comparing the data of the present test with those of the base case test, the following results are obtained.

(1) The present test experienced a significant oscillation, which was not observed in the base case test. The oscillation was periodic and its period was 5.7 s.

(2) Thermal equilibrium by mixing of ECC water and steam flowing in the intact loops was not established at the downcomer in the present test, and hence, downcomer fluid temperature was observed to be subcooled and lower than in the base case test. This is expected to be the cause of the oscillation mentioned above.

+ Department of Fuel Safety Research

(3) However, fluid temperature at the core inlet was higher than in the base case test. This higher fluid temperature is attributed to mixing of lower plenum fluid with core fluid due to the large oscillation. Quenching of heater rods were slightly later than in the base case test. This is attributed to the higher core inlet fluid temperature mentioned above. However, at the top part above 3 m elevation, difference in quench time tended to get smaller.

(4) Although thermo-hydrodynamic behavior through the system was oscillatory in the present test, average values of the oscillatory data were nearly identical to those of the base case test except for the differences mentioned in items (2) and (3) above. This suggests, for analysis or prediction of core cooling for the downcomer injection case, it would be possible to use the same models, methods or computer codes as used for the cold leg injection case with adding a modification on predicting the fluid temperature at the core inlet.

Keywords: Reactor Safety, LOCA, ECCS, PWR, Reflood Experiment, Heat Transfer, Hydrodynamics, Two-phase Flow

大型再冠水円筒第２次炉心試験Ｃ２－ＡＡ２（Run 58）評価報告書
― ダウンカマ注水の効果の検討 ―

東海研究所原子炉工学部伝熱流動研究室
大久保　努・井口　　正・杉本　　純[+]
秋本　　肇・村尾　良夫

（１９８９年12月21日受理）

本報告書は，円筒第２次炉心試験Ｃ２－ＡＡ２（Run 58）の評価報告書である。本試験では，ダウンカマ注水試験に於ける熱水力挙動の特徴を調べることを目的として，ＥＣＣ水を健全コールドレグとともにダウンカマにも注入した。また，上記の目的のため，ＥＣＣ水の注入場所が異る点を除いて他の条件は全て基準試験Ｃ２－４（Run 62）と同一に設定された。基準試験での注水位置はコールドレグのみであった。

本試験のデータを基準試験のデータと比較検討して，以下のような結果が得られた。

(1) 本試験に於いては，基準試験では見られない大きな振動が観測された。振動は周期的で周期は５.７秒であった。

(2) 本試験では，ダウンカマに於けるＥＣＣ水と健全ループを流れる蒸気との混合が熱的に非平衡に起こり，そのため，ダウンカマ水温はサブクールを示し基準試験の場合に比べて低かった。この点が上記の振動の原因と考えられる。しかし，炉心入口水温は基準試験に比べ高かった。これは，大きな振動により下部プレナムの水が炉心の水と混合したためである。

(3) 発熱体のクエンチは，基準試験の場合よりやや遅れていた。これは，上述のように炉心入口水温が高かったためである。しかし，３ｍ以上の炉心頂部では，クエンチ時間の差が小さくなる傾向にあった。

(4) 系全体に渡って，熱水力挙動は振動的であったが，振動的なデータの平均値は，上記項目(2)および(3)で述べた相違を除けば，基準試験のデータとほぼ同一であった。このことは，ダウンカマ注水の場合に対する炉心冷却の解析や予測に当たって，コールドレグ注水の場合に対して用いられているのと同じモデル・手法あるいは計算コードを，炉心入口水温の予測に関する修正を加えることにより使用可能であることを示唆している。

[+] 燃料安全工学部

目　　次

Contents

List of Tables

List of Figures

1. Introduction

A reflood test program[1] using large scale test facilities has been conducted at the Japan Atomic Energy Research Institute (JAERI). The facilities are the Cylindrical Core Test Facility (CCTF) and the Slab Core Test Facility (SCTF). This report presents evaluation for the CCTF Core-II downcomer injection test, Test C2-AA2 (Run 58).

The CCTF is an experimental facility designed to model a full-height core section, four primary loops and their components of a pressurized water reactor (PWR). This facility is used to provide information on fluid behaviors in the core, downcomer and upper plenum including the steam and water carry-over phenomena, and integral system effects during the refill and reflood phases of a hypothetical loss-of-coolant accident (LOCA) of a PWR.

The objectives of the test program using the CCTF are:

a. Demonstration of capability of emergency core cooling system (ECCS) during refill and reflood period.
b. Verification of reflood analysis codes.
c. Collection of information to improve the thermo-hydrodynamic models in reflood analysis codes, such as, (a) multi-dimensional core thermo-hydrodynamics including the radial power distribution effect, fall back effect and spatial oscillatory behavior, (b) flow behavior in the upper plenum and hot legs, (c) behavior of accumulated water at the bottom of the upper plenum including possible counter-current flow and sputtering effect, (d) hydrodynamic behavior of injected ECC water and water passing through the steam generator, (e) multi-dimensional thermo-hydrodynamic behavior in the hot annular downcomer and (f) overall oscillatory behavior in the system.

As the first series of the CCTF tests, twenty-seven CCTF Core-I tests were conducted. This series of tests presented a lot of information[2] on the system thermo-hydrodynamic behavior as well as the core behavior during the refill and reflood phases of a LOCA in a PWR. The CCTF Core-I test series was initiated in March 1979 and terminated in April 1981. Subsequently, as the second series of the CCTF tests, the CCTF Core-II test series was initiated in March 1982. The special purposes of the CCTF Core-II test program are to investigate the effects of alternative ECCS such as the combined and the downcomer injections as well as to extend the ex-

perimental range of the Core-I test series.

Test C2-AA2 (Run 58) was conducted in order to investigate the effects of downcomer injection. In this test, ECC water was injected into the downcomer directly as well as into three intact cold legs simulating the injection mode of a couple of new Japanese PWRs[3]. The downcomer injection simulated the low pressure coolant injection (LPCI) and the cold leg injection was for simulation of the high pressure coolant injection system (HPCI). Since total ECC water injection rate was set equal to that for the base case test (cold leg injection only), the effects of the downcomer injection is expected to be investigated quantitatively comparing results of the present test with those of the base case test. Therefore, in this report, results of those two tests are compared and discussed.

Selected data of the present test are presented in Appendix for better understanding of the test results.

2. Test Description

2.1 Test Facility

The CCTF Core-II was designed in consideration of the following objectives and criteria:

a. Design objectives

(1) The facility should provide the capability to reasonably simulate the flow conditions in the primary system of a PWR during the refill and reflood phases of a LOCA.

(2) The downcomer design should provide ECC water flow behavior throughout the test which is reasonably representative of that of the PWR downcomer.

b. Design criteria

(1) The reference reactors are the Trojan reactor in the USA and in certain aspects the Ohi reactor in Japan.

(2) The vertical dimensions and locations of system components are kept as close to those of the reference reactors as possible.

(3) The flow areas of the system components are scaled down in proportion to the scaling factor of core flow area.

(4) The facility is equipped with four loops which are composed of three intact loops and one broken loop.

(5) A 200% cold leg large break is simulated in the broken loop.

(6) The ECCS consists of two accumulator systems (Acc) and low pressure coolant injection system (LPCI), and the injection locations are the upper plenum, the downcomer and the hot legs as well as the lower plenum and the cold legs.

(7) The maximum allowable pressure of the facility is 588 kPa (6 kg/cm^2 absolute).

(8) The maximum allowable temperature of the simulated fuel rods is 1173 K (900C).

(9) The maximum allowable temperature of the components in the primary system except the simulated fuel rod assembly is 623 K (350C).

(10) The reactor vessel contains approximately 2,000 electrically heated rods simulating the fuel rods.

(11) The design of upper plenum internals is based on that of a new Westinghouse 17 x 17 type fuel assembly.

(12) The flow resistance of each loop is adjusted by an orifice in the

pump simulator.

(13) The containment system consists of two tanks.

A bird's-eye view of the CCTF is shown in Fig. 2.1. The scaled dimensions of the components are given in Table 2.1.

The differences in the design of the Core-II facility from the Core-I are:

(1) Axial and local peaking factors of heater rods
(2) Edge shape of grid spacers
(3) Upper plenum structures (upper plenum internals, plugging devices in end box region and a upper ring)
(4) Vent valves
(5) Alternative ECCS (downcomer injection, upper plenum injection and hot leg injection)
(6) Instruments

2.1.1 Pressure Vessel and Internals

The pressure vessel is of a cylindrical type as shown in Figs. 2.2 and 2.3. The height is the same as the reference reactor pressure vessel. The radial direction is scaled down by the flow area scaling ratio of 1/21.44. The upper ring was newly installed in the Core-II facility for the installation of the upper plenum ECC water injection lines and the instruments. Four vent valves and two downcomer ECC water injection nozzles, which are called Core Flooding Nozzle (CFN), are also newly equipped in the Core-II facility as shown in Figs. 2.2 and 2.3. Vent valves and CFNs are for the simulation of a Babcock & Wilcox (B & W) type PWR. Downcomer injection nozzles also exist in a couple of recent Japanese PWRs[3]. The location of Core Flooding Nozzles are shown in Fig. 2.4 in detail.

The cross section of the pressure vessel is shown in Fig. 2.3 and the dimensions are given in Fig. 2.5. The core consists of thirty-two 8 x 8 electrically heated rod bundles arranged in a cylindrical configuration and simulates a Westinghouse 15 x 15 type fuel assemblies.

The downcomer is an annulus of 61.5 mm gap. In determining the gap size, the flow area of the core baffle region was added to that of the downcomer region. Thus, the core baffle flow area is included in the downcomer simulation and is not simulated separately in the vessel inserting stainless steel fillers to prevent fluid flow.

The vessel wall is constructed of carbon steel which is cladded with the 5 mm thick stainless steel plate. The wall is 90 mm thick to simulate the stored energy as reasonably as possible during ECC water injection.

The design of upper plenum internals is based on that of the new Westinghouse 17 x 17 type fuel assemblies instead of the old type simulated in the Core-I facility. The internals consists of ten control rod guide tubes, ten support columns and twelve open holes as shown in Fig. 2.6. The radius of each internals is scaled down by factor 8/15 from that of an actual reactor. They are illustrated in Fig. 2.7. Flow resistance baffles are inserted into the control rod guide tubes. The baffles consist of two kinds of baffle plates and a shaft. The baffle plates are shown in Fig. 2.8.

End boxes are attached beneath the UCSP. The structure for one heater rod bundle is shown in Fig. 2.9. Plugging devices are installed newly in the Core-II facility as shown in Figs. 2.9 and 2.10 to simulate the flow resistance more correctly.

2.1.2 Heater Rod Assembly

The heater rod assembly simulating the fuel assembly consists of thirty-two 8 x 8 array rod bundle. Each bundle consists of fifty-seven electrically heated rods and seven non-heated rods as shown in Fig. 2.11. The core is usually subdivided into three regions to achieve a desired radial power distribution. This is shown in Fig. 2.3. The high, medium and low power regions are named A, B and C regions, respectively. The local peaking factor of heated rods in a bundle is unity, that is, all heated rods in a bundle have the same power density in the Core-II facility.

A heater rod consists of a nichrome heating element, magnesium oxide (MgO) and boron nitride (BN) insulators, and Inconel-600 sheath. BN is used for only central part of the heated region and MgO for the other part as shown in Fig. 2.12. The heated length and the outer diameter of the heater rods are 3.66 m and 10.7 mm, respectively, which are identical to the corresponding dimensions of actual PWR fuel rods. The sheath wall thickness is 1.0 mm and is thicker than the actual fuel cladding, because of the requirements for thermocouple installation. The heating element is a helical coil with a varying pitch to generate a 17 steps chopped cosine axial power profile as shown in Fig. 2.13. The peaking factor is 1.40, in-

stead of 1.492 for a Core-I rod.

Non-heated rods are either stainless steel pipes or solid bars of 13.8 mm O.D. All the pipes are utilized for installation of instruments such as superheated steam probes and thermocouples. All the bars are used for carrying the assembly loads.

The heated rods and non-heated rods are held in radial position by grid spacers which are located at six elevations along the axial length as shown in Fig. 2.13. A grid spacer is a lattice structure composed of stainless steel plates of 0.4 mm and 0.8 mm thick and 40 mm high. The rod pitch is 14.3 mm which is the same as that of the reference PWR.

The heater rods penetrate through the bottom plate of the vessel to facilitate lead out of the power cables from the bottom of the vessel. The outer diameter of the rods in the lower plenum is reduced to 8.6 mm. Three-phase electric current is used for heating the heater rods and the electrical neutral point is at the top of the rods where they are interconnected to each other.

2.1.3 Primary Loops and ECCS

Primary loops consist of three intact loops and a broken loop. Each loop consists of hot leg and cold leg pipings, a steam generator simulator and a pump simulator. The 200 percent cold leg large break is simulated for the broken loop. The broken cold leg is connected to two containment tanks through blowdown valves. The primary loop arrangement is shown in Figs. 2.14 and 2.15.

The inner diameter of the piping is scaled down in proportion to the core flow area scaling. The length of each piping section is almost the same as the corresponding section of the reference PWR.

The steam generator simulators are of the U-tube and shell type as shown in Fig. 2.16. The tube length is about 5 m shorter than in the reference PWR. The vertical height of the steam generator simulators is also about 5 m lower than in the reference PWR. The primary coolant passes through the tube side and the secondary coolant is stagnant in the shell side. The steam generator simulators of two loops are housed in a single shell assembly which has two compartment, one simulator for each loop in one compartment. The wall thickness of the U-tube is 2.9 mm compared to 1.27 mm of the reference PWR, because of a higher pressure difference be-

tween the primary and secondary sides in the simulator.

The pump simulator consists of the casing and duct simulators and an orifice plate as shown in Fig. 2.17. The loop flow resistance is simulated with the orifice plate. Each orifice plate has a hole with diameter and thickness of 95 mm and 10 mm, respectively.

ECCS consists of two Accs and a LPCI. The injection points are at each cold leg, hot leg, lower plenum, upper plenum and downcomer. The upper plenum, downcomer and hot leg injection system was newly installed after Test C2-2 (Run 56) for the alternative ECCS tests. In the new injection system, two accumulator tanks are used for ECC water injection.

2.1.4 Instrumentation

The instrumentation is divided into two groups. One of them is JAERI-supplied instruments measuring the temperatures, absolute pressures, differential pressures, water levels and flow rates. Thermocouples measure the temperatures of the rod surface, fluid and structure. The absolute pressures are measured in the upper and lower plena, steam generator plena and containment tanks. The differential pressure measurements are carried out at many locations covering the whole system almost completely. In the ECC water supply tanks and the containment tank 1, the liquid levels are measured. The flow meters measure the ECC water flow rates. Furthermore, flow rates in the downcomer, loop seal pipings and the vent line from the containment tank 2 to the atmosphere are measured with drag disk flow meters, pitot tubes and a ventulli tube, respectively. The total number of the JAERI-supplied instruments is 1338 channels as summarized in Table 2.2 and the signals from these instruments are recorded on a magnetic tape.

The other group of the instrumentation is the USNRC-supplied instruments. They are the advanced instrumentation for the two-phase flow measurement. The kinds and quantities of those are tabulated in Table 2.3. The total number is 540 channels.

2.2 Test Conditions and Procedures

2.2.1 Test Conditions

The summary of the test conditions are presented in Table 2.4. The distinctive feature of the present test is that the ECC water was injected into the downcomer directly. Except the difference in injection location,

the other conditions were set equal to those in the base case test.

2.2.2 Test Procedures

In preparation for the test, the accumulator tanks, the LPCI tank, the saturated water tank and the secondary sides of the steam generator simulators were filled with water which was purified with ion exchange resin. After all the components and instruments were inspected for mechanical and electrical leakages, the instruments were checked for zero points and sensitivity.

After these preparatory operation, the primary system was heated with the preheaters to its specified temperature (393 K) and pressurized to a specified pressure (200 kPa) by substituting steam for nitrogen gas in the system. The water in the accumulator tanks was electrically heated to its specified temperature (308 K) and pressurized with nitrogen gas to provide sufficient head to drive the injection flow required. The water in the LPCI tank was also heated to its specified temperature (308 K) and was circulated through the circulation line including the LPCI line so as to preheat the line to the same temperature as the water. The water in the saturated water tank was heated up near saturation temperature (393 K) of the expected primary system pressure (200 kPa). The water in the secondary side of each steam generator simulator was also heated and pressurized to the specified temperature (539 K) and pressure (5.3 MPa).

After establishing the initial conditions of the test, electric power for preheating was turned off and the lower plenum was filled to a specified level (0.9 m) directly from the saturated water tank. When the water level in the lower plenum reached the specified level and other initial conditions of the test stabilized at the allowable tolerance, electric power was applied to the heater rods in the core and the data recording was started. This is the initiation of the test, *i.e.* 0 s. The temperature rise of the rods were monitored by using a computer. At 85 s, Acc injection (0.096 m^3/s) into the lower plenum was initiated. LPCI injection (8.9×10^{-3} m^3/s) into the downcomer was also initiated at the same time using the newly installed Acc tank. The initiation time for ECC injection, *i.e.* 85 s, was scheduled to coincide with the timing when the clad temperature of 995 K was reached by four rods. This specified clad temperature (995 K) of the heater rods for initiation of coolant injection was predetermined by

interpolation between the clad temperature (393 K) after preheating and the clad temperature (1073 K) assumed for the time of bottom of core recovery (BOCREC). The system pressure was maintained at the specified initial pressure (200 kPa) throughout the test by controlling the outlet valve of containment tank 2. Decay of power input to the rods was programmed to begin when the water reached bottom of the heated region of the core. The specified power decay was obtained by normalizing the decay curve of the ANS standard x 1.2 + ^{238}U capture decay at 30 seconds after shutdown.

At 97 s, Acc injection location was switched from the lower plenum to three intact cold legs. Since the BOCREC was scheduled to occur at 94 s, some amount of steam generated in the core was expected to flow in the primary loops prior to switching of the Acc injection location. This procedure was for preventing an unrealistic condensation from occurring at the cold legs. At a specified time (23 s) after the initiation of Acc injection, the Acc injection mode was transferred to the LPCI injection mode. This mode simulated HPCI injection in an actual PWR. A injection rate of 2.2×10^{-3} m^3/s was maintained constantly in parallel with downcomer injection until the ECC injection was turned off. The sequence of the ECC water injection of the present test is compared with that of the base case test in Fig. 2.18.

The generated steam and the entrained water flowed via broken and intact loops to the containment tanks. The steam was then vented to the atmosphere to maintain the pressure in the containment tanks constant.

When all thermocouples on the surface of heater rods indicated quenching of the rods, the power supply to heater rods and the ECC water injection were turned off. After this the data recording was ended terminating the test.

The chronology of events are presented in Table 2.5.

Table 2.1 CCTF component scaled dimensions

COMPONENT		PWR	JAERI	RATIO
PRESSURE VESSEL				
VESSEL INSIDE DIAMETER	(mm)	4394 (173")	1084	
VESSEL THICKNESS	(mm)	216 (8 1/2")	90	
CORE BARREL OUTSIDE DIAMETER	(mm)	3874	961	
CORE BARREL INSIDE DIAMETER	(mm)	3760	929	
THERMAL SHIELD OUTSIDE DIAMETER	(mm)	4170		
THERMAL SHIELD INSIDE DIAMETER	(mm)	4030		
DOWNCOMER LENGTH	(mm)	4849	4849	1/1
DOWNCOMER GAP	(mm)	114.3	61.5	
DOWNCOMER (+ BUFFLE) FLOW AREA	(m^2)	4.23	0.197	1/21.44
LOWER PLENUM VOLUME	(m^3)	29.6	1.38	1/21.44
UPPER PLENUM VOLUME	(m^3)	43.6	2.04	1/21.44
FUEL (HEATER ROD) ASSEMBLY				
NUMBER OF BUNDLES	(—)	193	32	
ROD ARRAY	(—)	15 × 15	8 × 8	
ROD HEATED LENGTH	(mm)	3660	3660	1/1
ROD PITCH	(mm)	14.3	14.3	1/1
FUEL ROD OUTSIDE DIAMETER	(mm)	10.72	10.7	1/1
THIMBLE TUBE DLAMETER	(mm)	13.87	13.8	1/1
INSTRUMENT TUBE DIAMETER	(mm)	13.87	13.8	1/1
NUMBER OF HEATER RODS	(—)	39372	1824	1/21.58
NUMBER OF NON-HEATED RODS	(—)	4053	224	1/18.09
CORE FLOW AREA	(m^2)	5.29	0.25	1/21.2
CORE FLUID VOLUME	(m^3)	17.95	0.915	1/19.6
PRIMARY LOOP				
HOT LEG INSIDE DIAMETER	(mm)	736.6 (29")	155.2	1/4.75
HOT LEG FLOW AREA	(m^2)	0.426	0.019	1/22.54
HOT LEG LENGTH	(mm)	3940	3940	1/1
PUMP SUCTION INSIDE DIAMETER	(mm)	787.4 (31")	155.2	1/5.07
PUMP SUCTION FLOW AREA	(m^2)	0.487	0.019	1/25.77
PUMP SUCTION LENGTH	(mm)	7950	7950	1/1

Table 2.1 (Cont'd)

COMPONENT		PWR	JAERI	RATIO
COLD LEG INSIDE DIAMETER	(mm)	698.5 (27.5")	155.2	1/4.50
COLD LEG FLOW AREA	(m^2)	0.383	0.019	1/20.26
COLD LEG LENGTH	(mm)	5600	5600	1/1
STEAM GENERATOR SIMULATOR				
NUMBER OF TUBES	(—)	3388	158	1/21.44
TUBE LENGTH (AVERAGE)	(m)	20.5	15.2	1/1.35
TUBE OUTSIDE DIAMETER	(mm)	22.225 (0.875")	25.4	
TUBE INSIDE DIAMETER	(mm)	19.7 (0.05")	19.6	1/1
TUBE WALL THICKNESS	(mm)	1.27	2.9	
HEAT TRANSFER AREA	(m^2)	4784 (51500 ft^2)	192	1/24.92
TUBE FLOW AREA	(m^2)	1.03	0.048	1/21.44
INLET PLENUM VOLUME	(m^3)	4.25	0.198	1/21.44
OUTLET PLENUM VOLUME	(m^3)	4.25	0.198	1/21.44
PRIMARY SIDE VOLUME	(m^3)	30.50 (1077 ft^3)	1.2	1/25.41
SECONDARY SIDE VOLUME	(m^3)	157.33 (5556 ft^3)	2.5	1/62.93
CONTAINMENT TANK - I	(m^3)		30	
CONTAINMENT TANK - II	(m^3)		50	
STORAGE TANK	(m^3)		25	
ACC. TANK	(m^3)		5	
SATURATED WATER TANK	(m^3)		3.5	
ELEVATION				
BOTTOM OF HEATED REGION IN CORE	(mm)	0	0	
TOP OF HEATED REGION IN CORE	(mm)	3660	3660	0
TOP OF DOWNCOMER	(mm)	4849	4849	0
BOTTOM OF DOWNCOMER	(mm)	0	0	0
CENTERLINE OF COLD LEG	(mm)	5198	4927.	- 271
BOTTOM OF COLD LEG (INSIDE)	(mm)	4849	4849	0
CENTERLINE OF LOOP SEAL LOWER END	(mm)	2056	2047	- 9
BOTTOM OF LOOP SEAL LOWER END	(mm)	1662	1959	+ 297

Table 2.1 (Cont'd)

COMPONENT		PWR	JAERI	RATIO
CENTER OF HOT LEG	(mm)	5198	4927	− 271
BOTTOM OF HOT LEG (INSIDE)	(mm)	4830	4849	+ 19
BOTTOM OF UPPER CORE PLATE	(mm)	3957	3957	0
TOP OF LOWER CORE PLATE	(mm)	− 108	− 50	+ 58
BOTTOM OF TUBE SHEET OF STEAM GENERATOR SIMULATOR	(mm)	7308	7307	− 1
LOWER END OF STEAM GENERATOR SIMULATOR PLENUM	(mm)	5713	5712	− 1
TOP OF TUBES OF STEAM GENERATOR SIMULATOR (avg)	(mm)	17952.7	14820	

Table 2.2 List of items measured with JAERI-supplied instruments

Item	Number of channels
Rod surface temperature	673
Core fluid temperature	40
Core barrel wall temperature	10
UP fluid temperature	120
UP wall temperature	36
DC fluid temperature	20
DC wall temperature	40
LP fluid temperature	8
LP wall temperature	4
SG primary side fluid temperature	24
SG secondary side fluid temperature	66
Primary loop piping fluid temperature	94
Primary loop piping wall temperature	4
Water supply tank fluid temperature	12
Core differential pressure	28
DC differential pressure	20
UP differential pressure	8
LP differential pressure	1
SG primary side differential pressure	8
Primary loop differential pressure	52
Pressure	15
Water level	7
Flow rate	39
Electric power	9
Total	1338

Note

UP : Upper plenum, DC : Downcomer

LP : Lower plenum, SG : Steam generator

Table 2.3 List of USNRC-provided instruments

Instrument	Number of sets	Number of sensors
DC FDG	18	162
DC VOP	1	1
DC drag disk	4	8
Core velocimeter	4	4
Core flag probe	12	24
Core LLD	6	96
LP LLD	3	15
End box turbine meter	8	8
UP turbine meter	4	4
UP FDG	11	110
UP film probe	2	4
UP prong probe	2	4
UP VOP	1	1
VV turbine meter	2	2
VV string probe	2	2
HL film probe	2	4
HL VOP	1	1
Reference probe	1	1
Spool piece	8	89
Total	92	540

Note

DC : Downcomer, FDG: Fluid distribution grid,
VOP: Video optical probe, LLD: Liquid level detector,
LP : Lower plenum, UP : Upper plenum,
VV : Vent valve

Table 2.4 Summary of test conditions

1. Test type: Downcomer and cold leg combined injection test
2. Test No.: C2-AA2 (Run 58)
3. Test Date: March 30, 1983
4. Power: Total; 9.36 MW, Average linear; 1.40 kW/m
5. Radial power distribution:

   A : B : C

   1.91 : 1.68 : 1.07 kW/m
6. Pressure (MPa):

   Upper plenum ; 0.26

   Containment ; 0.2
7. Temperature (K):

   Downcomer wall; 481, Vessel internals; 395

   Primary piping; 395, Lower plenum liquid; 395

   ECC liquid; 308, Steam generator secondary; 540
8. ECC injection type: Downcomer and cold leg combined injection
9. Pump K-factor: 15
10. ECC injection rates and duration:

    Acc; 81×10^{-3} m^3/s from 87.5 to 111.3 s (at half maximum)

    LPCI; 2.2×10^{-3} m^3/s from 111.0 to 1008.0 s

    New Acc; 8.9×10^{-3} m^3/s from 85.5 to 1008.0 s

    ECC injection to lower plenum; from 85.5 to 103.0 s
11. Initial water level in lower plenum: 0.86 m
12. Power decay: ANS × 1.2 + Actinide (30 s after scram)
13. Peak clad temperature at BOCREC: 1067 K

Table 2.5 Chronology of events

Event	Time (s)
Test initiated (Heater rods power on) (Data recording initiated)	0.0
Accumulator injection initiated (New Accumulator injection initiated)	85.5
Bottom of core recovery (BOCREC)	93.0
Power decay initiated	94.5
Accumulator injection switched from lower plenum to cold legs	97.0
LPCI injection initiated	111.0
Accumulator injection ended	116.0
All heater rods quenched	722.0
Power off	1008.0
LPCI injection ended (New Accumulator injection ended)	1008.0
Test ended (Data recording ended)	1038.0

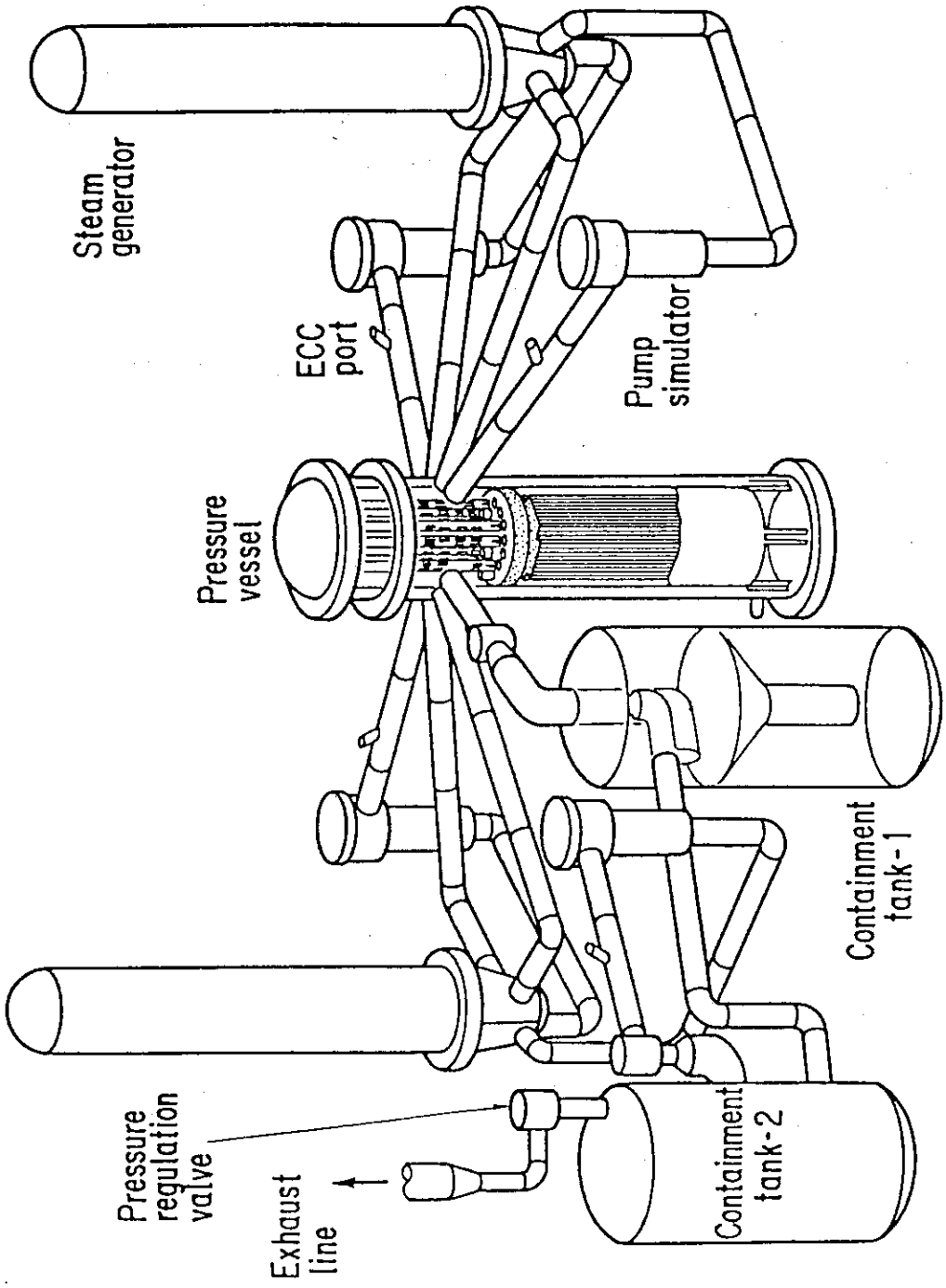

Fig. 2.1 Brid's-eye view of CCTF

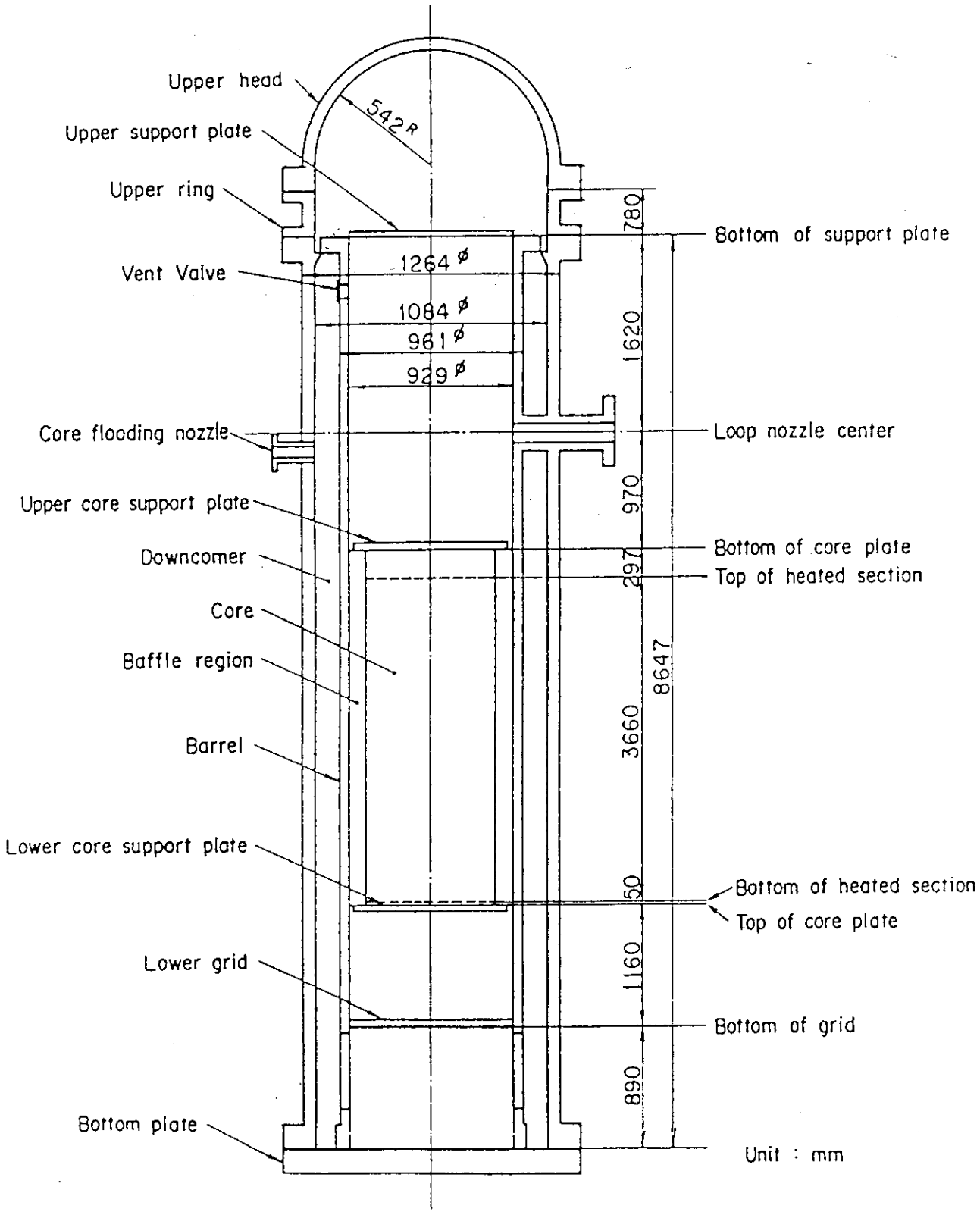

Fig. 2.2 CCTF Core-II pressure vessel

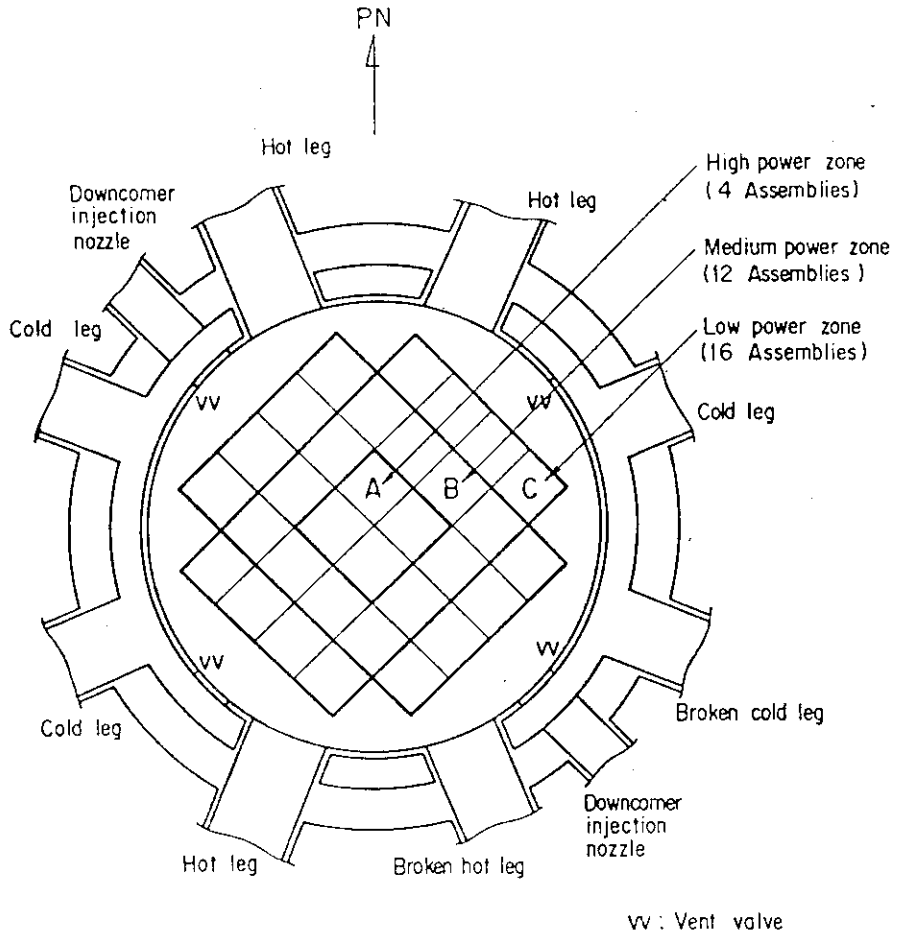

Fig. 2.3 Cross section of CCTF Core-II pressure vessel

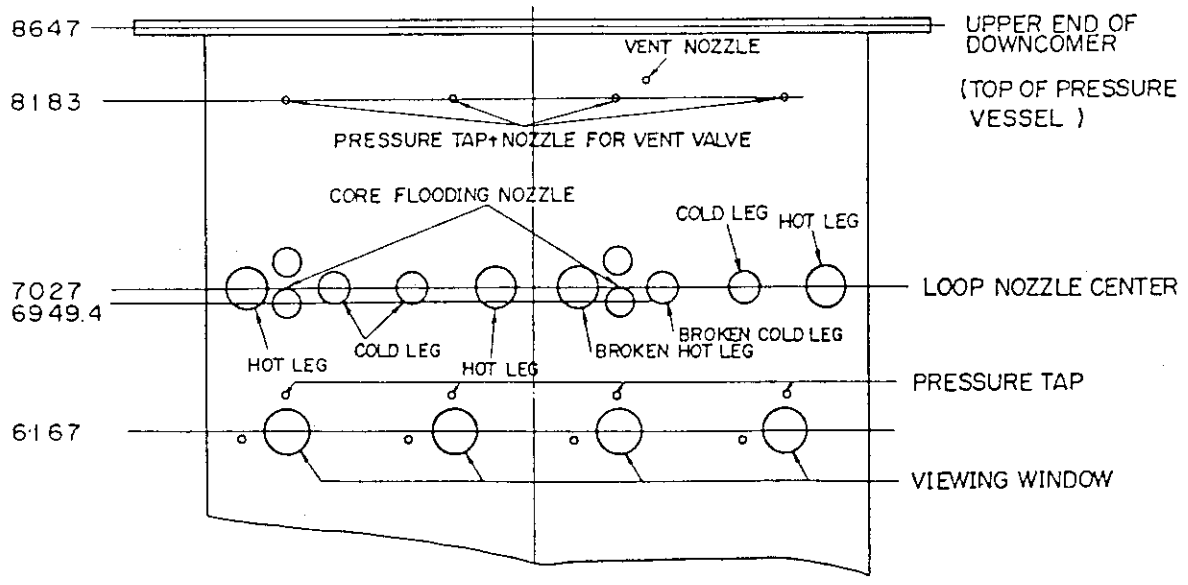

Fig. 2.4 Location of Core Flooding Nozzles

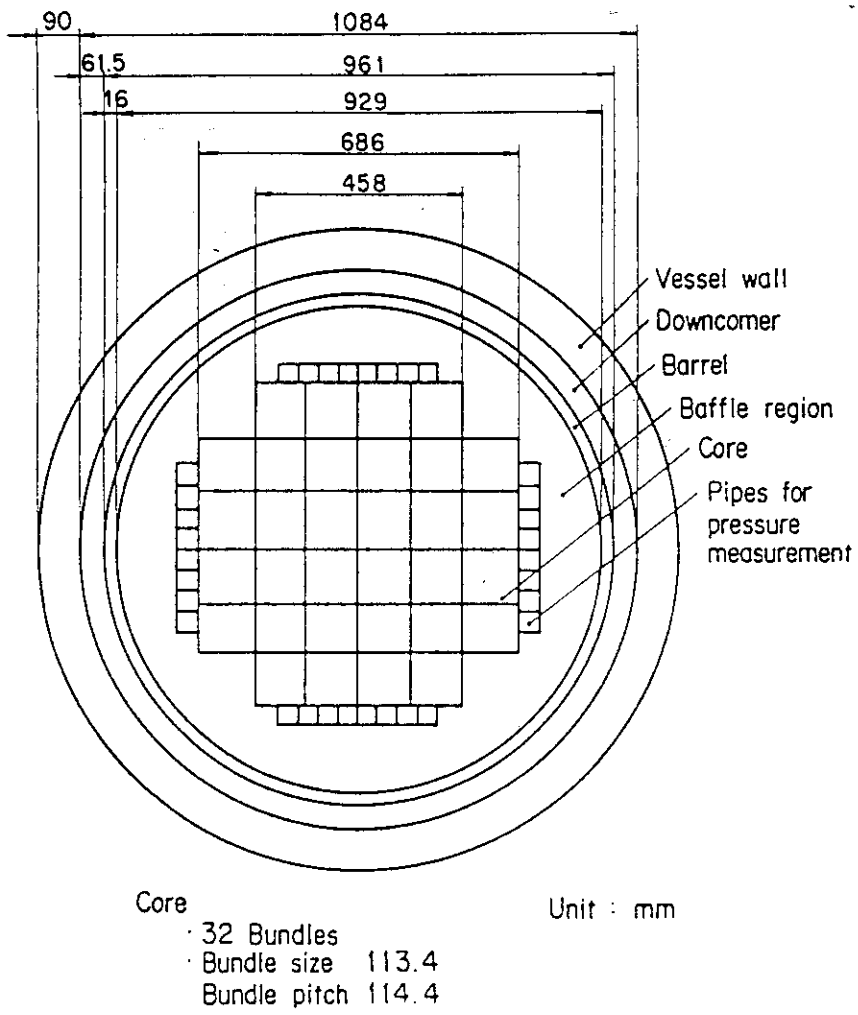

Fig. 2.5 Dimension of CCTF Core-II pressure vessel cross section

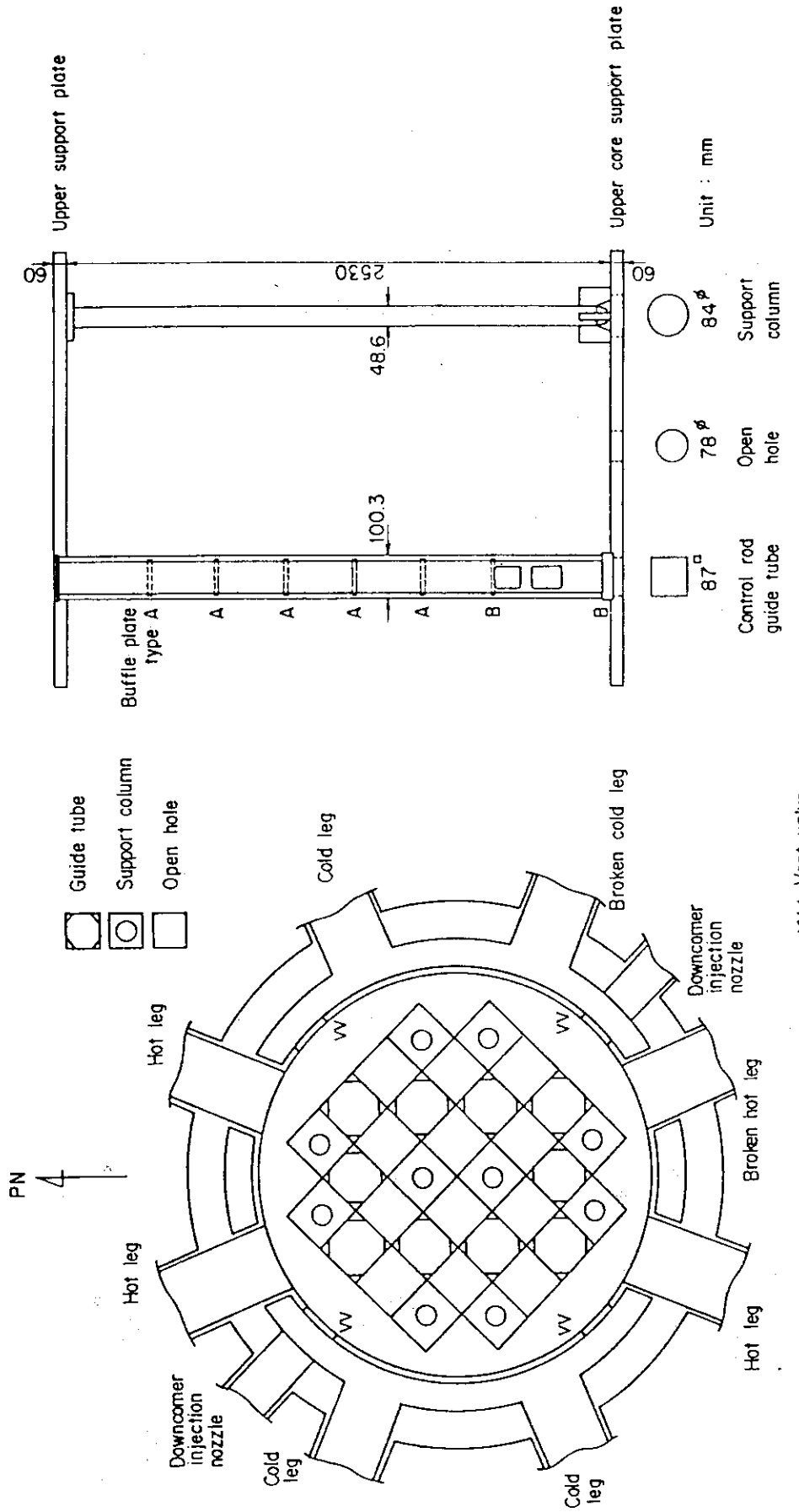

Fig. 2.6 Arrangement of upper plenum internals

Fig. 2.7 Upper plenum internals

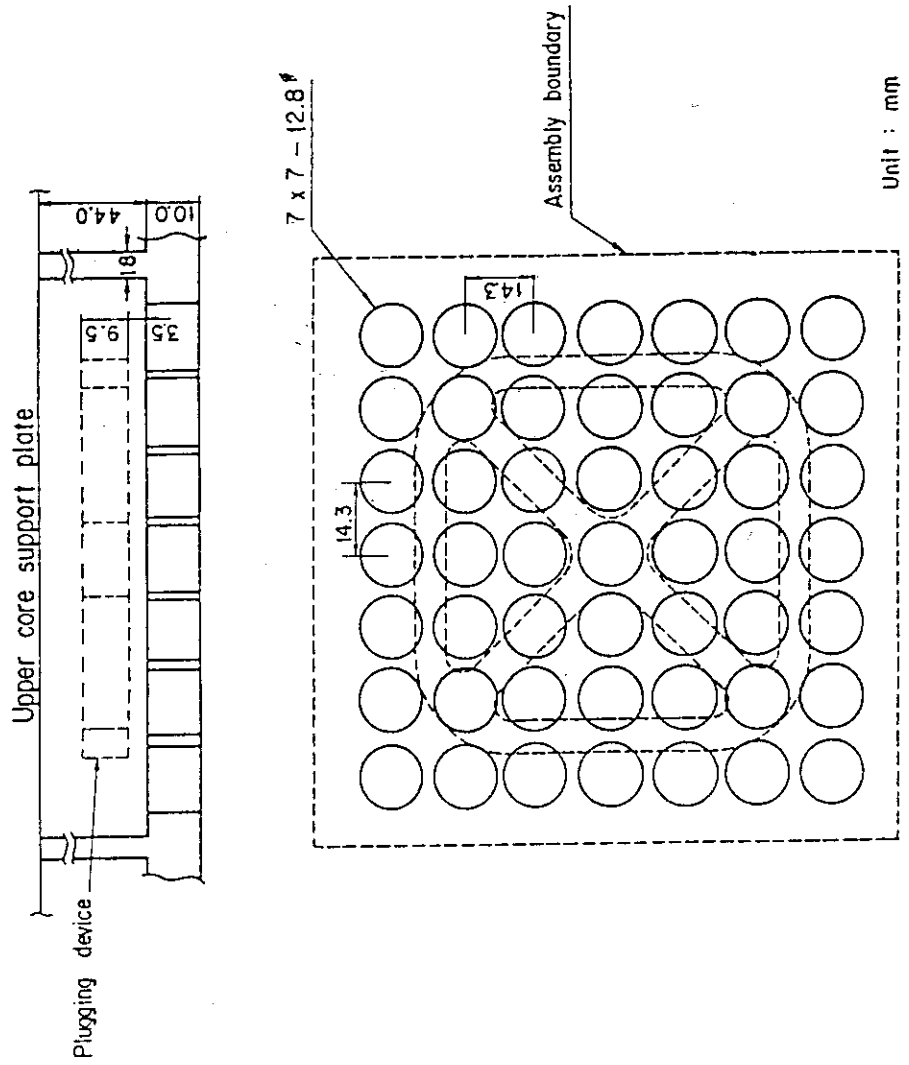

Fig. 2.9 End box

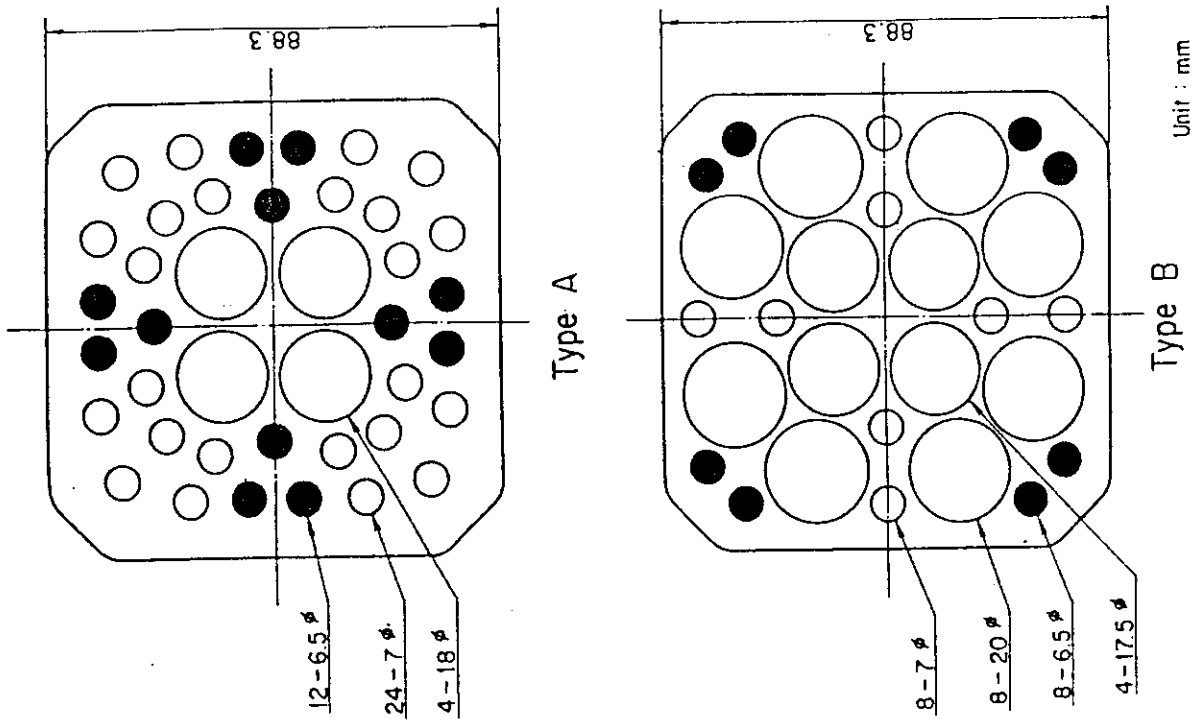

Fig. 2.8 Baffle plates in control rod guide tube

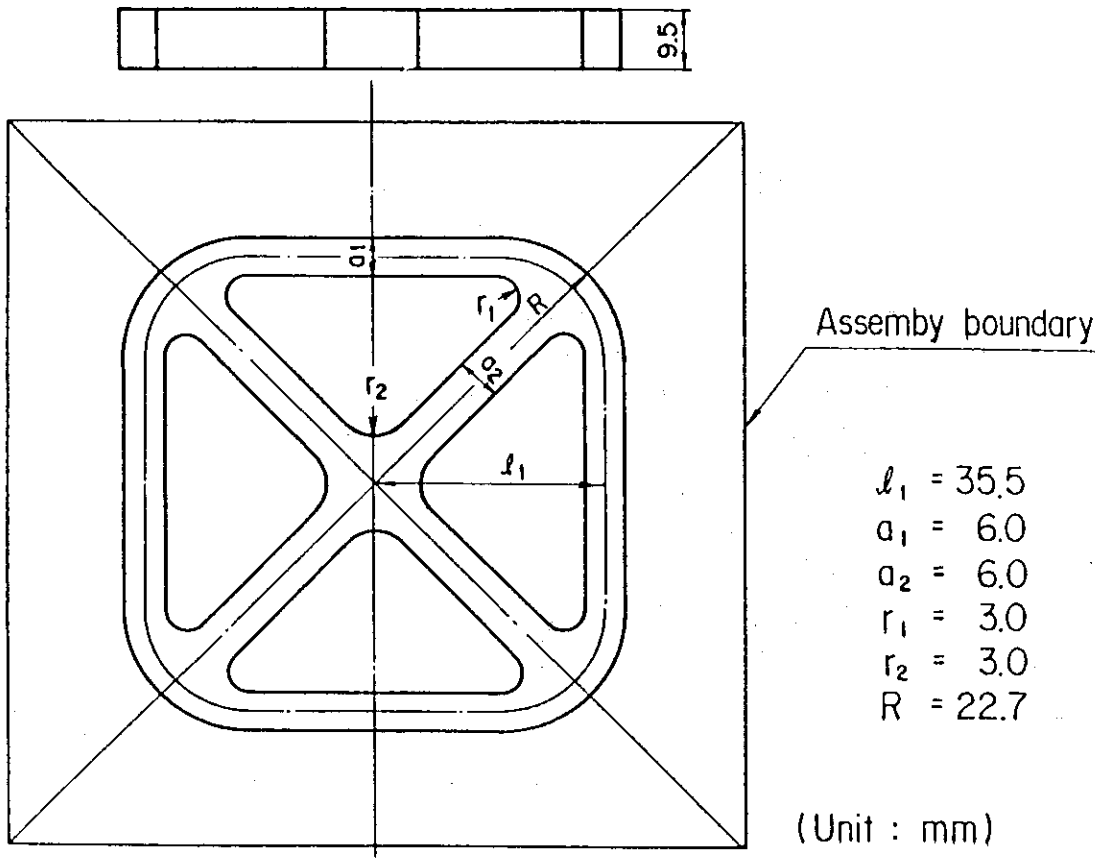

Fig. 2.10 Dimensions of plugging device

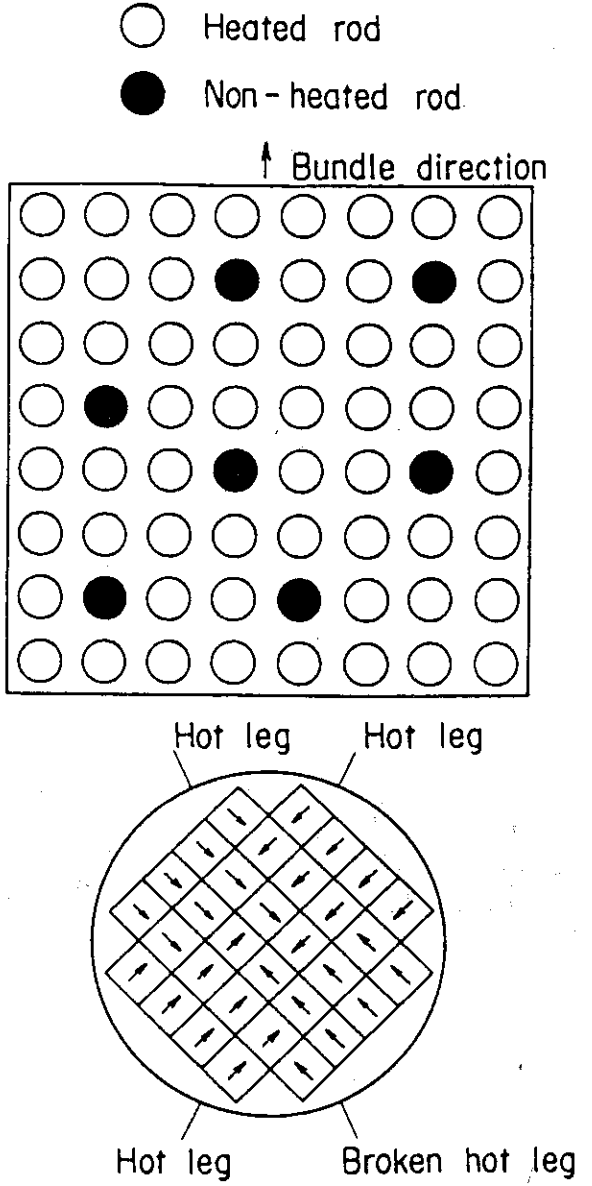

Fig. 2.11 Arrangement of non-heated rods and bundle direction

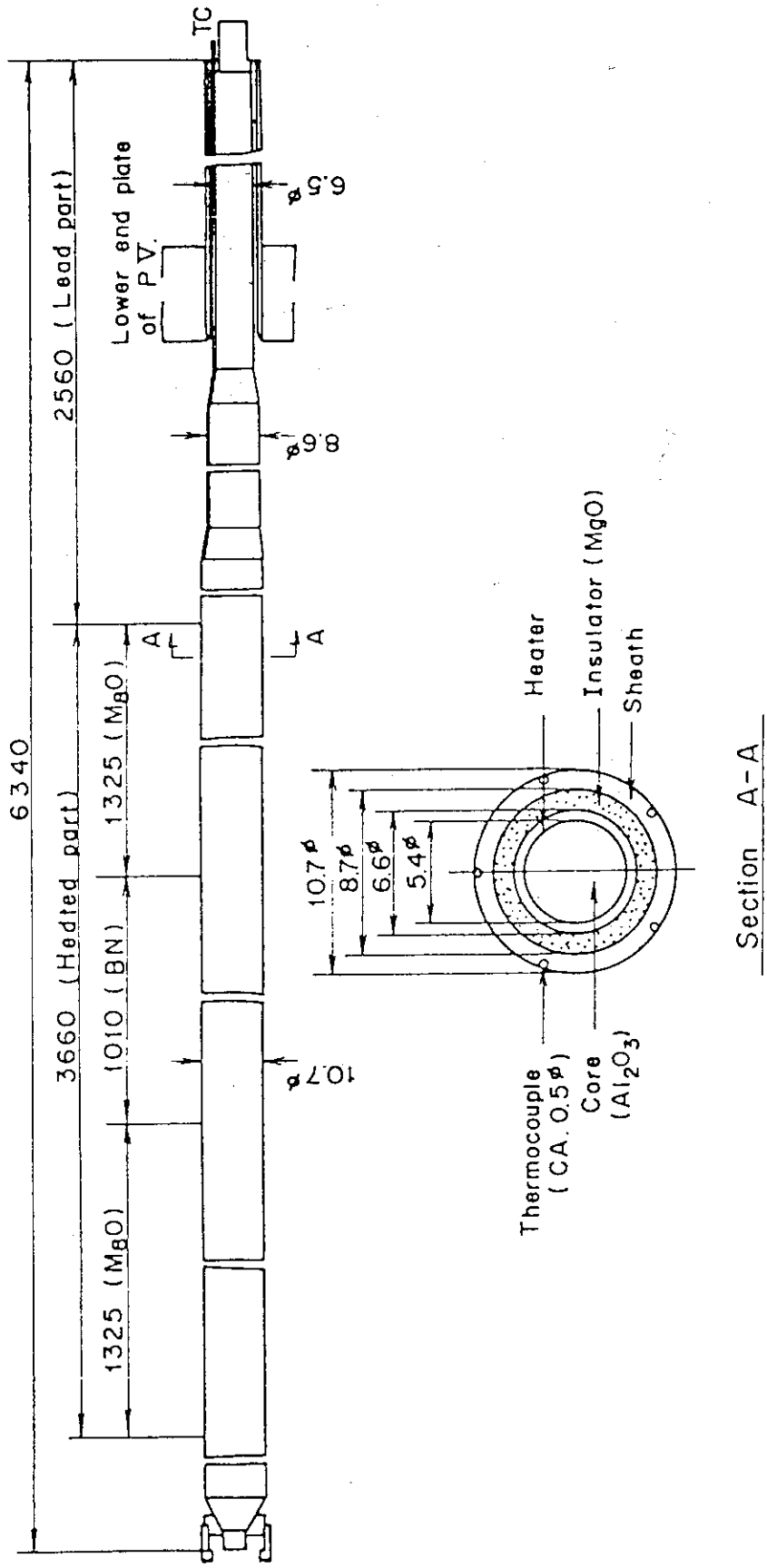

Fig. 2.12 Heater rod

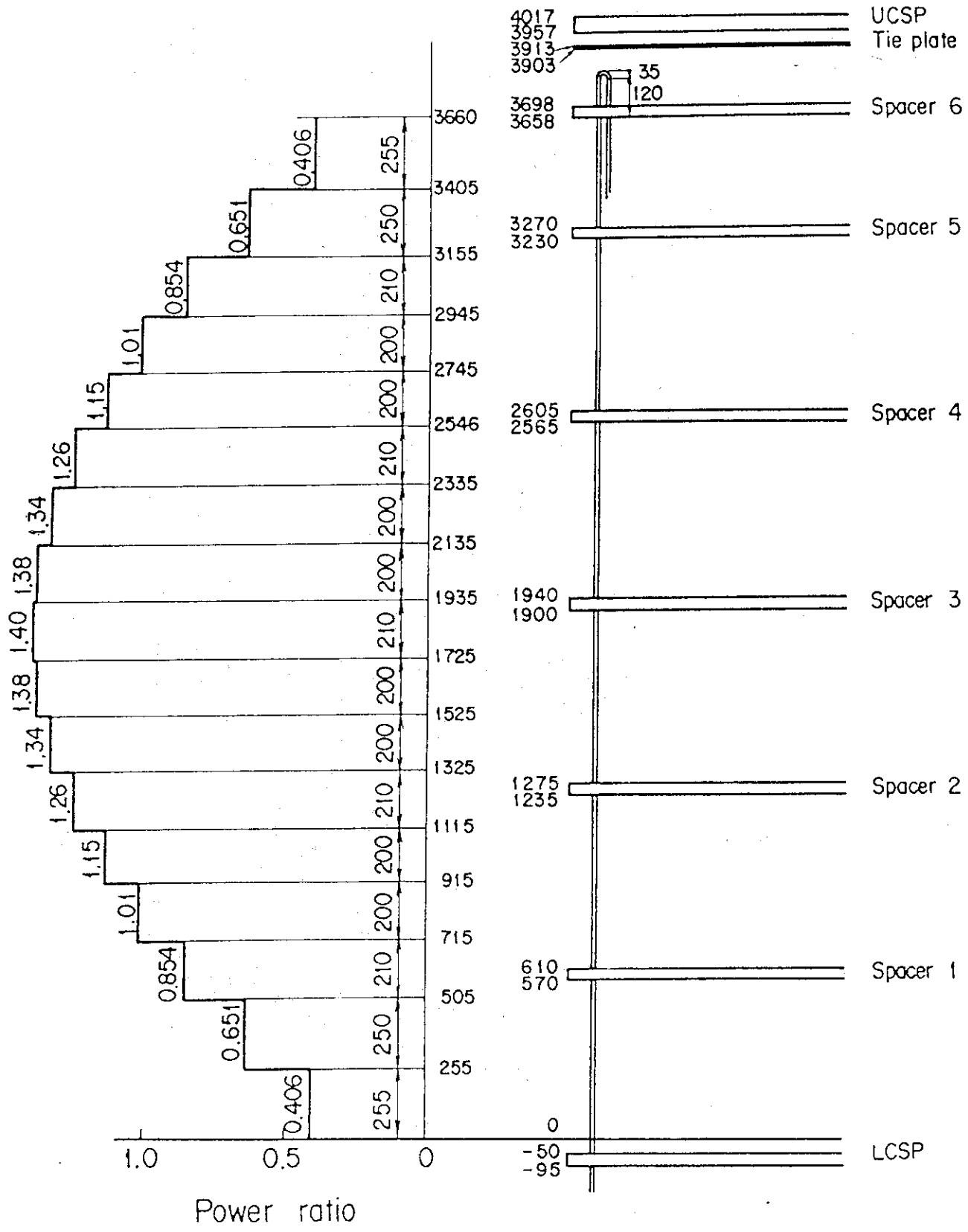

Fig. 2.13 Axial power profile of CCTF Core-II heater rod

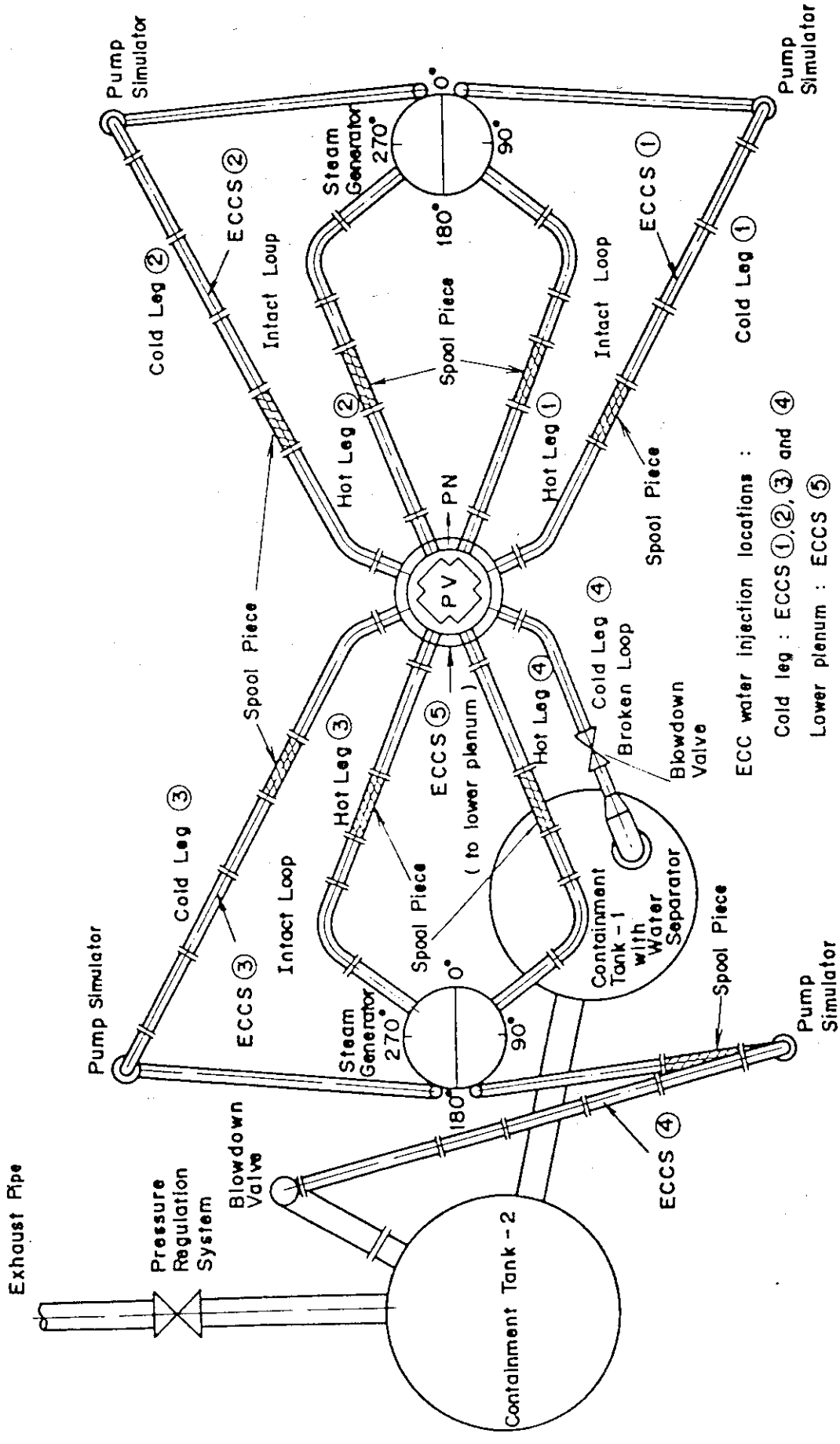

Fig. 2.14 Top view of primary loop pipings

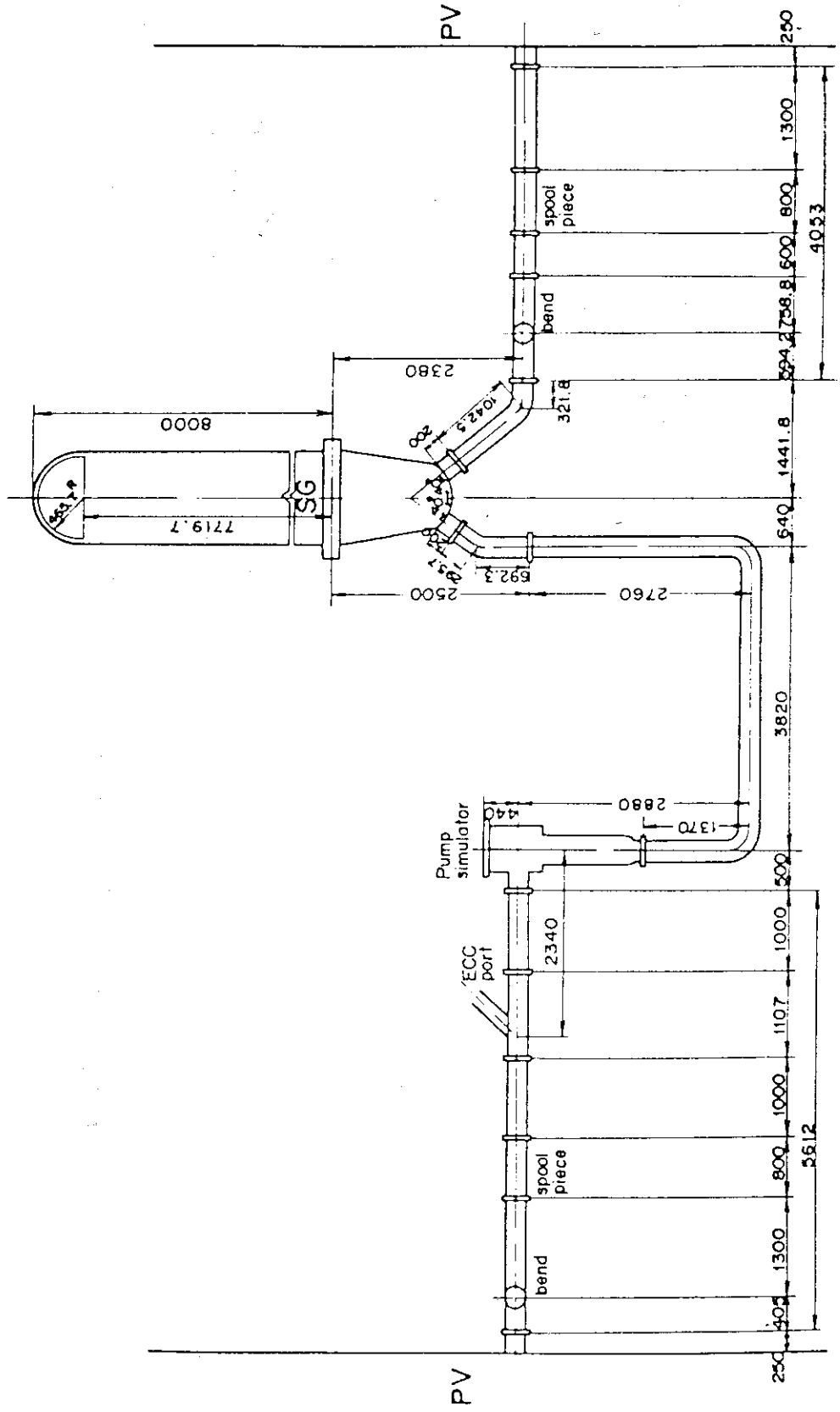

Fig. 2.15 Dimensions of primary loop

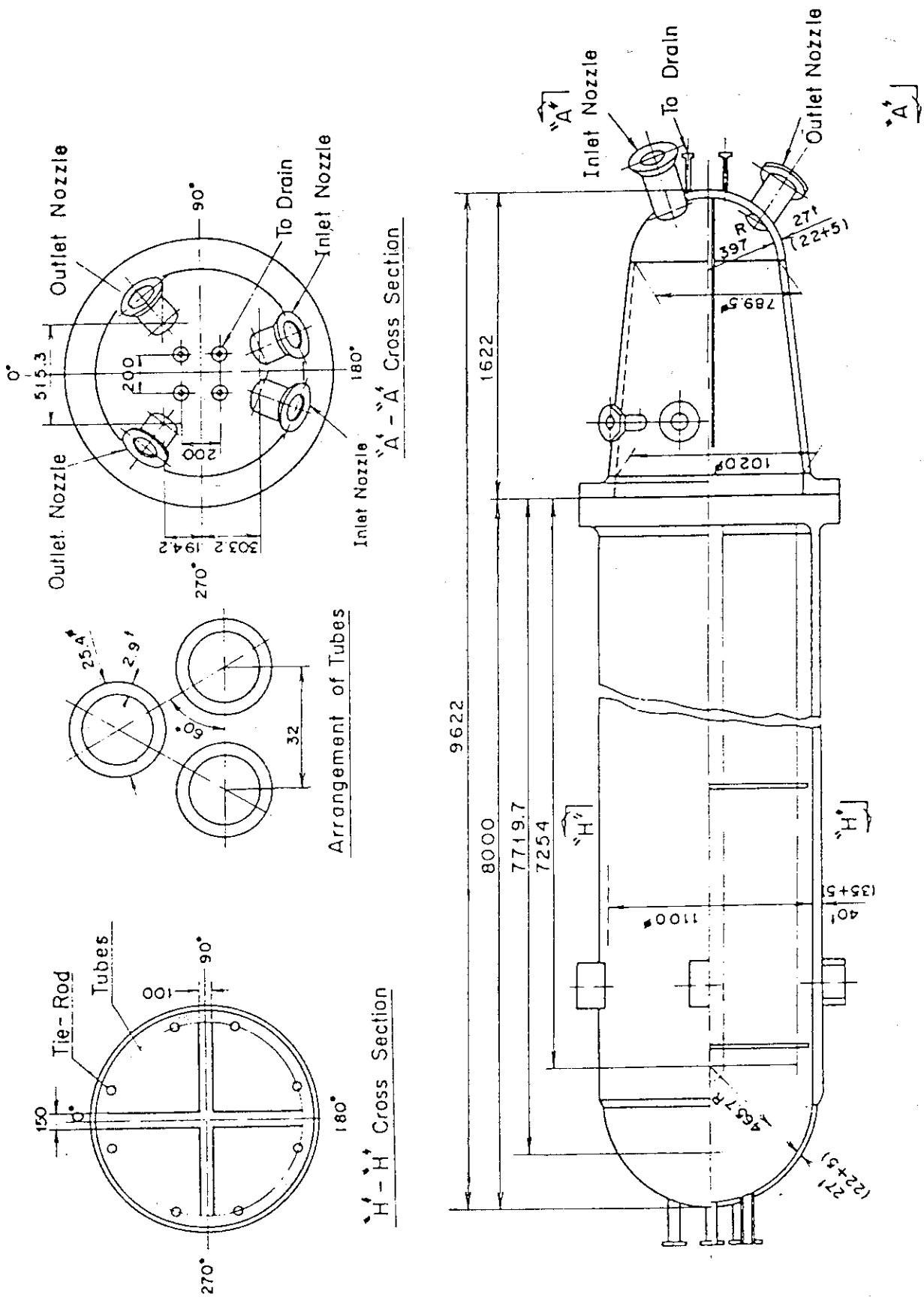

Fig. 2.16 Steam generator simulator

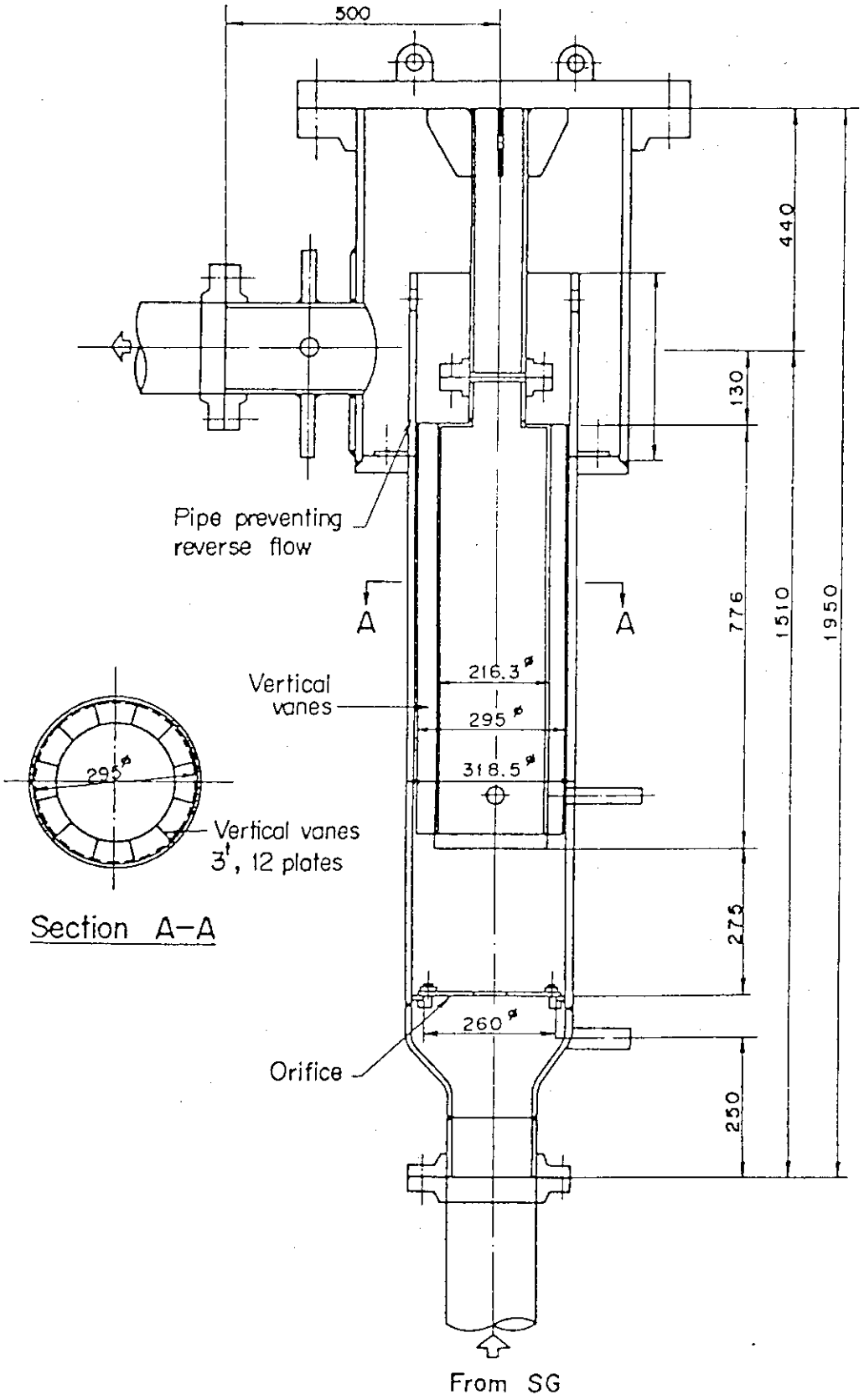

Fig. 2.17 Pump simulator

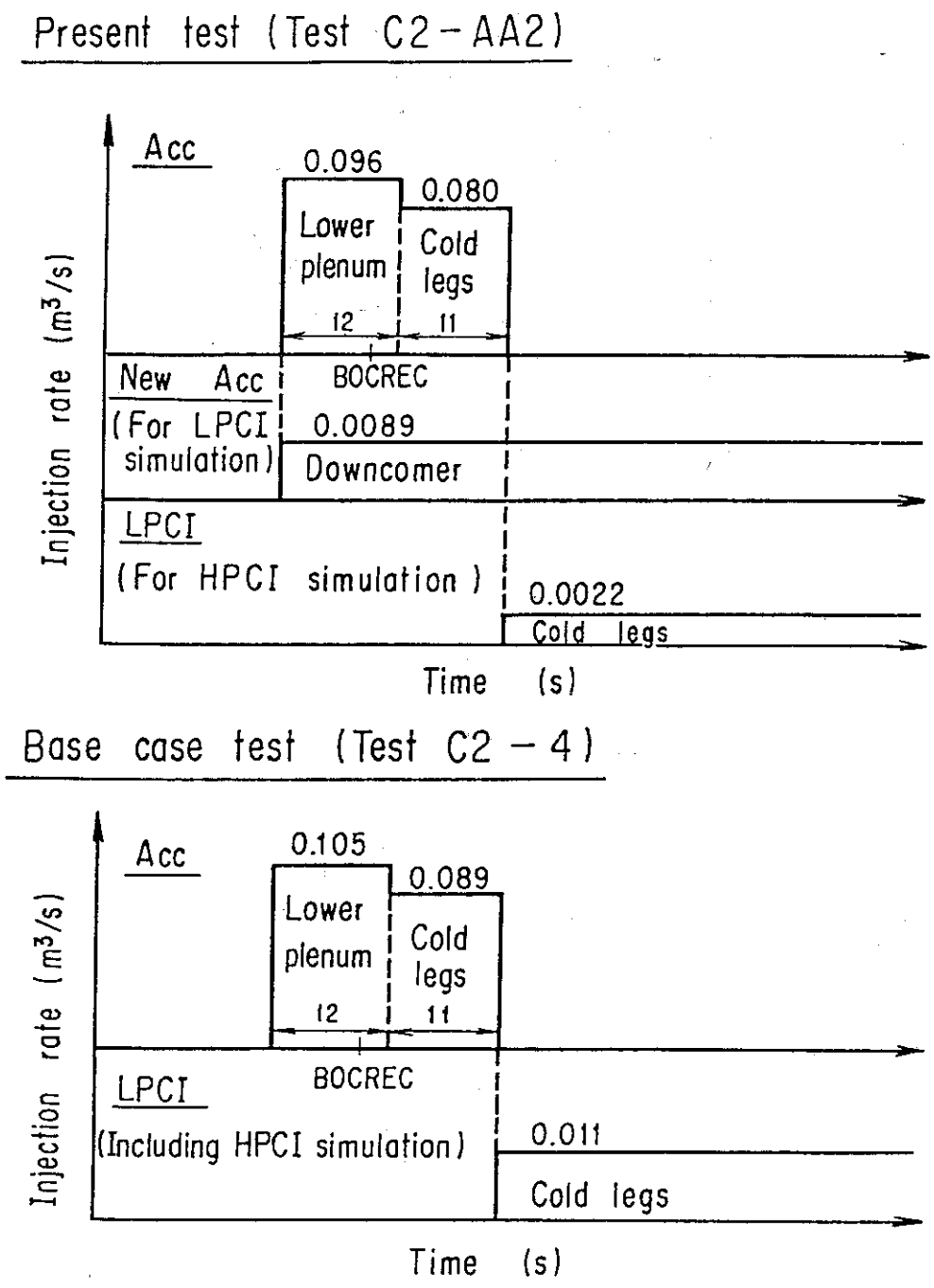

Fig. 2.18 Schematic of ECC water injection sequence

3. Test Results and Discussion

3.1 System Behavior

In the present test, C2-AA2, a significant oscillation is observed in pressure and differential pressure data as shown in Fig. 3.1 for instance. Even in fluid temperature data, the same kind of oscillation is observed (for example, Fig. 3.2). The oscillation is repeated periodically. Its pattern is unique and different from that observed in the lower plenum injection tests[4]. The oscillation observed in the present test is investigated in detail in Section 3.3.

Figure 3.1 shows a comparison of downcomer differential pressure between the present test and the base case test C2-4[5]. Average value for the base case test is smaller than that for the present test during the period from 100 s to 280 s and after that they become almost identical. The decrease of the differential pressure for the base case test is caused by voiding of the downcomer water due to heat release from initially superheated downcomer outside wall[6]. For Test C2-AA2, however, decrease of the downcomer differential pressure is not noticeable. This is considered to result from lower and subcooled downcomer fluid temperature in this test, as shown in the following.

Figures 3.2(a) through 3.2(e) show comparisons of downcomer fluid temperature at five elevations and indicate that downcomer fluid temperature for Test C2-AA2 is lower and subcooled at every elevation. This suggests no voiding in the downcomer mentioned above. The difference in the temperature between the two tests tends to be larger at the higher elevation. The lower and subcooled downcomer fluid temperature in Test C2-AA2 is attributed to thermal non-equilibrium in mixing of LPCI water and steam, which flows through the intact loops, at the top section of the downcomer due to direct injection of subcooled LPCI water into the downcomer. In the base case test, however, subcooled LPCI water is injected into the intact cold legs and is heated up to the saturation temperature before it arrives at the downcomer due to condensation of steam, and hence, thermal equilibrium is established between LPCI water and steam.

There are two injection nozzles in the downcomer as shown in Figs. 2.2 through 2.4, and Figs. 3.2(a) through (e) show data at location just below the injection nozzle. In order to check influence of injection location on fluid temperature, Figs. 3.3(a) through (c) show fluid temperatures at

locations just below the injection nozzle and below between the two injection nozzles. These figures indicate that there is influence of injection location on fluid temperature. Although temperatures below between two injection nozzles is higher than that just below injection nozzle as shown in Figs. 3.3(a) through (c), they are still lower than those for the base case test and subcooled. The temperatures in the base case test are almost the same as the saturation temperature.

Figure 3.4 shows a comparison of core differential pressure. In an early period, the differential pressure for the present test is a little lower on the average. This is attributed to the higher fluid temperature at the bottom section of the core. This is discussed in the next section (Figs. 3.19(a) and 3.20). From 140 s through 260 s, however, the differential pressure for the present test is slightly higher on the average and then both of them become identical on the average.

Figure 3.5 shows differential pressures through the intact and broken loops. Behavior of intact loop differential pressure is similar to that of the downcomer differential pressure shown in Fig. 3.1. That is, the data for the present test is larger during the period from 100 s to 280 s and after that they are almost identical on the average. The broken loop differential pressure for the present test is much smaller in an early period. These differential pressure data suggest that the mass effluence from the core is smaller in the present test until 160 s.

Figure 3.6 presents total mass flow rate in four primary loops and indicates total mass flow rate is smaller in the present test until 160 s. Since the core inlet subcooling is smaller in the present test as is shown later (Fig. 3.12), above result is inconsistent with the result of other two CCTF tests[7] (initial downcomer wall temperature effects tests in Core-I series). In these tests, core inlet subcoolings were different, whereas core flooding rates and other conditions were almost identical, and total primary loop mass flow rate was larger for the test in which core inlet subcooling was smaller. This result is easy to understand because liquid with smaller subcooling can be easily vaporized resulting in larger steam generation in the core. In the present test, however, total mass flow rate in the primary loops are smaller than in the base case test, although core inlet subcooling is smaller as is described later (Fig. 3.12). One reason for this may be the oscillation in the present test. The significant oscillation of liquid in the core in an early period may reduce

total heat transferred to liquid due to emptying the core during reversal flow period.

Figure 3.7 shows a comparison of differential pressure through the broken cold leg, which is difference of the broken and intact loop differential pressures shown in Fig. 3.5. They are not identical and the differential pressure for Test C2-AA2 is smaller on the average in an early period.

Figure 3.8 shows a comparison of pressures at the containment tank 2 and the upper plenum. The containment pressures are nearly identical, although there appear several step-wise increases due to problems of pressure control system in the present test. The upper plenum pressures follow the same trend as the broken loop differential pressures shown in Fig. 3.5.

Figures 3.9(a) and (b) show fluid temperatures in the broken cold leg near the broken cold leg nozzle for Test C2-AA2 and the base case test, respectively. They are almost identical on the average after 40 s and indicate the saturation temperature. In Fig. 3.9(a), however, there exist some periodic spikes indicating subcooling which is not observed in Fig. 3.9(b).

Figure 3.10 shows a comparison of fluid temperature at the bottom of the core. The fluid temperature for the present test is higher than that for the base case test. As shown in Fig. 3.2(a), however, the fluid temperature in the downcomer at 0.983 m from the bottom of the lower plenum is lower for the present test. Therefore, these data suggest that fluid in the lower plenum mixes well with fluid in the core due to the large oscillation in Test C2-AA2, and hence, fluid temperature in the lower plenum increases resulting in the high fluid temperature at the bottom of the core. This can be confirmed by data shown in Fig. 3.11. Figure 3.11 shows a comparison of lower plenum fluid temperatures at two elevations (0.3 m and 0.6 m from the bottom of the lower plenum). The temperatures for Test C2-AA2 are much higher than those of the base case test at both elevations indicating better fluid mixing in the present test. Figure 3.12 shows a comparison of core inlet subcooling. Subcooling for the present test is much smaller than for the base case test.

Figure 3.13 shows a comparison of the differential pressure through the upper plenum, which indicates water accumulation above the UCSP. There is a significant difference between them during 100 s through 300 s.

A comparison of core flooding rate is shown in Fig. 3.14. They are

evaluated by mass and energy balance calculation, and averaging, *i.e.* smoothing, of the data is performed so as to compare mean value. The core flooding rates are nearly identical on the average.

3.2 Core Behavior

Figure 3.15(a) shows a comparison of quench times in each power region. Lines present mean values. In Figs. 3.15(b) and (c), standard deviations σ_{n-1} are shown (with symbols) as well as mean values for Test C2-AA2 and the base case test, respectively. Figure 3.15 (a) indicates that the quenching occurs later in Test C2-AA2 than in the base case test above about 1 m elevation and the difference between them gets larger at higher elevations. This is attributed to the smaller core inlet subcooling in Test C2-AA2 shown in Fig. 3.12. Above about 3 m, however, the differences tend to become smaller gradually.

Rod surface temperatures are compared in Figs. 3.16(a), (b) and (c) for A, B and C regions, respectively. These figures indicate that the cooling is worse after the turnaround in the present test than in the base case test up to 1.83 m elevation and this tendency is more significant at higher elevations. However, above 2.44 m elevation, the cooling is better in the present test around the period when the temperatures turnaround, although quenching occurs later as observed at the lower elevations. Figure 3.17 shows comparisons of rod surface temperature at the top part of the core in A region. These data confirms the tendency observed in Figs. 3.16 (a) through (c).

Heat transfer coefficients calculated from the experimental data are shown in Fig. 3.18. This figure shows the heat transfer coefficients for the thermocouples in A region and their temperature histories are shown in Fig. 3.16(a). At 3.05 m elevation, the considerable decrease of the value for the base case test is observed from 100 s to 280 s, whereas such the decrease is not observed for Test C2-AA2. This difference corresponds to that in temperature as shown in Fig. 3.16(a).

As shown in Fig. 3.13, water accumulation behavior above the UCSP is different between the two tests. This difference may have a relation with the difference in cooling at the top of the core.

Sectional core differential pressures are compared in Figs. 3.19(a) through (f). Figure 3.19(a) indicates that the differential pressure at

the lowest section (0 - 0.61 m) for the present test is slightly smaller on the average than in the base case test until 200 s. This difference is attributed to the difference in fluid density in this section of the core due to difference in fluid temperature. Figure 3.20 shows core fluid temperatures at 0.38 m elevation and indicates that fluid temperature is higher in the present test at this elevation.

Figures 3.19(b) and (c) give the almost identical differential pressures for the two tests. Figures 3.19(d) through (f) indicate that the differential pressures for the present test is slightly higher on the average after about 100 s through about 250 s. In this time period, the differential pressure above the UCSP is significantly larger in the present test as shown in Fig. 3.13.

These slightly larger differential pressures seem to be the reason for the better cooling at the top part of the core during the time period from 100 s through 250 s, which is shown in Figs. 3.16(a) through (c) and 3.17. The reason for these slightly larger differential pressures is considered to be more water entrainment in the present test due to its smaller core inlet subcooling shown in Fig. 3.12.

From above discussion, it has been obtained that although thermo-hydrodynamic behavior through the system was oscillatory in the present test, average values of the oscillatory data were nearly identical to those of the base case test except for core inlet subcooling and a few related behavior to it. Therefore, this suggests, for analysis or prediction of core cooling for the downcomer injection case, it would be possible to use the same models, methods or computer codes as used for the cold leg injection case with adding a modification on predicting the fluid temperature at the core inlet.

3.3 Investigation of oscillation

In order to investigate the oscillation observed in the present test in detail, data except for temperature are plotted at the time interval of 0.2 s in this section instead of usual interval of 0.5 s. Figures 3.21 and 3.22 present downcomer and core differential pressures. From these figures it is recognized that the large oscillations appear with the time period of 5.7 s and a small oscillation appears between the two large oscillations. Figures 3.23 and 3.24 show the differential pressures through the intact

and broken loops. There also appear large and small oscillations one after the other at the same frequency as observed in Figs. 3.21 and 3.22.

Figure 3.25 shows the differential pressure defined as

$$\Delta P_D - \Delta P_C - \Delta P_I - \Delta P_U$$

where, symbols ΔP_D, ΔP_C, ΔP_I and ΔP_U are differential pressures in the downcomer, core, intact loop and upper plenum, respectively. This differential pressure means the driving force for core flooding and experiences the similar oscillations to the other differential pressure data. This oscillation of the differential pressure indicates that the core flooding experiences the U-tube type oscillation and its period is 2.9 s. The large and small oscillations also appear one after the other, and hence, the period of the large oscillation is 5.7 s.

Figure 3.26 shows differential pressure in the lower plenum, whose height is 2.1 m. Through the whole transient, the lower plenum is expected to be filled with solid water. Therefore, the oscillation of the differential pressure with the magnitude of 0.01 MPa around the value of 0.02 MPa is considered to be caused by accelerational and frictional pressure drops due to movement of water between the core and the downcomer. This confirms the U-tube type oscillatory core flooding shown in Fig. 3.25 takes place. The frictional pressure drop is not negligible in the lower plenum due to some flow restriction structures.

Pressure drop through the broken cold leg is presented in Fig. 3.27. This is differential pressure between the downcomer and the containment tank 2, *i.e.* the difference between the broken loop differential pressure (Fig. 3.24) and the intact loop differential pressure (Fig. 3.23). As shown in Fig. 3.27 the differential pressure decreases significantly in a periodic manner at the period of 5.7 s. When it decreases, the differential pressure through the intact loop increases significantly as shown in Fig. 3.23. It has been known[8] that the pressure drop in the broken cold leg is mainly determined by steam quality of the two-phase flow there and smaller steam quality tends to give smaller pressure drop. Therefore, Fig. 3.27 suggests that steam quality becomes significantly small periodically in the broken cold leg.

Figure 3.28 shows differential pressure in the top section of the downcomer, *i.e.* between 6.383 m and 8.183 m elevations. Since the bottom of primary loop pipings locates at 6.949 m elevation, the overflow level

corresponds to 5.2 kPa in the figure at the saturation condition. As shown in Figs. 3.2(d) and (e), the downcomer water is subcooled. Therefore, when the differential pressure in the top section of the downcomer increases, the condensation of steam in the downcomer is expected to increase resulting in decrease of pressure drop through the broken cold leg as shown in Fig. 3.27.

Figure 3.29 shows the downcomer fluid temperature at 6.743 m elevation, *i.e.* 0.206 m below the overflow level. There appear periodical decreases in the temperature and their magnitude are 50 K at maximum. Timings of the temperature decreases correspond to those of increases in the downcomer differential pressure shown in Fig. 3.28. This confirms that the downcomer fluid temperature at 6.743 m indicates subcooling due to arrival of downcomer water level at that elevation.

Total water injection rate into the downcomer is shown in Fig. 3.30. The injection rate varies around the preset value of 0.0088 m^3/s due to the pressure change at the injection locations. The downcomer injection was driven by the pressure difference between the injection tank and the downcomer. The deviations are within -10 percent to +30 percent of the preset value. Timings of appearance of the peaks in this figure tend to coincide with those of the increases in the downcomer differential pressure shown in Fig. 3.28. The increase in the injection rate of the water is also expected to result in the increase in the steam condensation. However, although the increases in the differential pressure in the top section of the downcomer (Fig. 3.28) coincide with the increases in the downcomer water injection rate (Fig. 3.30), the increase in the downcomer differential pressure is judged not to be caused by the increase in the downcomer injection rate but by the U-tube type oscillation. This is because the deviation of the downcomer injection rate is evaluated to be too small to cause the observed increase in the downcomer differential pressure shown in Fig. 3.28.

From the above discussion for Figs. 3.27 through 3.30, the increase in the subcooled downcomer water level reduces the steam flow rate in the broken cold leg, and hence, the pressure drop through the broken cold leg. Figure 3.31 shows differential pressure between the two containment tanks and indicates the magnitude of the steam flow rate coming from the broken cold leg. The large decreases in this differential pressure coincide with the decreases in the pressure drops through the broken cold leg, indicating

the decreases of the steam flow at those timings. This support the discussion above.

Figures 3.32(a) and (b) show relation among downcomer fluid temperature at 6.743 m, broken cold leg differential pressure and intact loop differential pressure. From these figures it is confirmed that timings of oscillations in these data are the same.

Summarizing the discussion in this section, the mechanism of the oscillation in the present test can be explained as follows; During the U-tube oscillation between the core and the downcomer, the downcomer water level oscillates. When the water level comes near the overflow level, steam condensation around the top of the downcomer increases. This increase causes decrease in the pressure drop through the broken cold leg, and hence, increases the intact loop differential pressure as shown in Figs. 3.32. The increase in the intact loop differential pressure results in decrease in the driving force for core flooding as shown in Fig. 3.25, and hence, pushes up the downcomer water level further. This is considered to cause more steam condensation at the top of the downcomer due to the supply of subcooled water. However, in a short time, the steam condensation becomes little due to saturation of the subcooled water, and subsequently water in the downcomer starts to go to the core. In this manner, the magnitude of the U-tube oscillation is increased significantly. After this large oscillation, a small oscillation appears. This is because, after the large oscillation, subcooled water at the top section of the downcomer is a little due to the significant steam condensation occurred just before, and hence, another large steam condensation cannot occur. After the small oscillation, however, there appears a large oscillation again because subcooled water gradually accumulates at the top section of the downcomer by this time and can cause significant steam condensation again.

In the case of the cold leg injection, however, temperature of water coming from the cold leg is almost the saturation temperature as shown Fig. 3.2. This is because complete mixing between the ECC water and steam flowing in the intact loops takes place at downstream side from the ECC ports in the cold leg pipings. The length of this section is about 4 m. Therefore, large oscillation was not observed in the base case test.

Incidentally, large oscillation observed in the present test is expected to occur in a PWR with the downcomer injection type ECCS under the

"single-failure" assumption, which is a typical assumption in the safety analysis and is applied in both tests concerned here. This is because the cause of the large oscillation is considered to be the incomplete mixing between the ECC water and steam flowing in the intact loops and this incomplete mixing is also expected to occur in the PWR. However, under the case of no failure of the LPCI pumps, injection rate of the ECC water is twice of the single-failure assumption case, and hence, all the steam flowing in the intact cold legs is evaluated to be condensed with the ECC water. In such situation, reflooding behavior is no longer expected to be oscillatory.

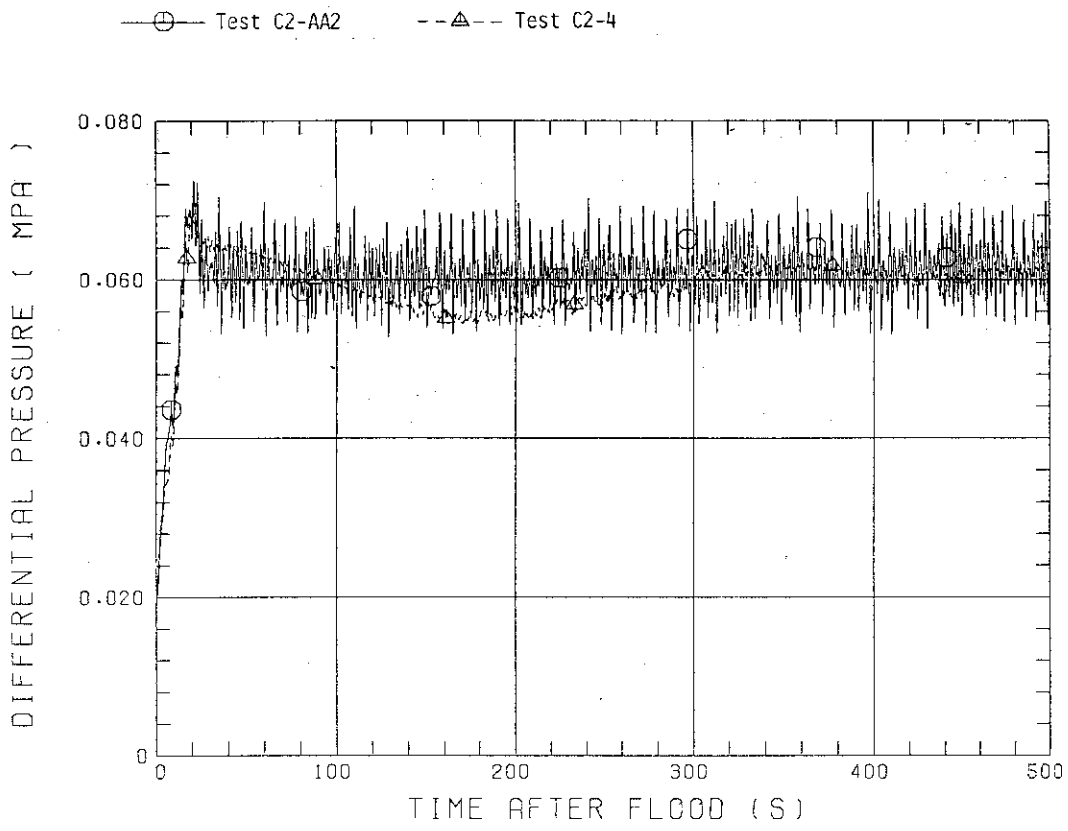

Fig. 3.1 Downcomer differential pressure

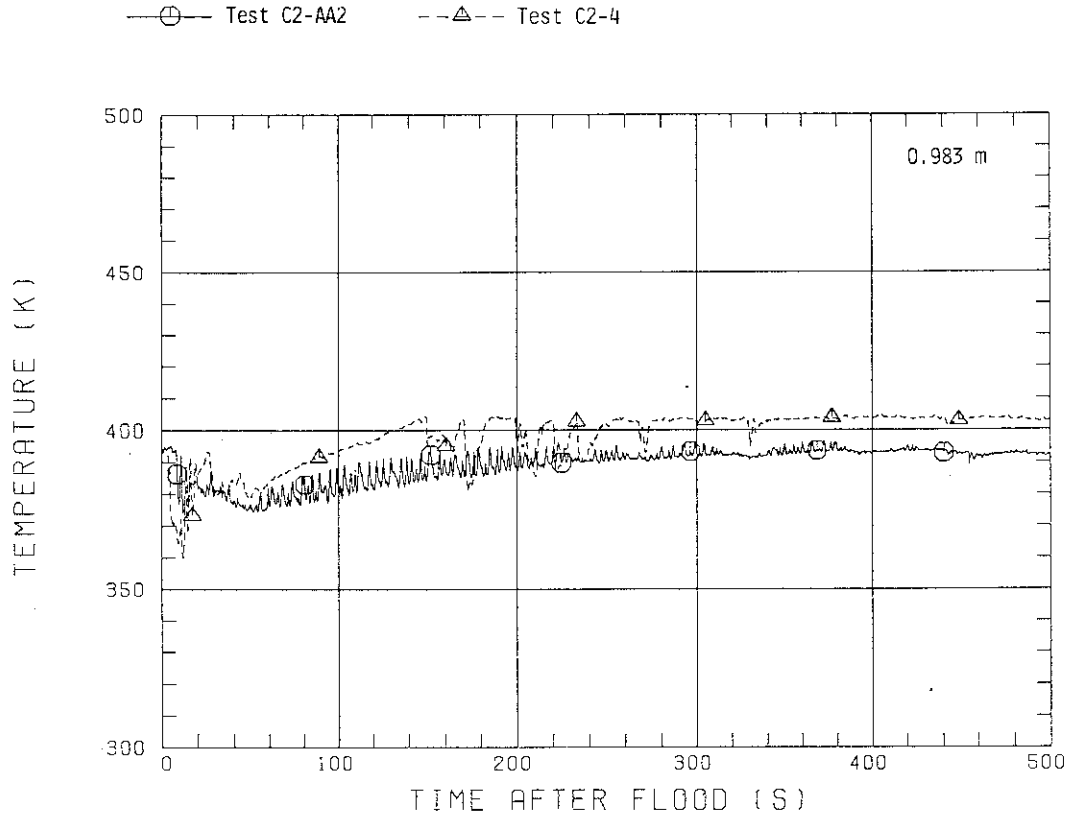

Fig. 3.2(a) Downcomer fluid temperatures at 0.983 m

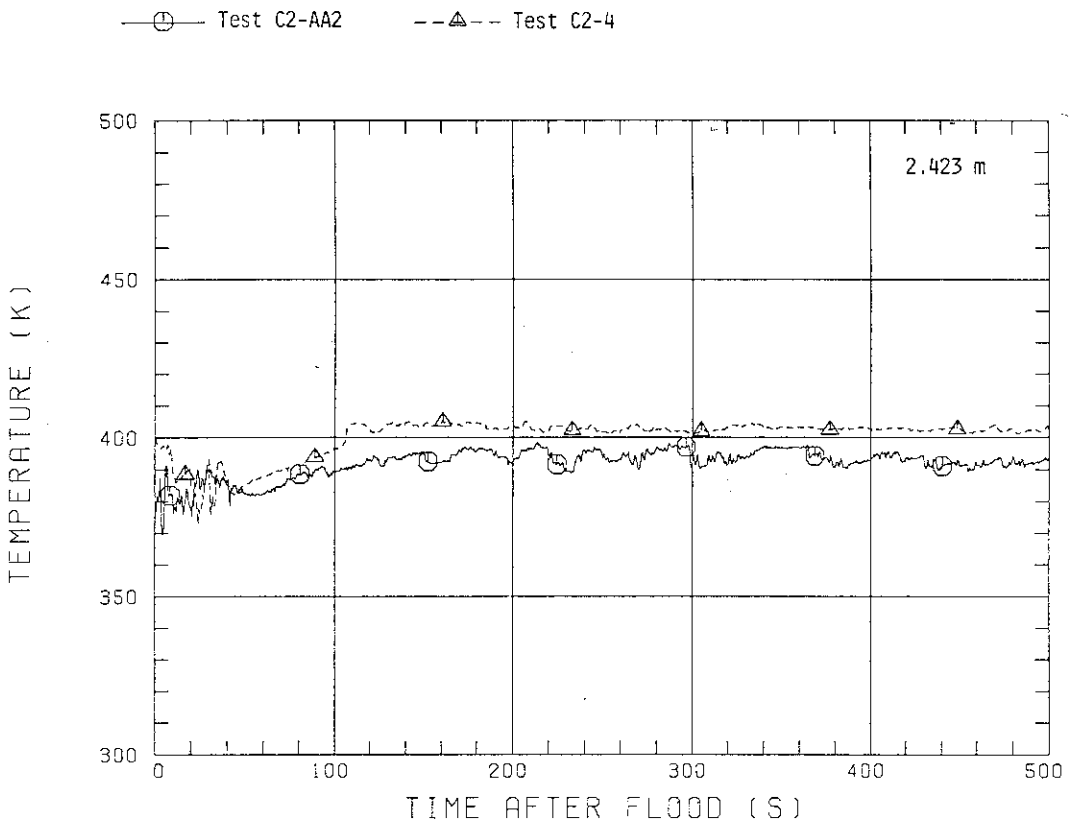

Fig. 3.2(b) Downcomer fluid temperatures at 2.423 m

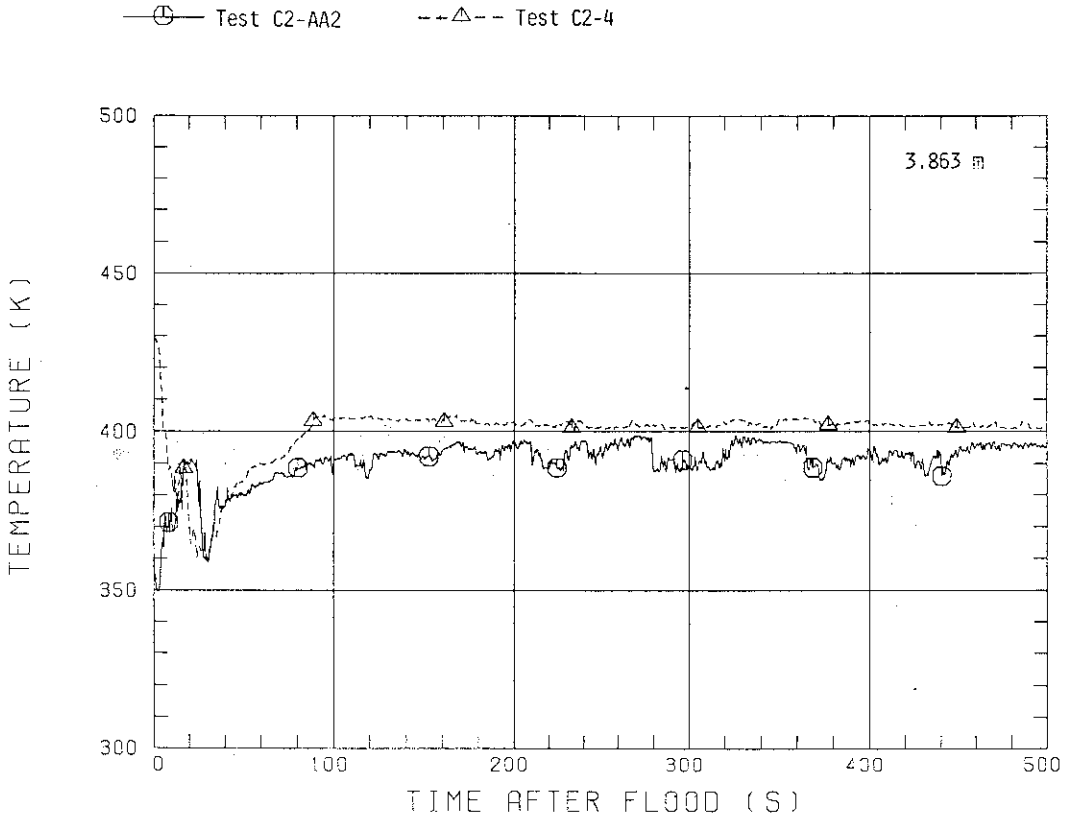

Fig. 3.2(c) Downcomer fluid temperatures at 3.863 m

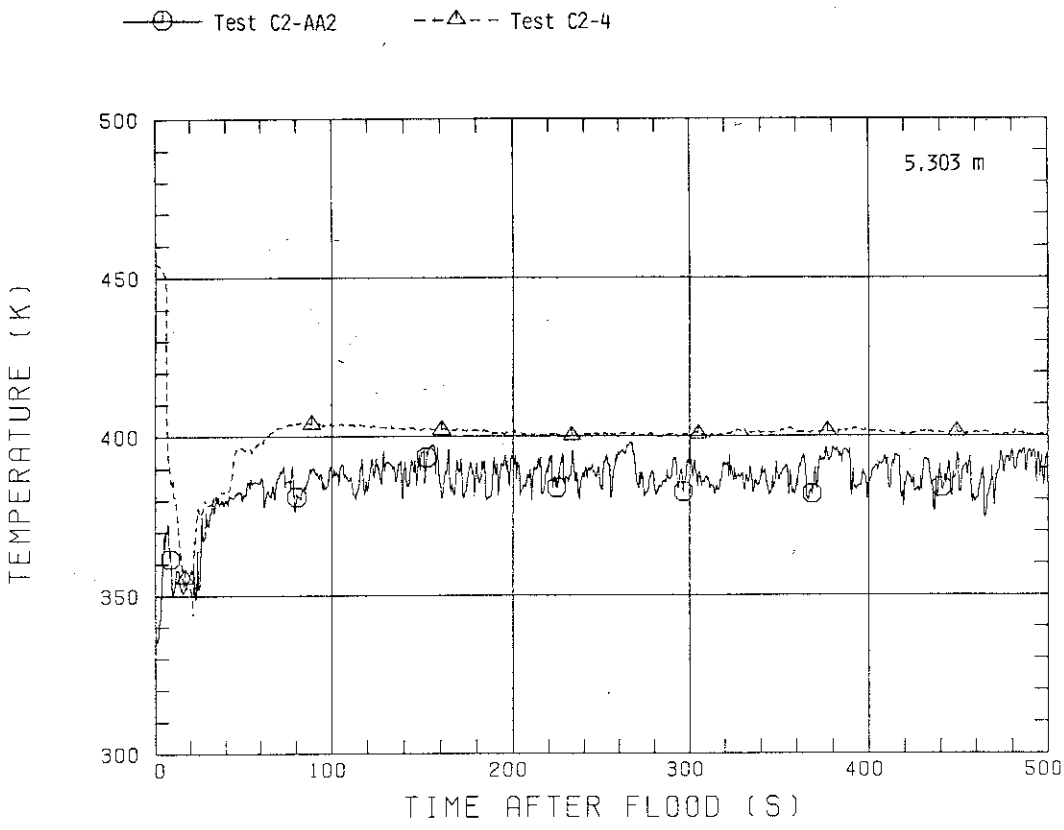

Fig. 3.2(d) Downcomer fluid temperatures at 5.303 m

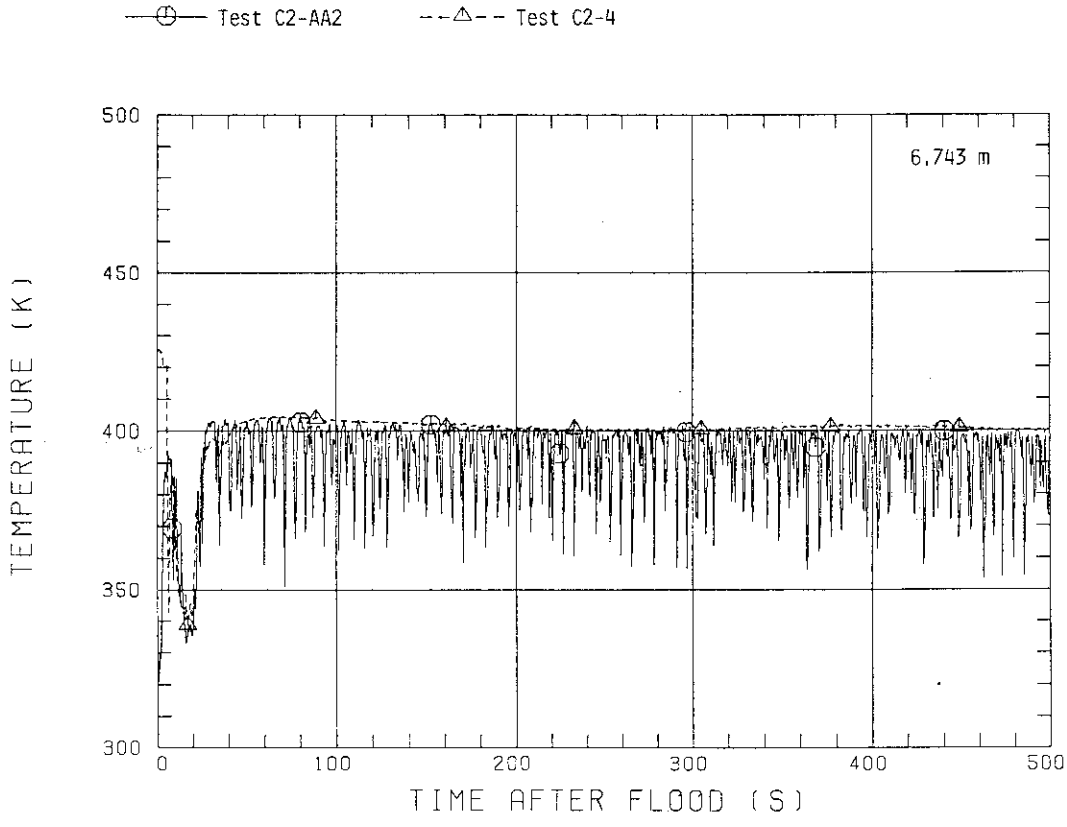

Fig. 3.2(e) Downcomer fluid temperatures at 6.743 m

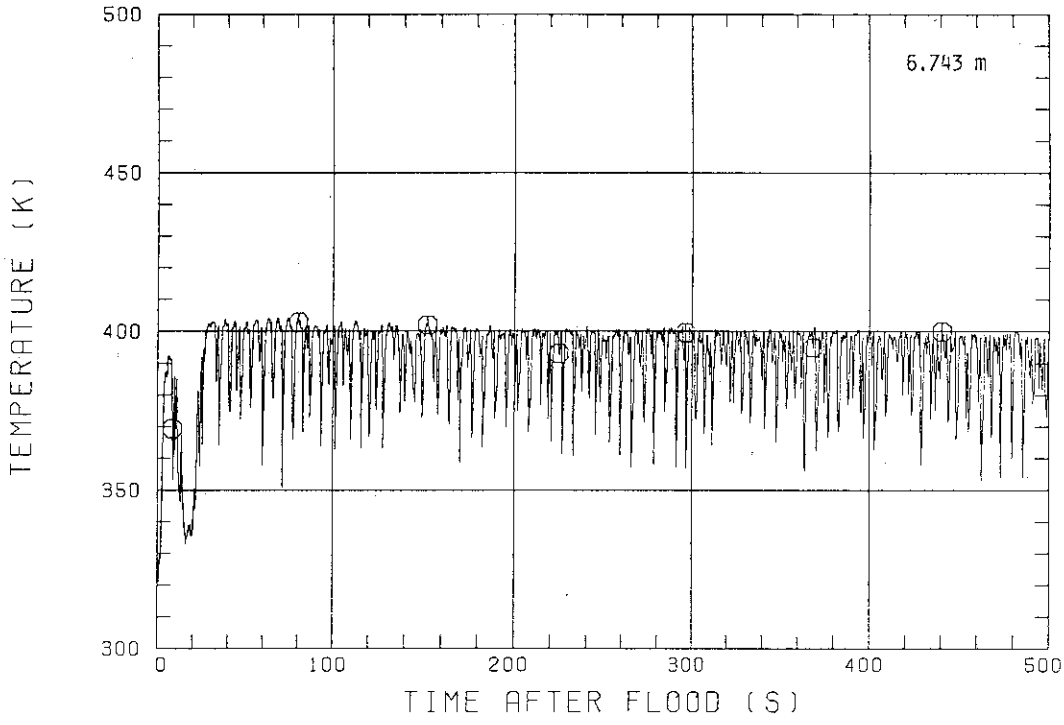

Fig. 3.3(a) Downcomer fluid temperatures at 6.743 m just below injection nozzle

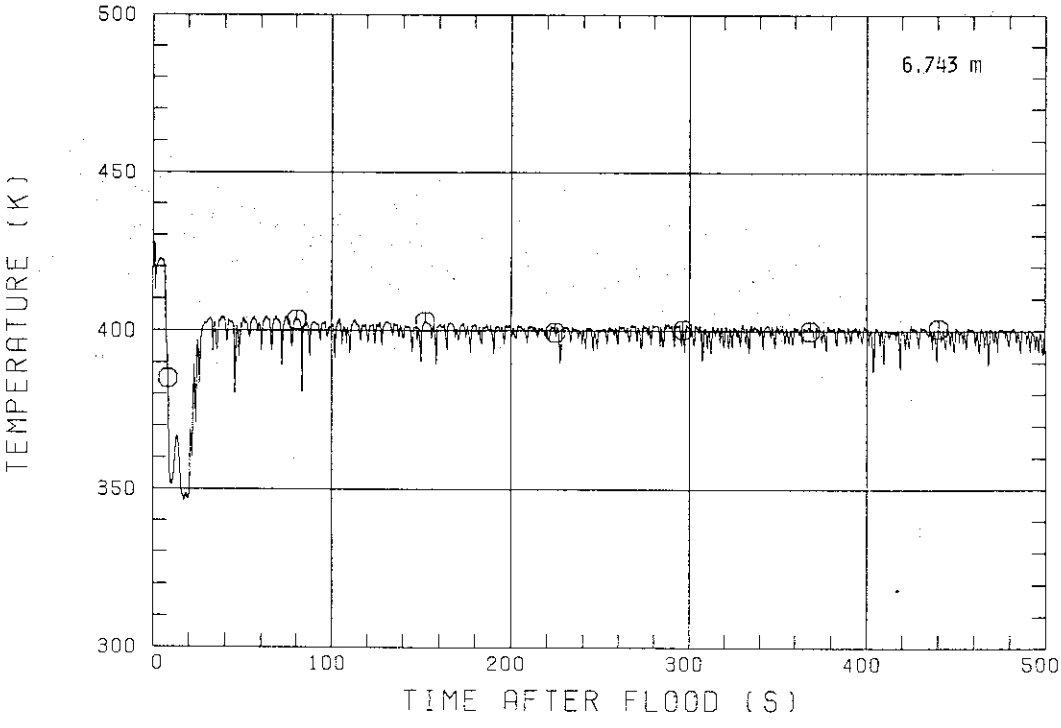

Fig. 3.3(b) Downcomer fluid temperatures at 6.743 m below between injection nozzles

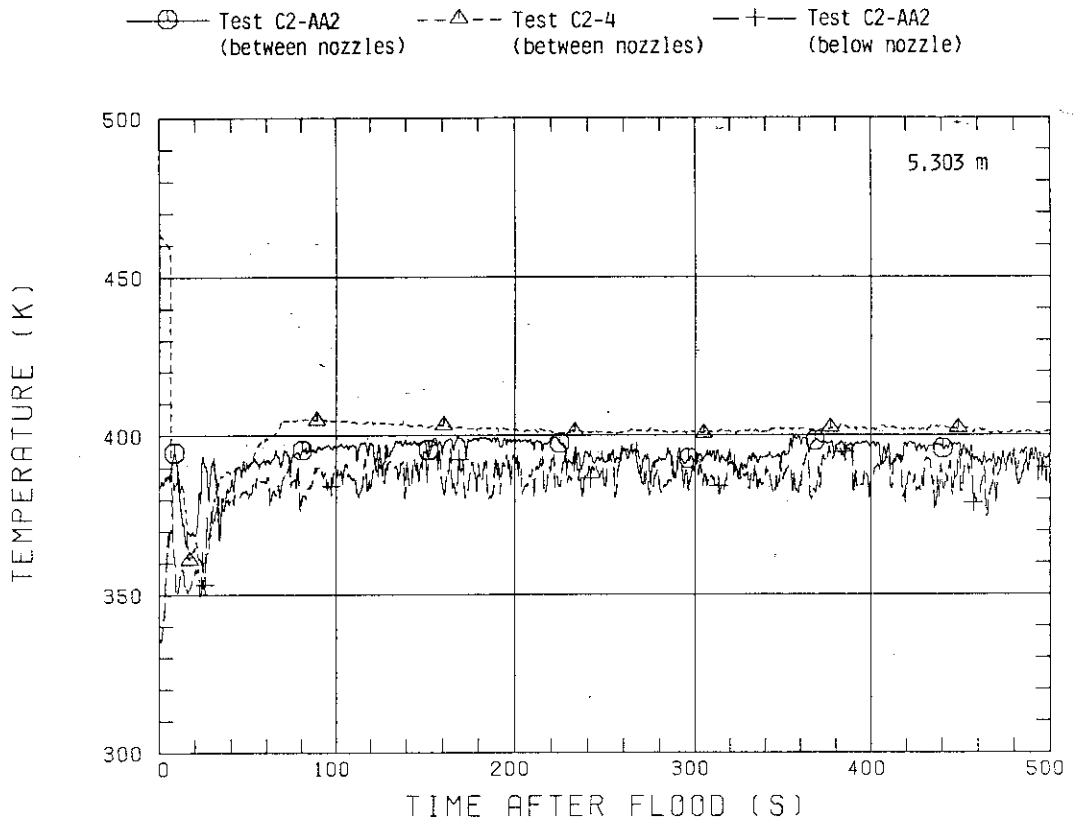

Fig. 3.3(c) Downcomer fluid temperatures at 5.303 m

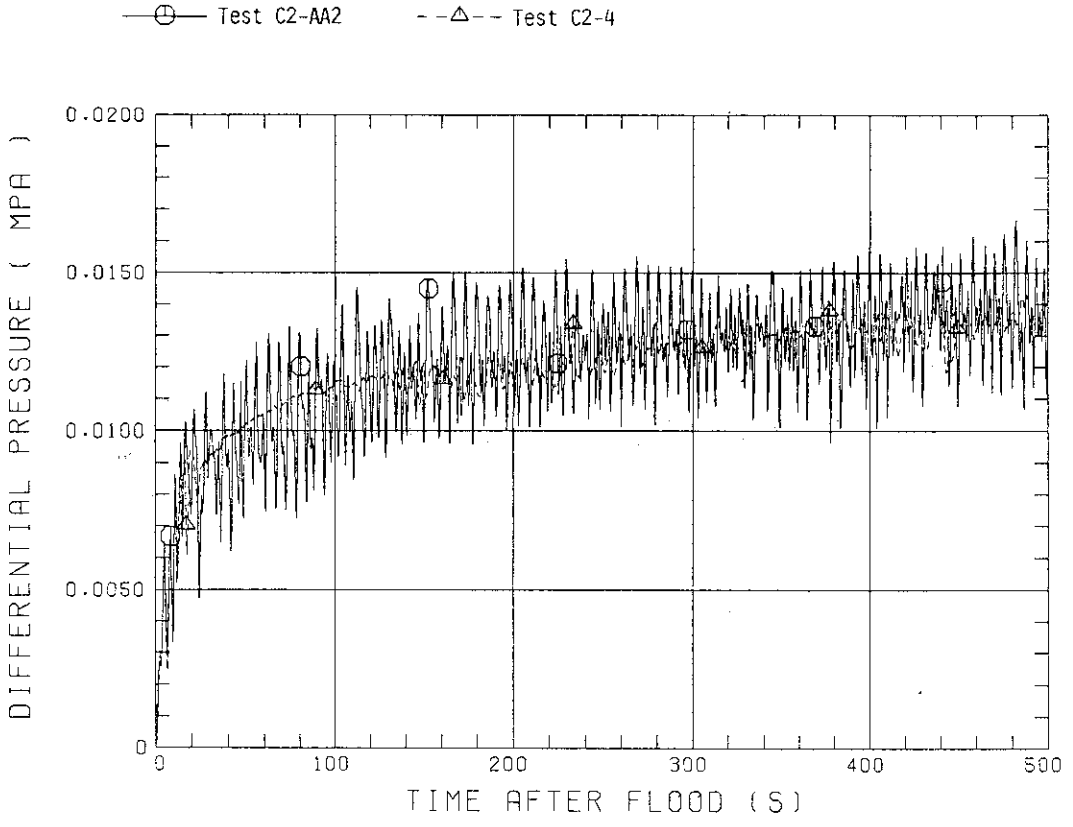

Fig. 3.4 Core differential pressures

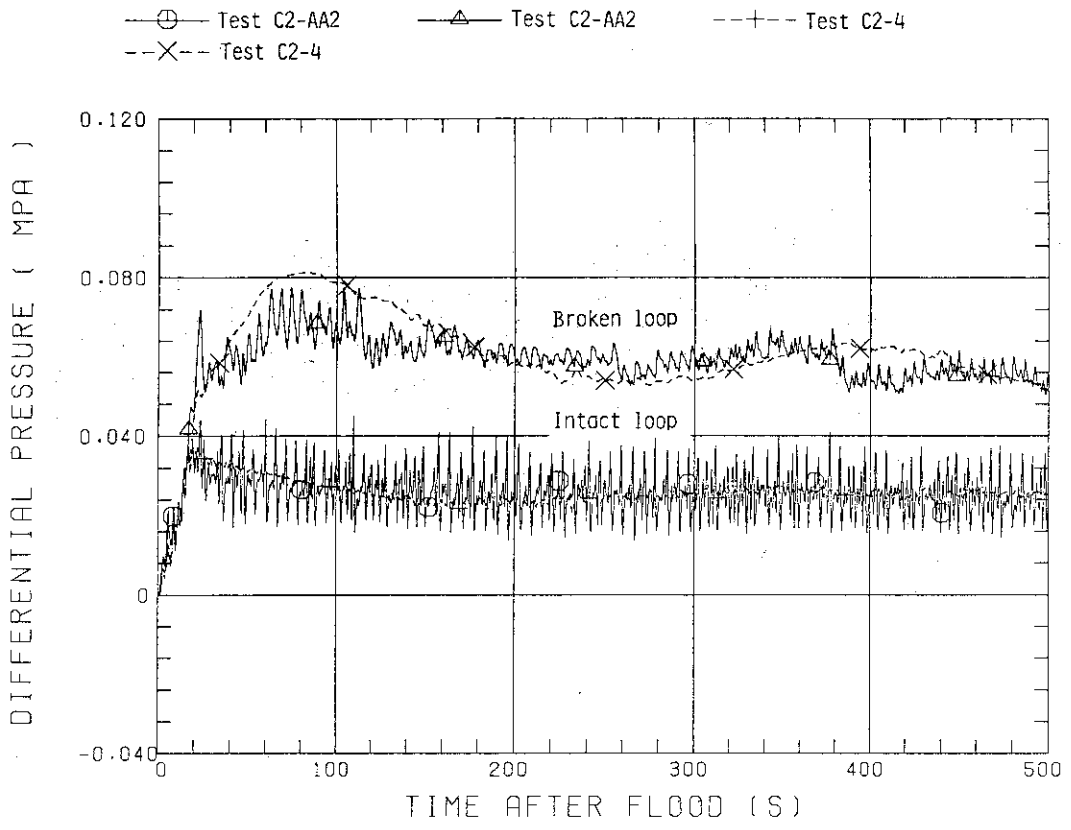

Fig. 3.5 Intact and broken loop differential pressures

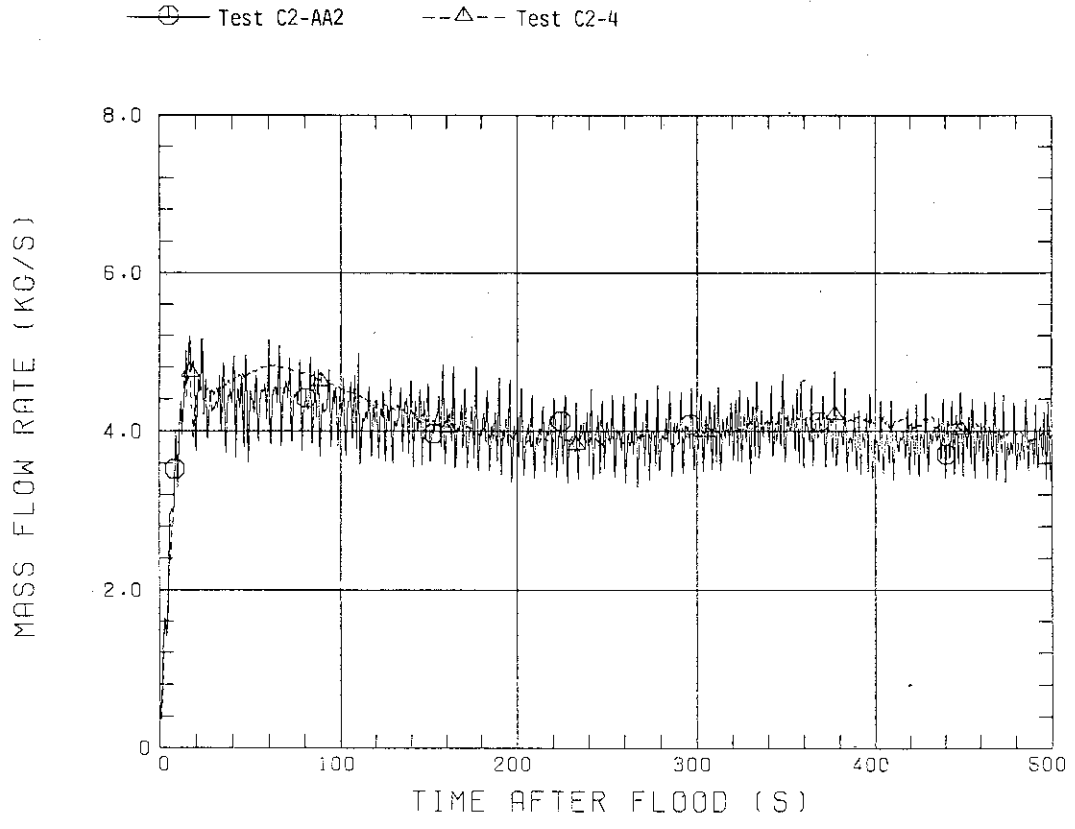

Fig. 3.6 Total steam mass flow rates

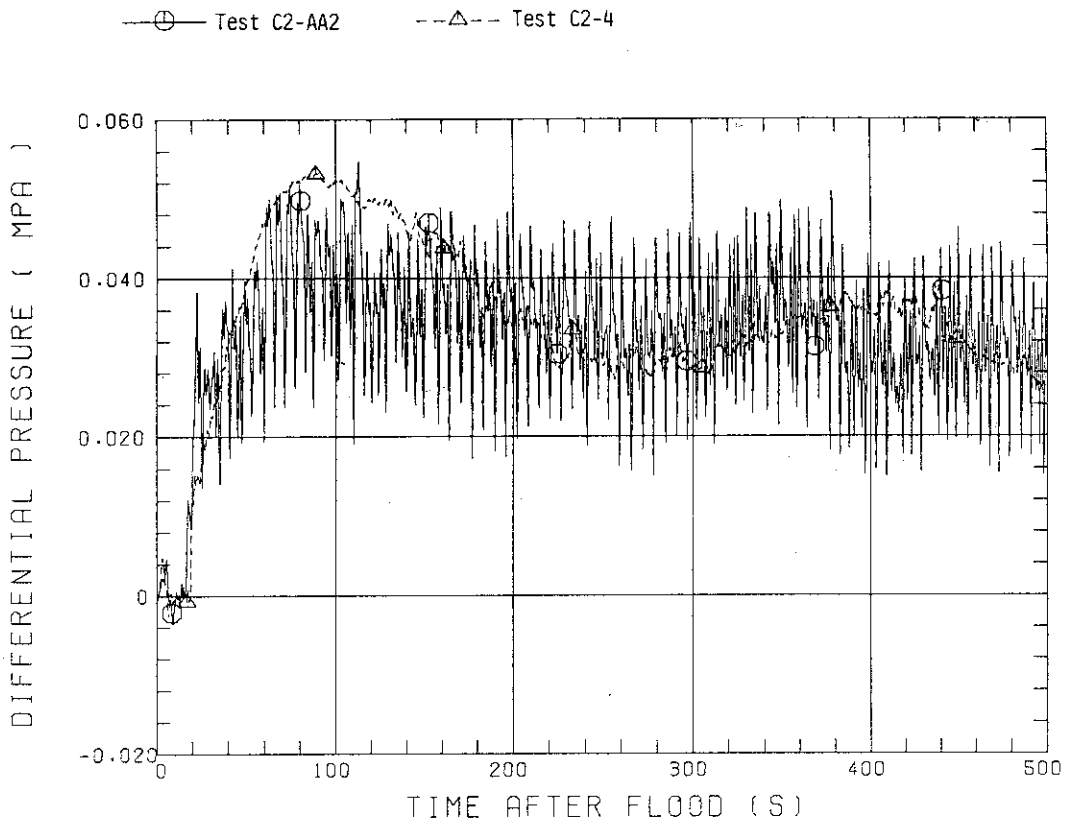

Fig. 3.7 Differential pressures through broken cold leg

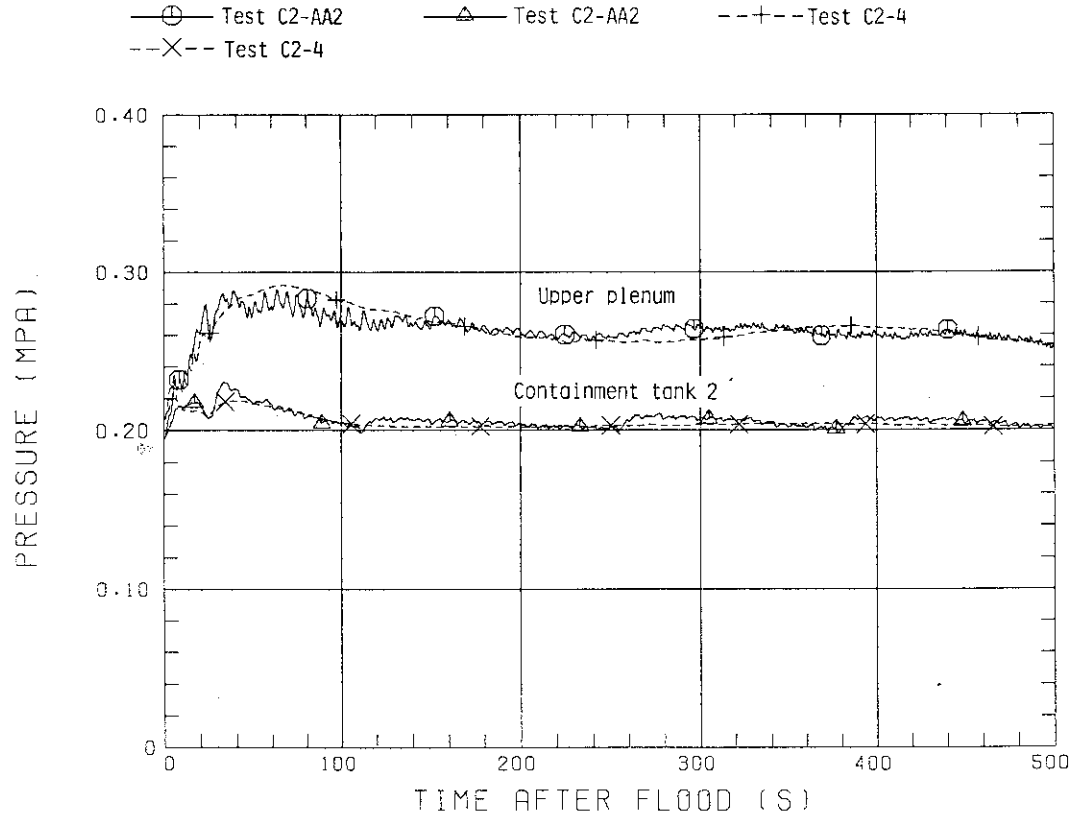

Fig. 3.8 Upper plenum and containment tank 2 pressures

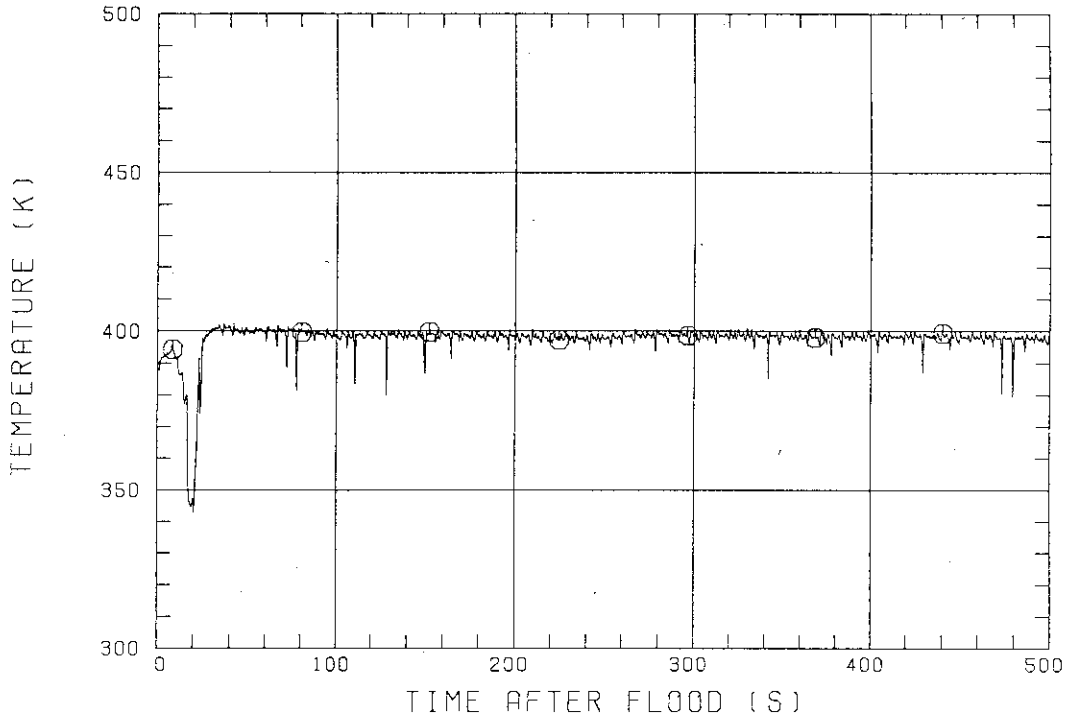

Fig. 3.9(a) Fluid temperature in broken cold leg near downcomer for Test C2-AA2

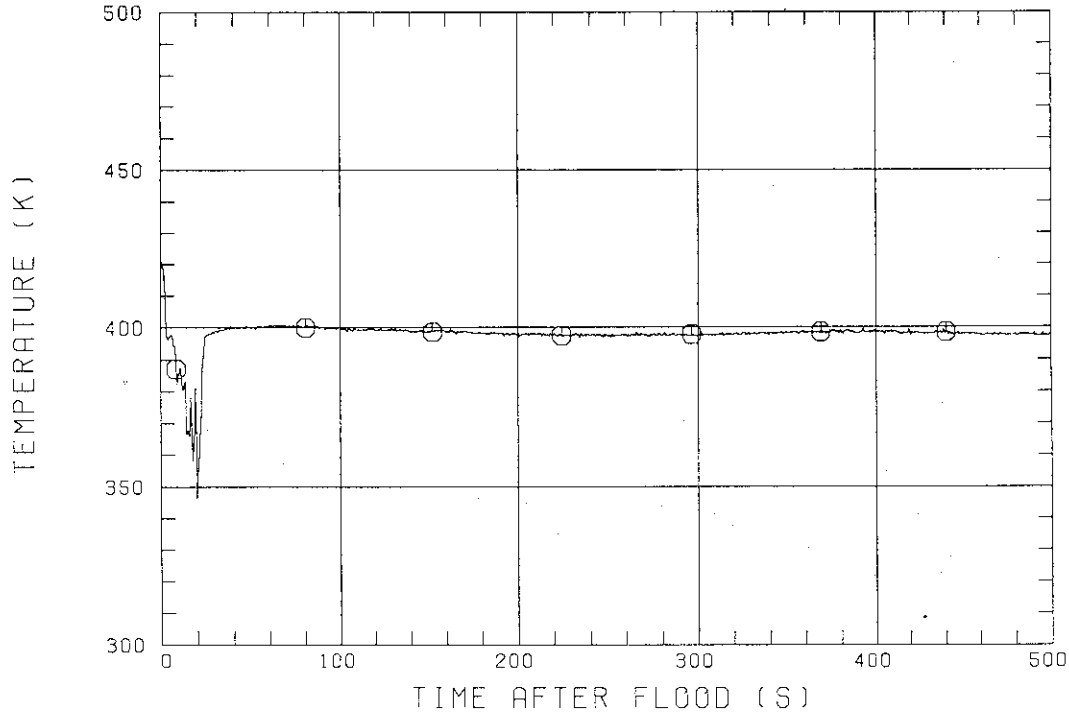

Fig. 3.9(b) Fluid temperature in broken cold leg near downcomer for base case test

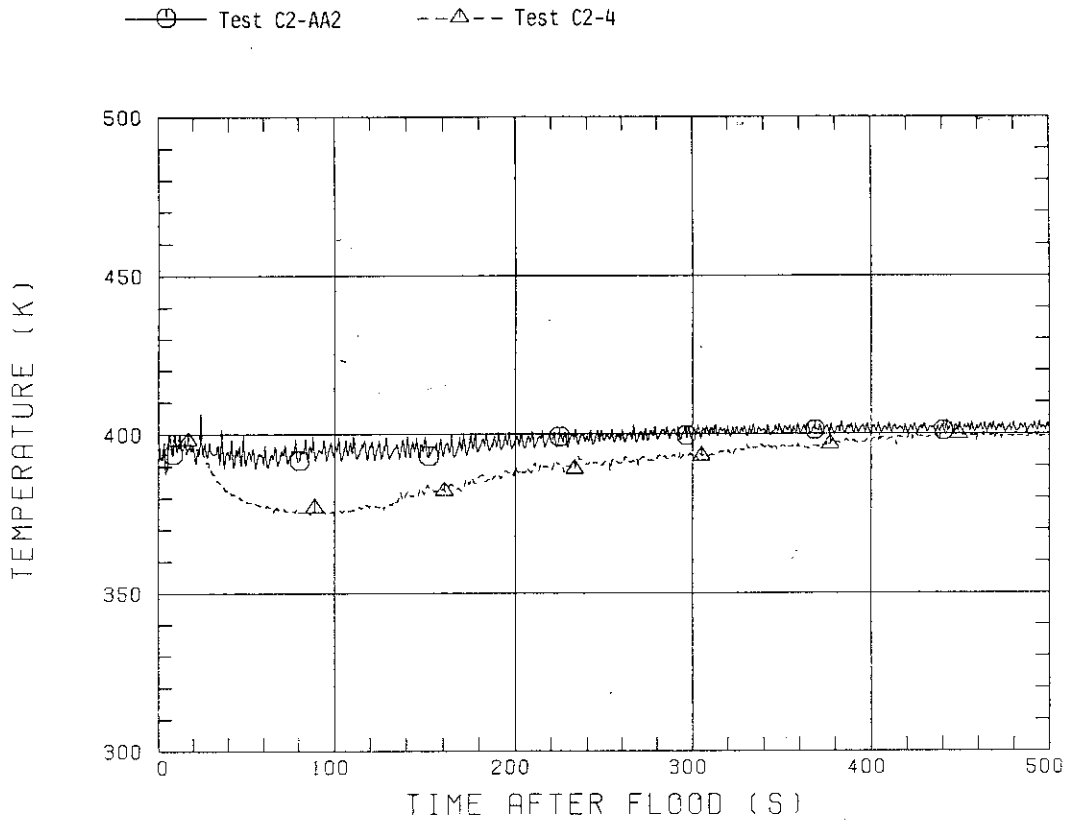

Fig. 3.10 Fluid temperatures at core inlet

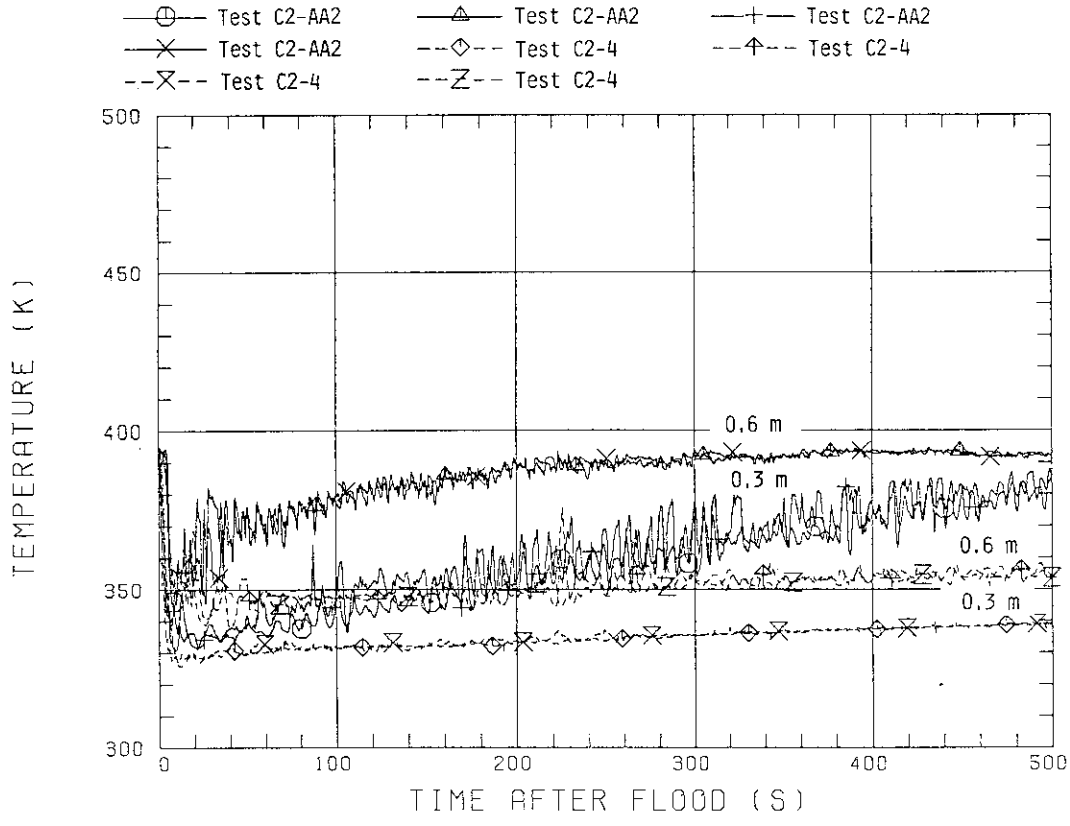

Fig. 3.11 Fluid temperatures in lower plenum at 0.3 and 0.6 m

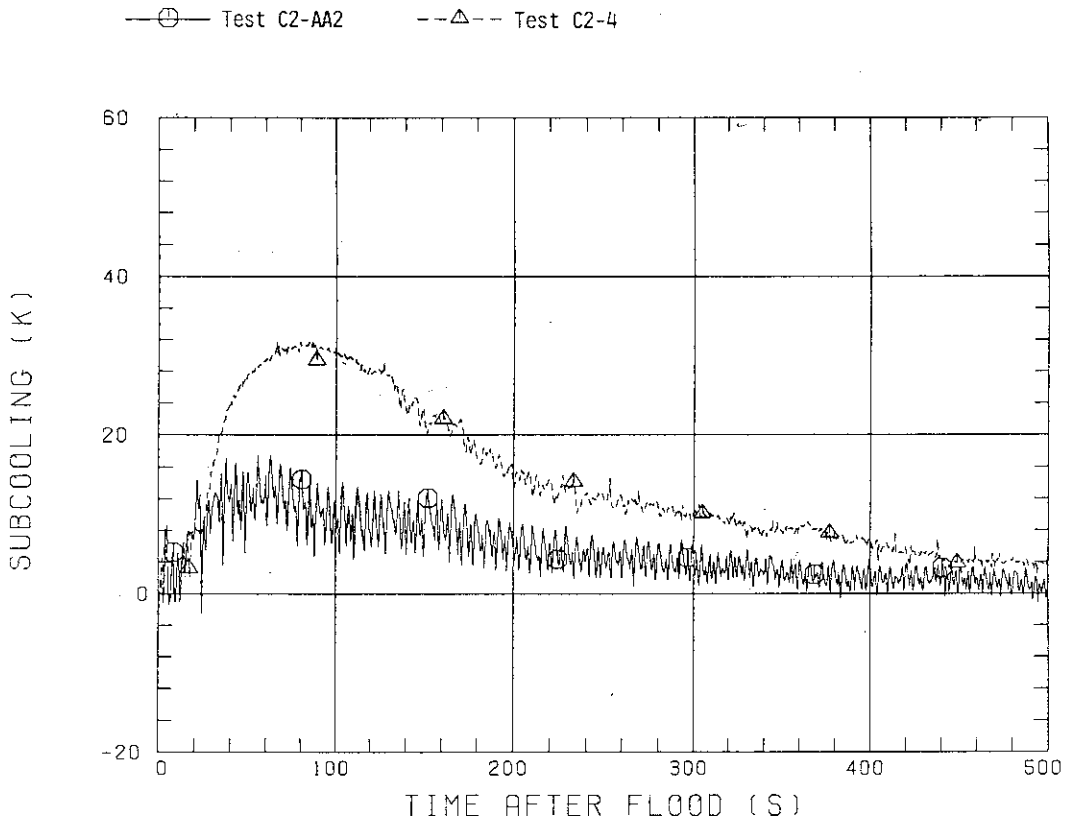

Fig. 3.12 Core inlet subcoolings

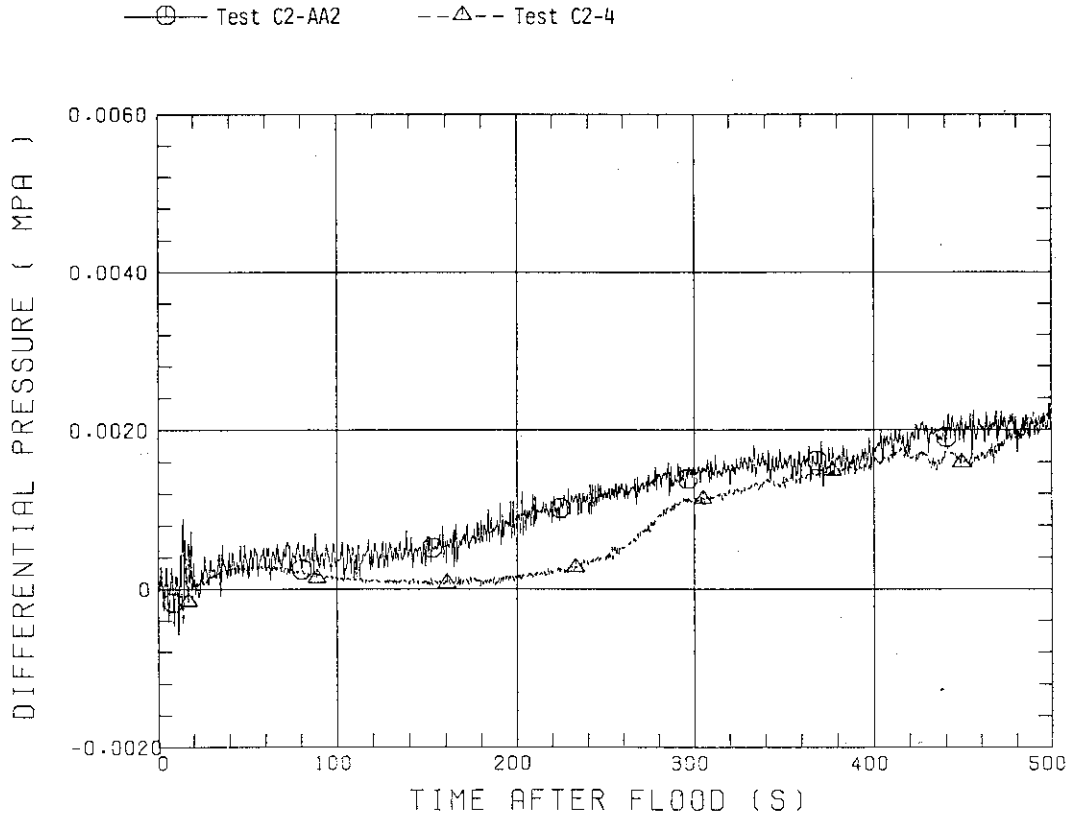

Fig. 3.13 Differential pressures above UCSP

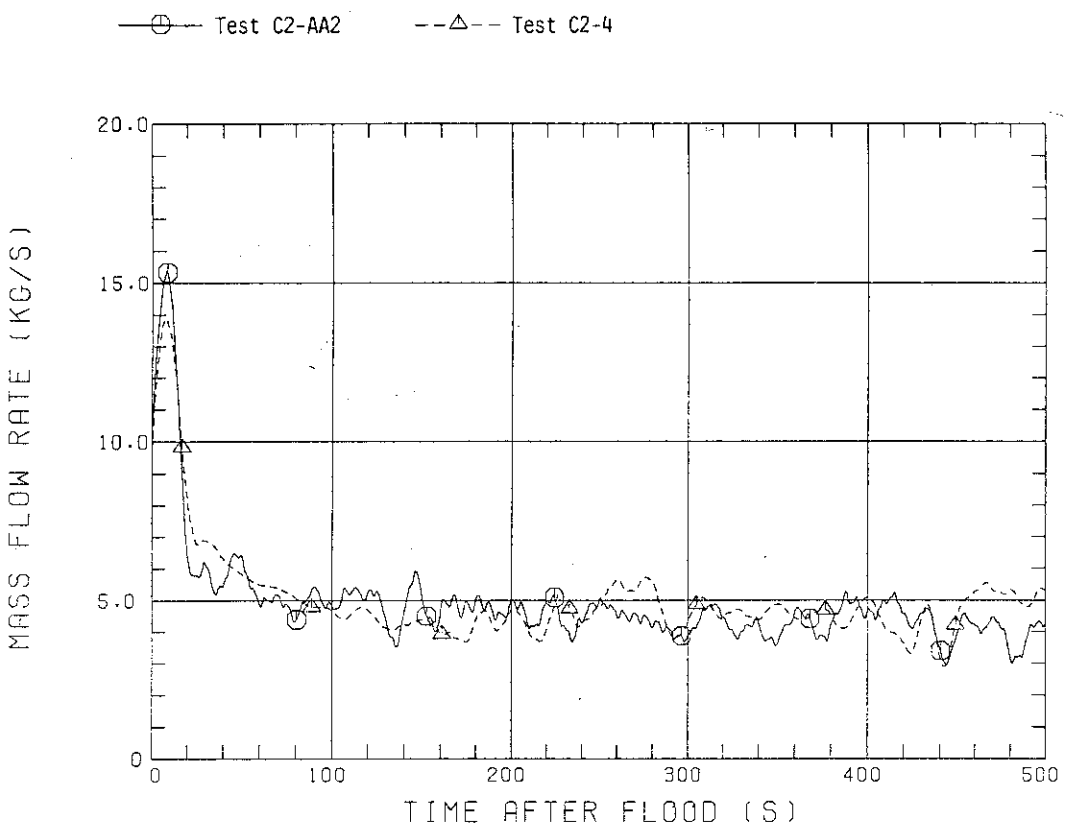

Fig. 3.14 Core flooding rates

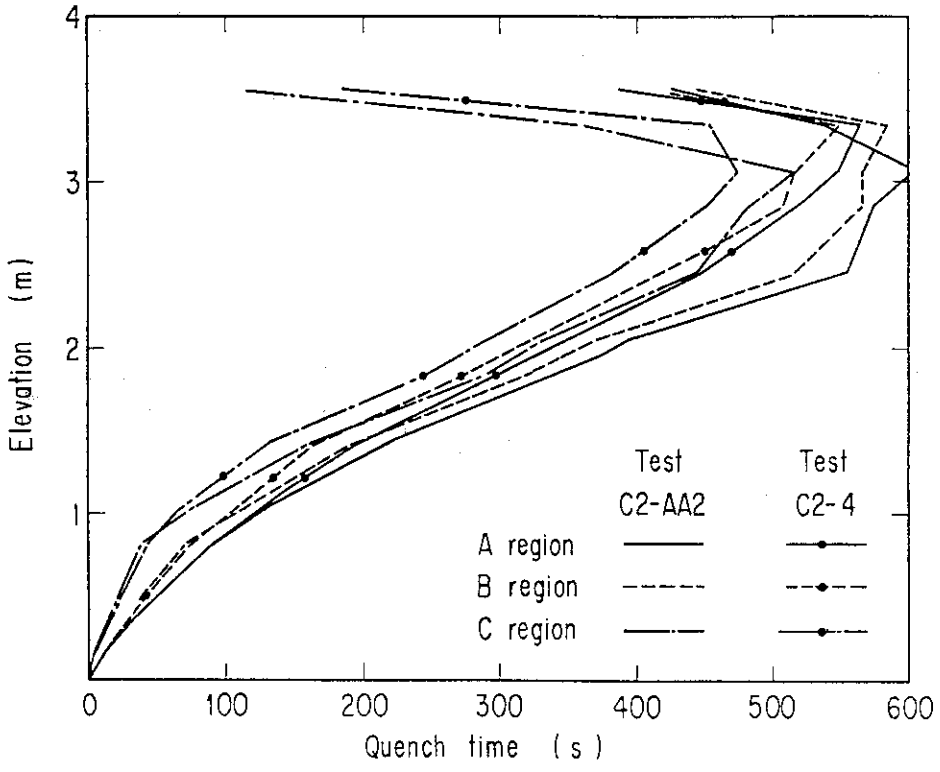

Fig. 3.15(a) Quench envelopes (mean values)

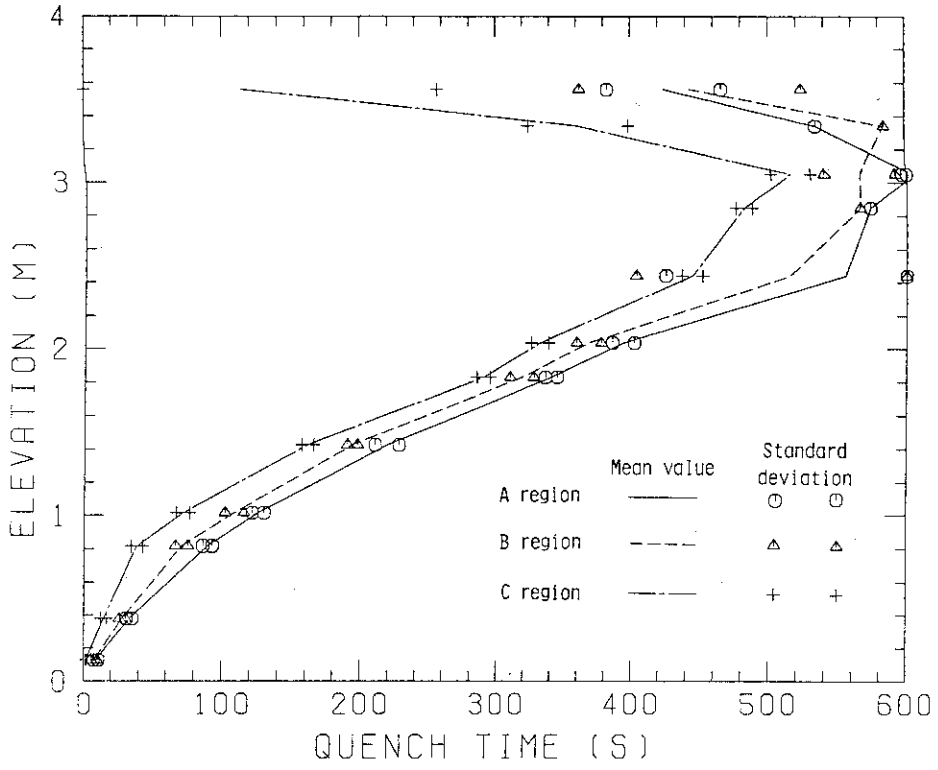

Fig. 3.15(b) Quench envelope for Test C2-AA2

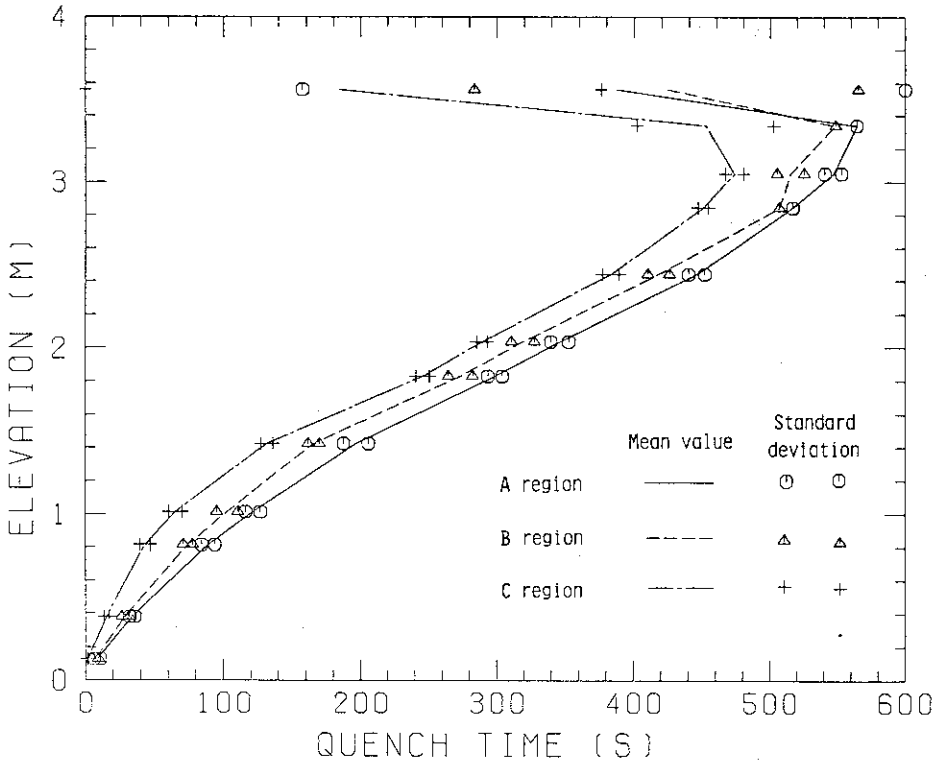

Fig. 3.15(c) Quench envelope for base case test

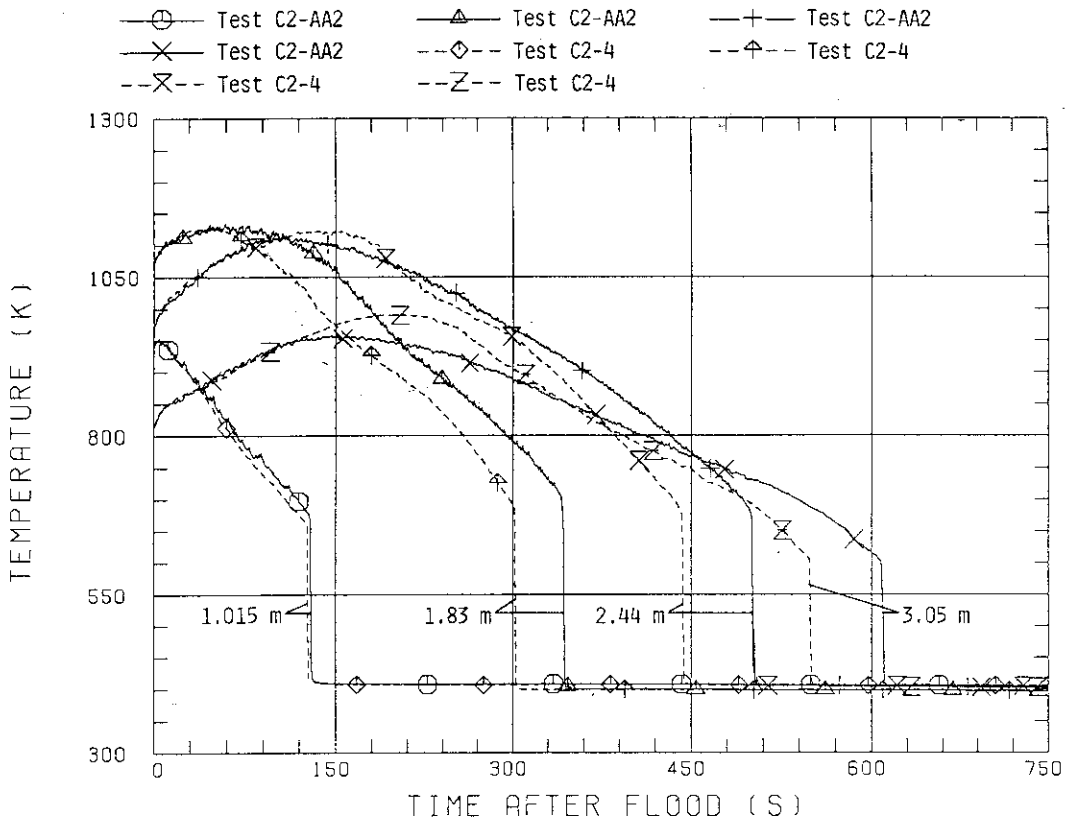

Fig. 3.16(a) Rod surface temperatures in A region

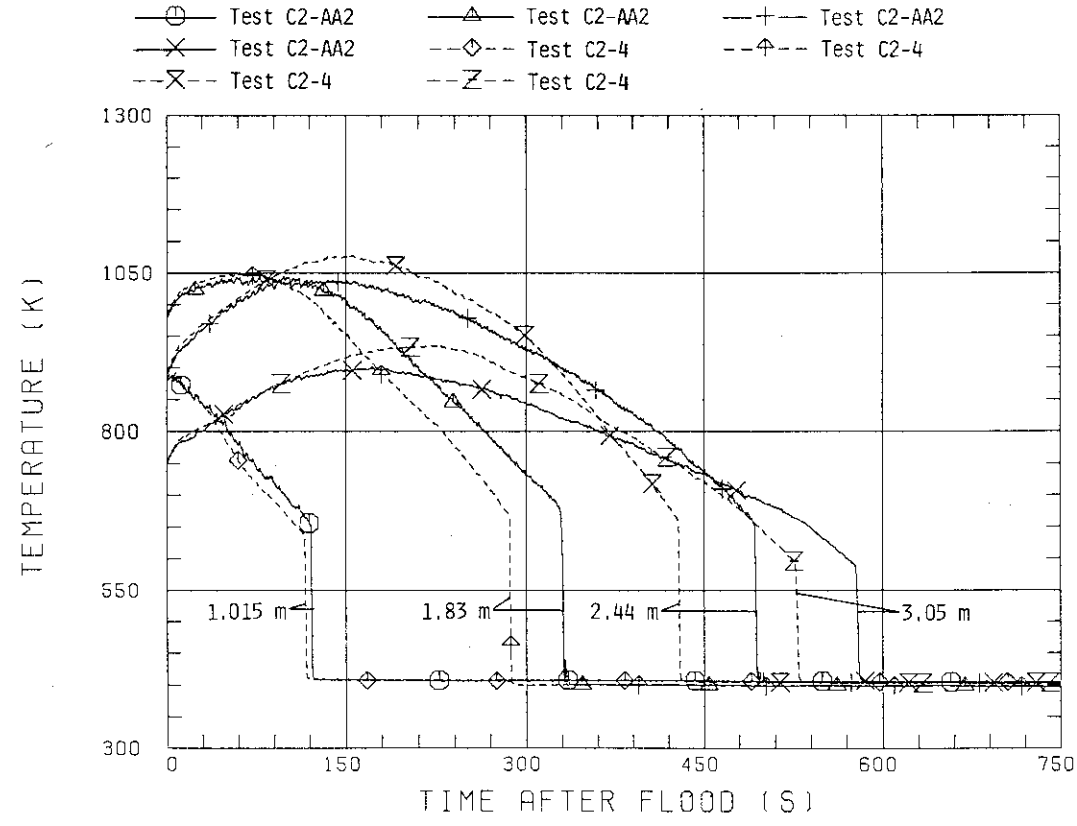

Fig. 3.16(b) Rod surface temperatures in B region

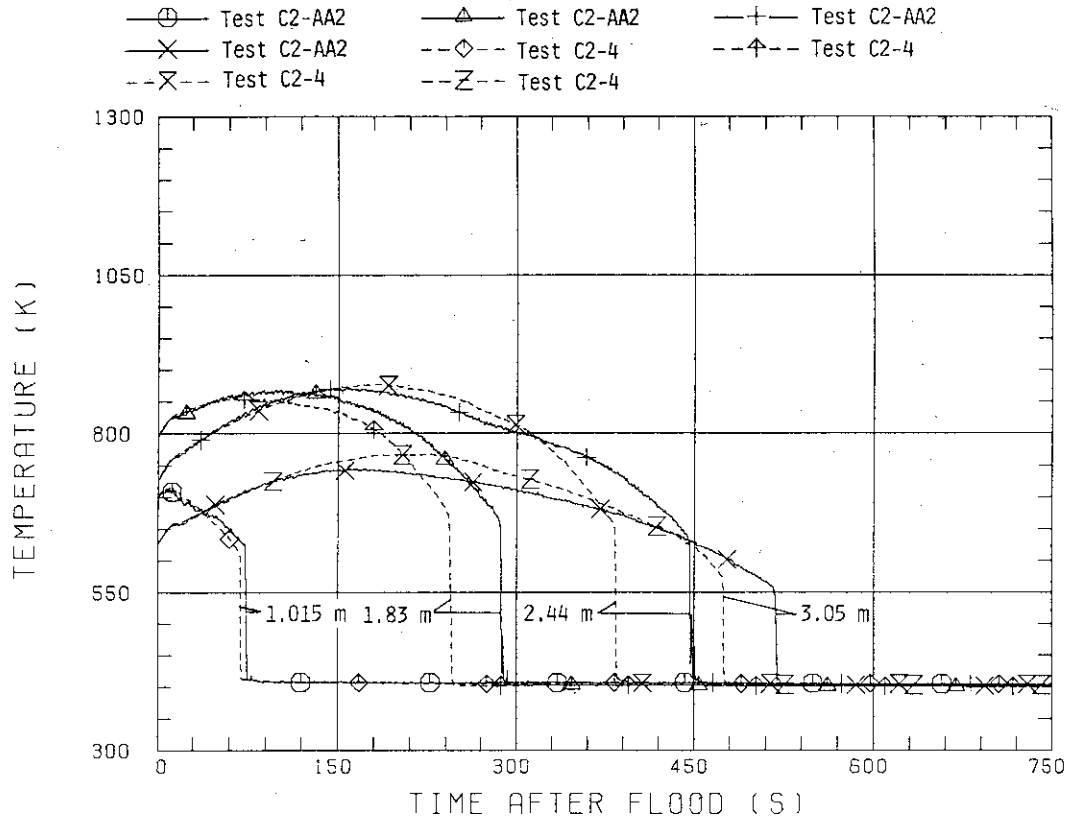

Fig. 3.16(c) Rod surface temperatures in C region

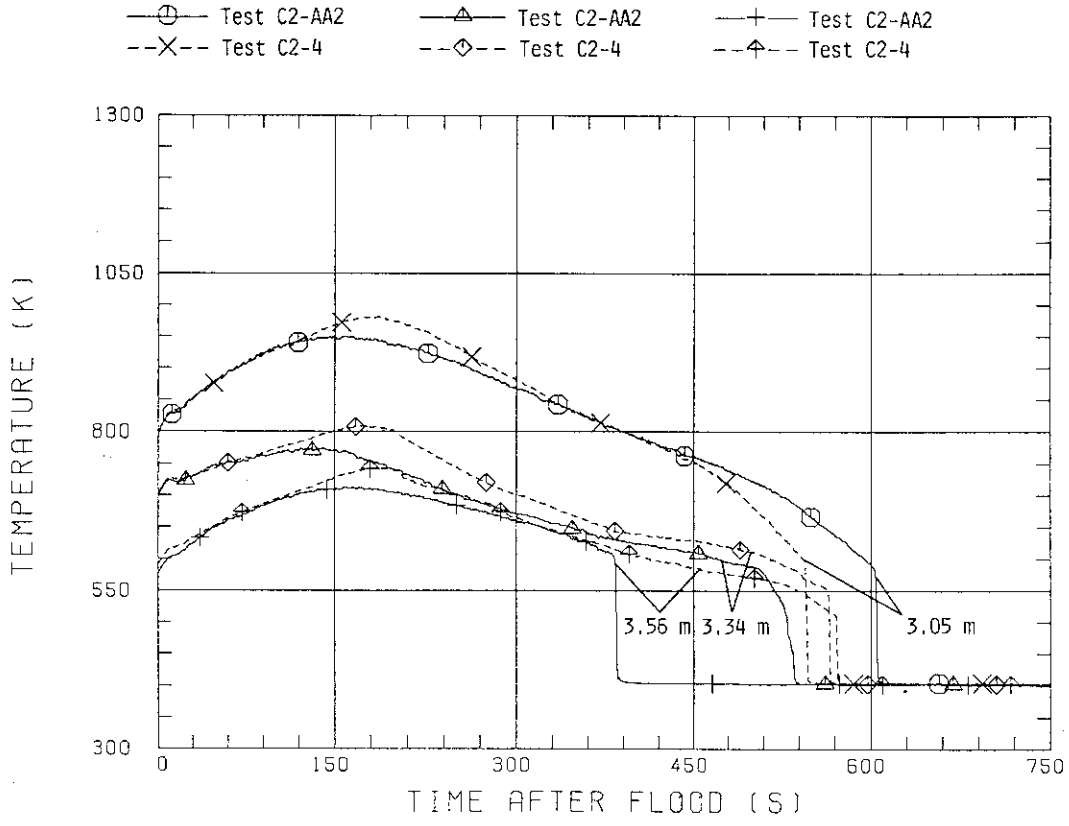

Fig. 3.17 Rod surface temperatures at top part in A region

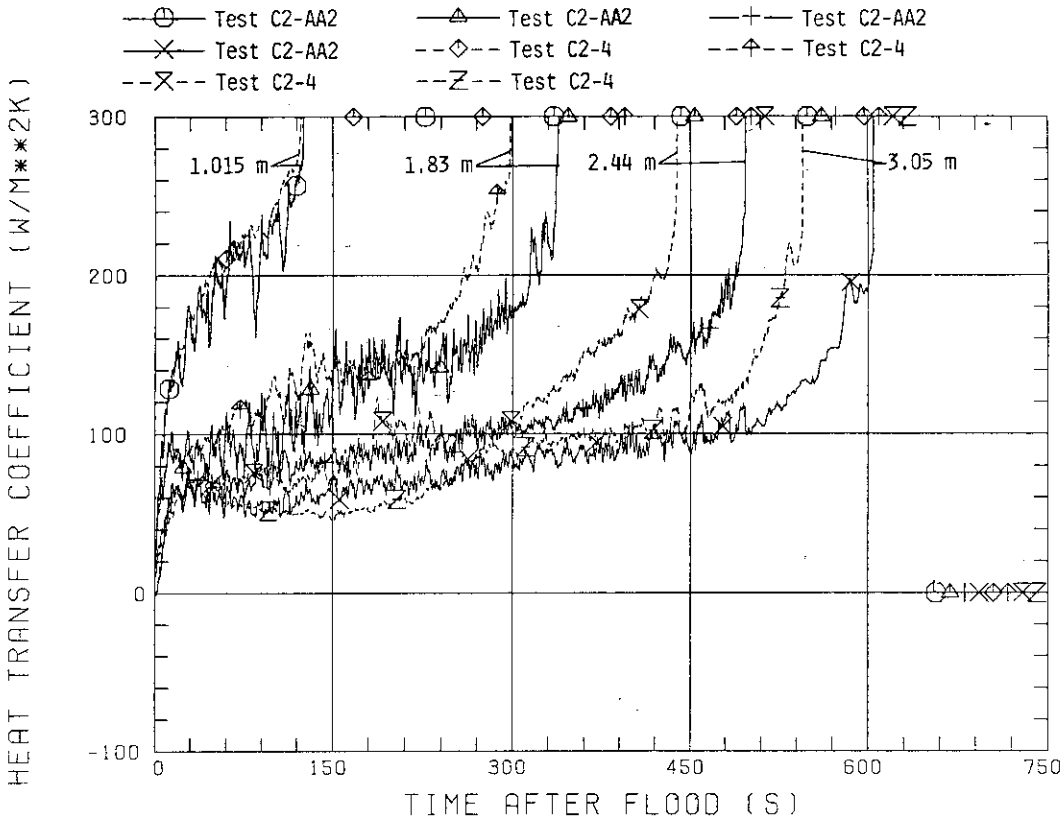

Fig. 3.18 Heat transfer coefficients in A region

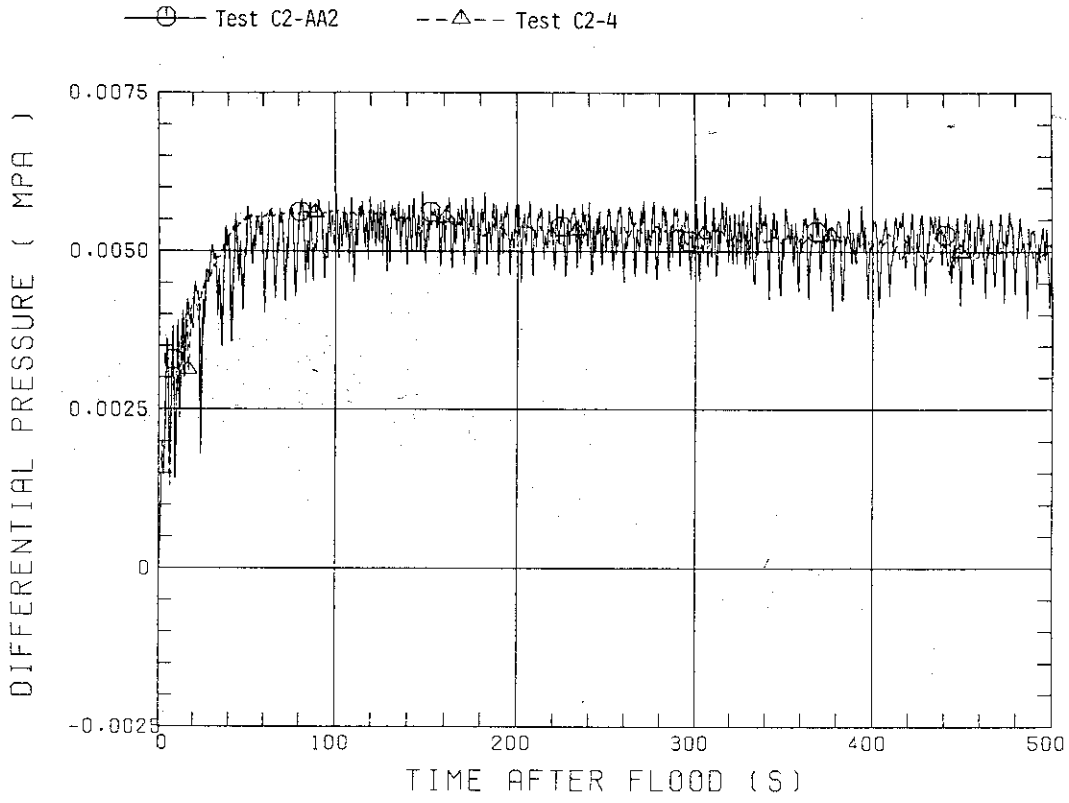

Fig. 3.19(a) Core sectional differential pressures between 0 and 0.61 m elevations

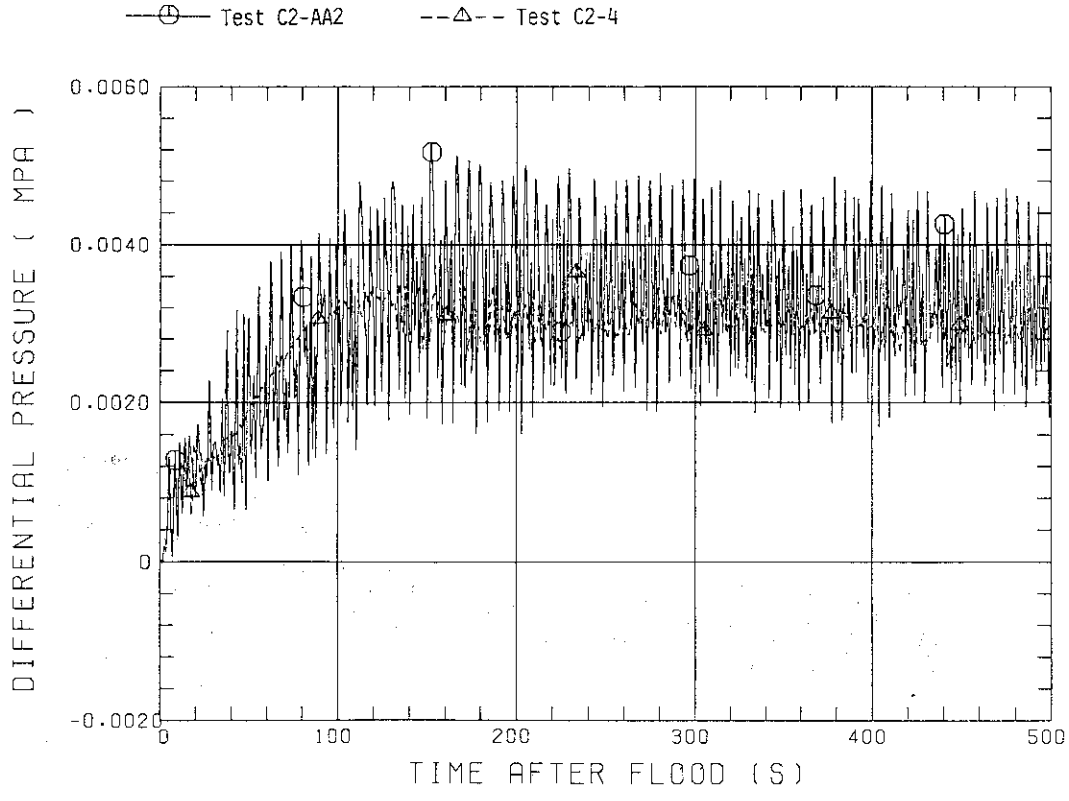

Fig. 3.19(b) Core sectional differential pressures between 0.61 and 1.22 m elevations

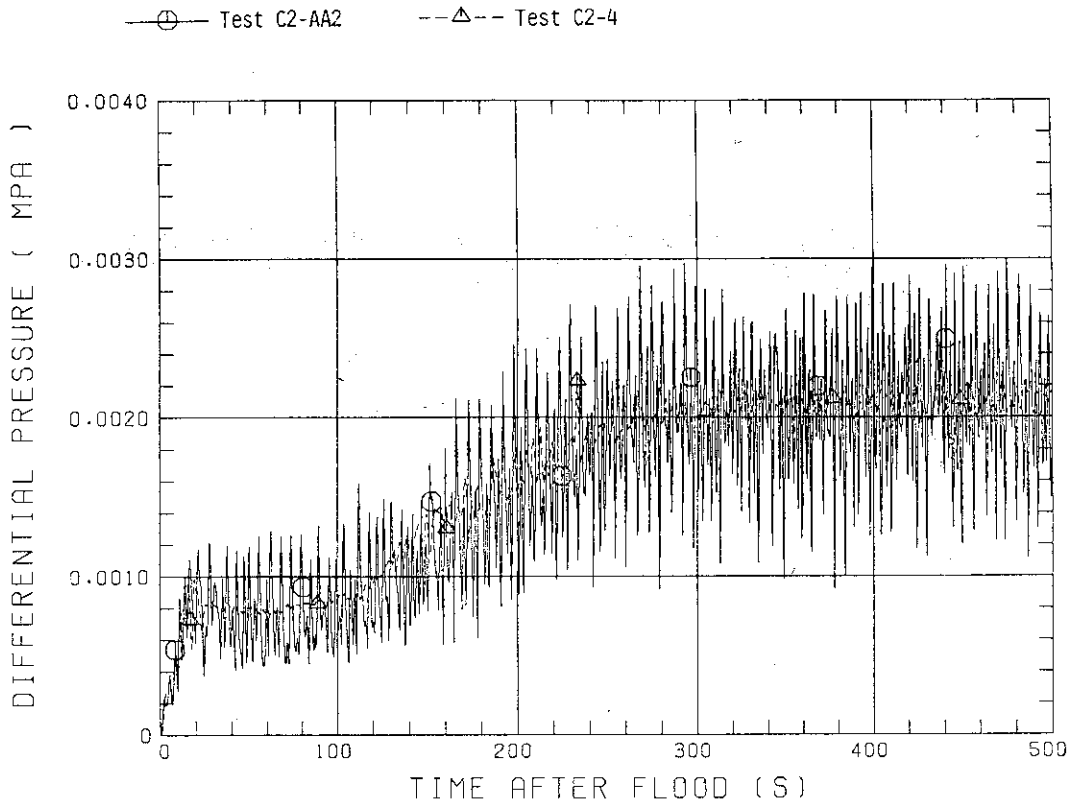

Fig. 3.19(c) Core sectional differential pressures between 1.22 and 1.83 m elevations

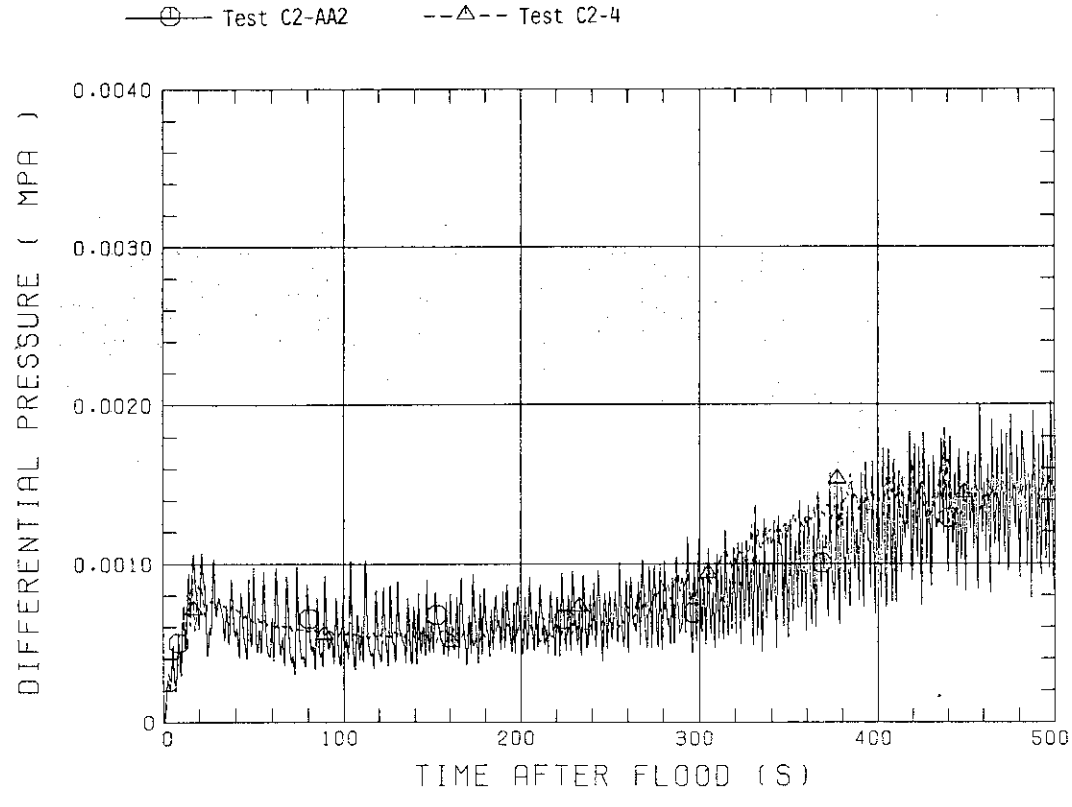

Fig. 3.19(d) Core sectional differential pressures between 1.83 and 2.44 m elevations

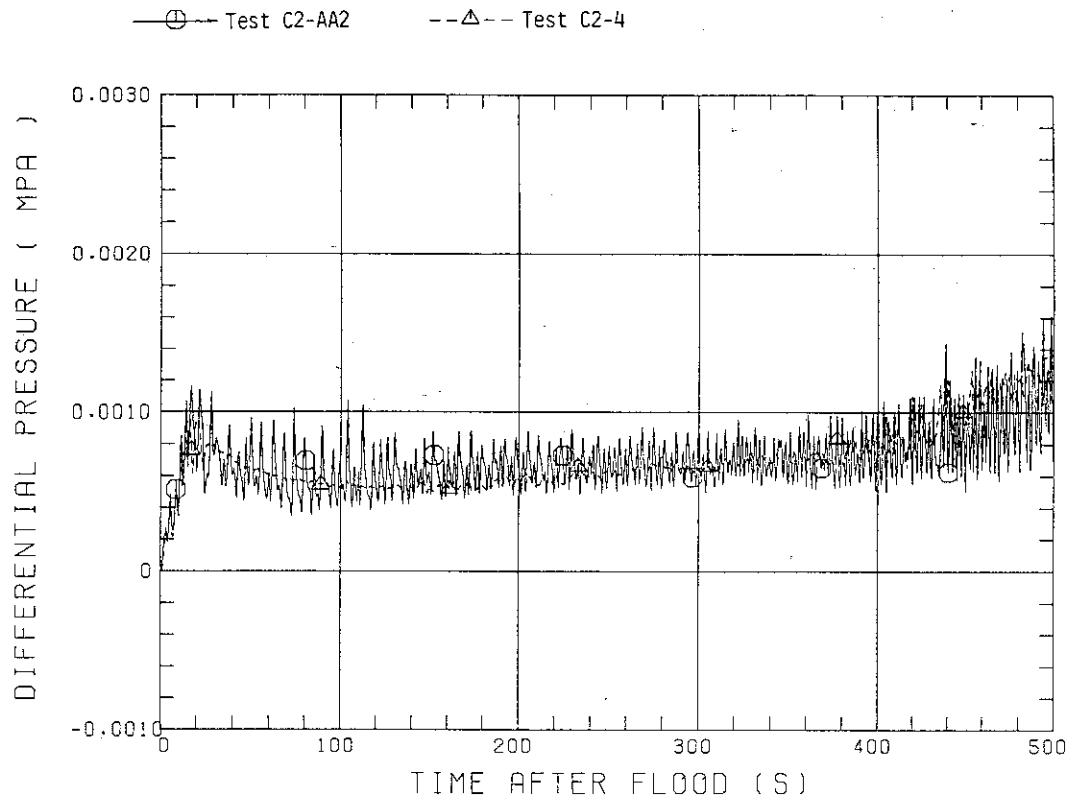

Fig. 3.19(e) Core sectional differential pressures between 2.44 and 3.05 m elevations

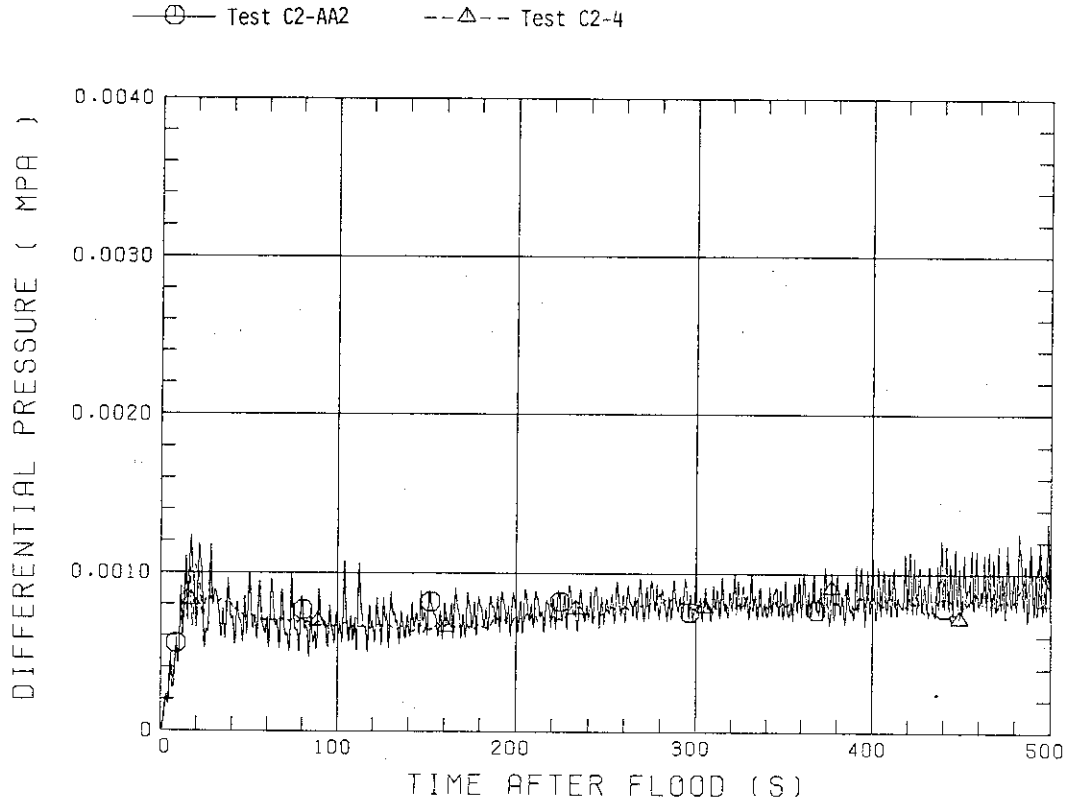

Fig. 3.19(f) Core sectional differential pressures between 3.05 and 3.66 m elevations

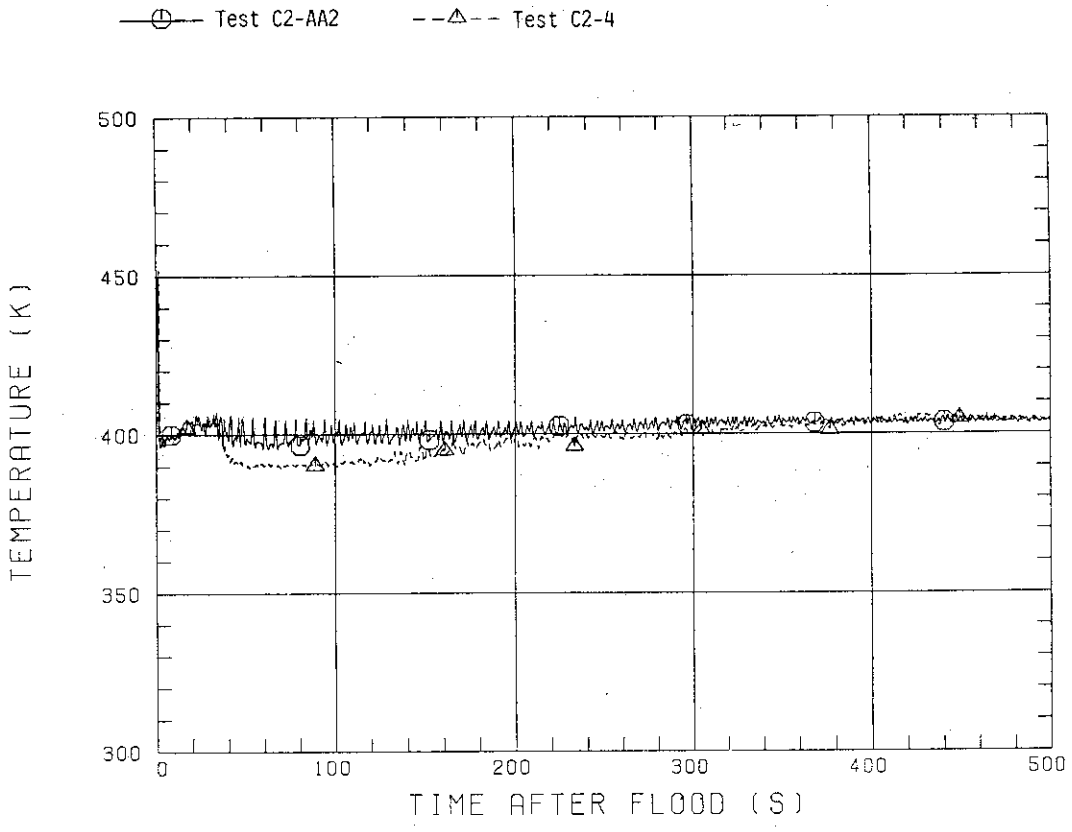

Fig. 3.20 Core fluid temperatures at 0.38 m

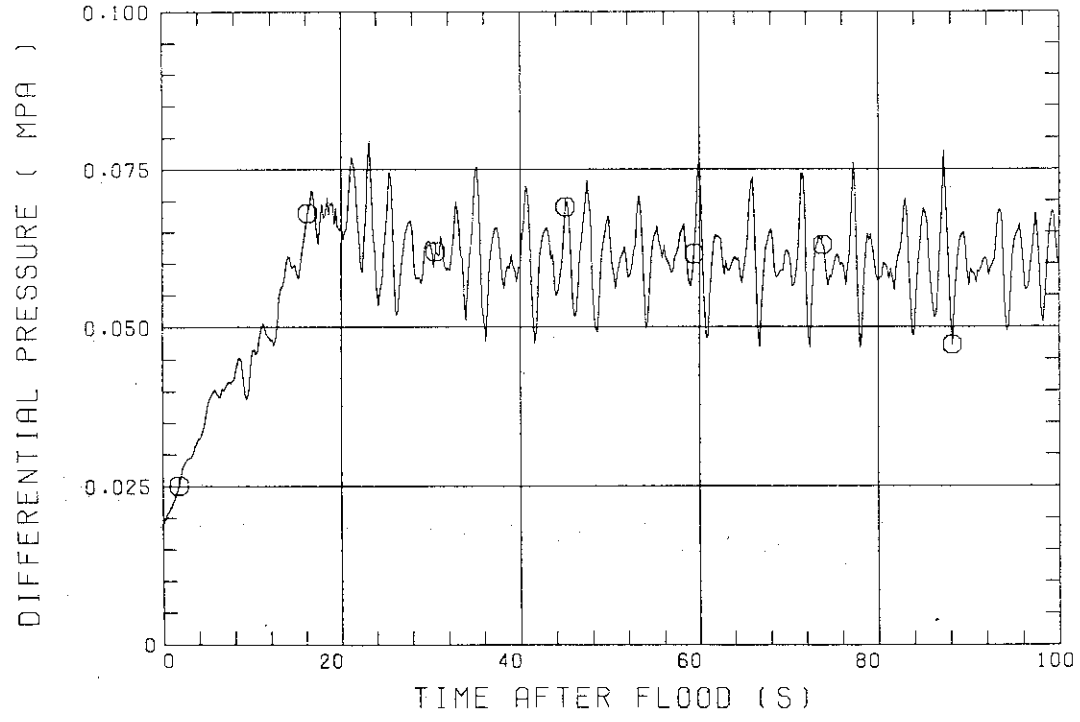

Fig. 3.21 Downcomer differential pressure

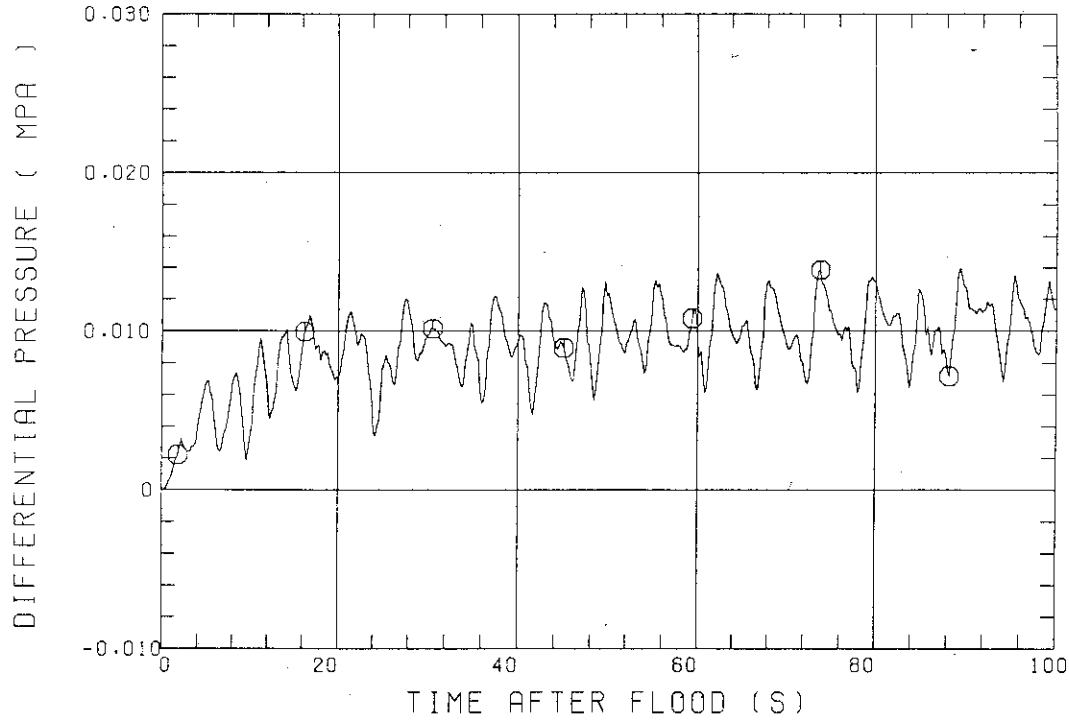

Fig. 3.22 Core differential pressure

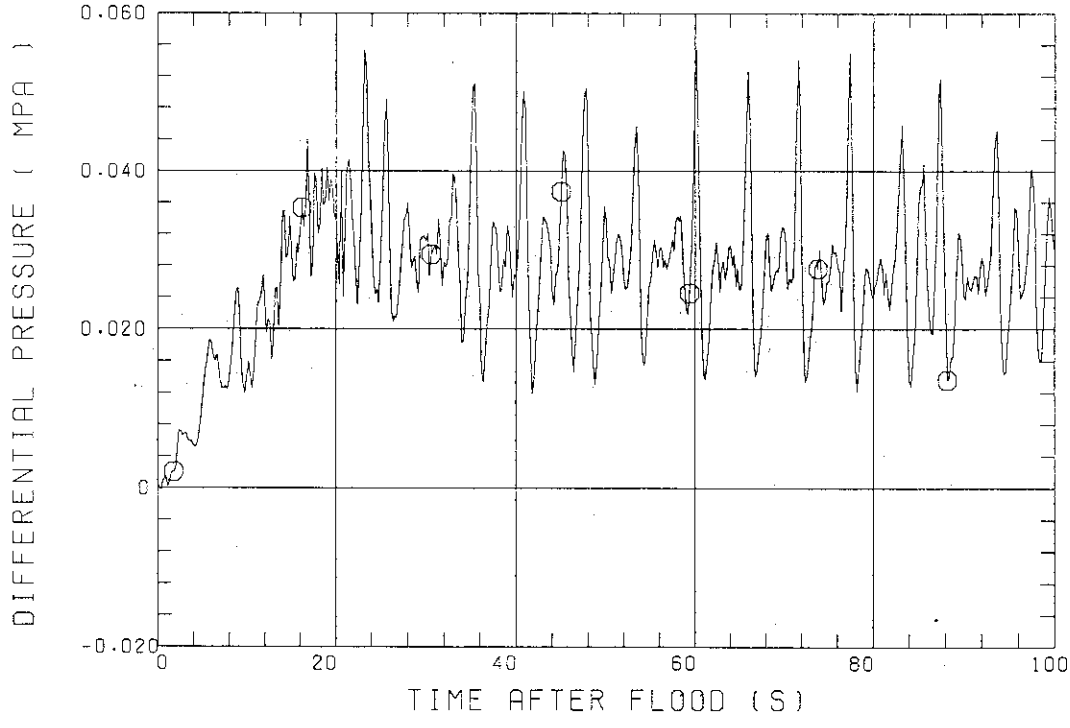

Fig. 3.23 Intact loop differential pressure

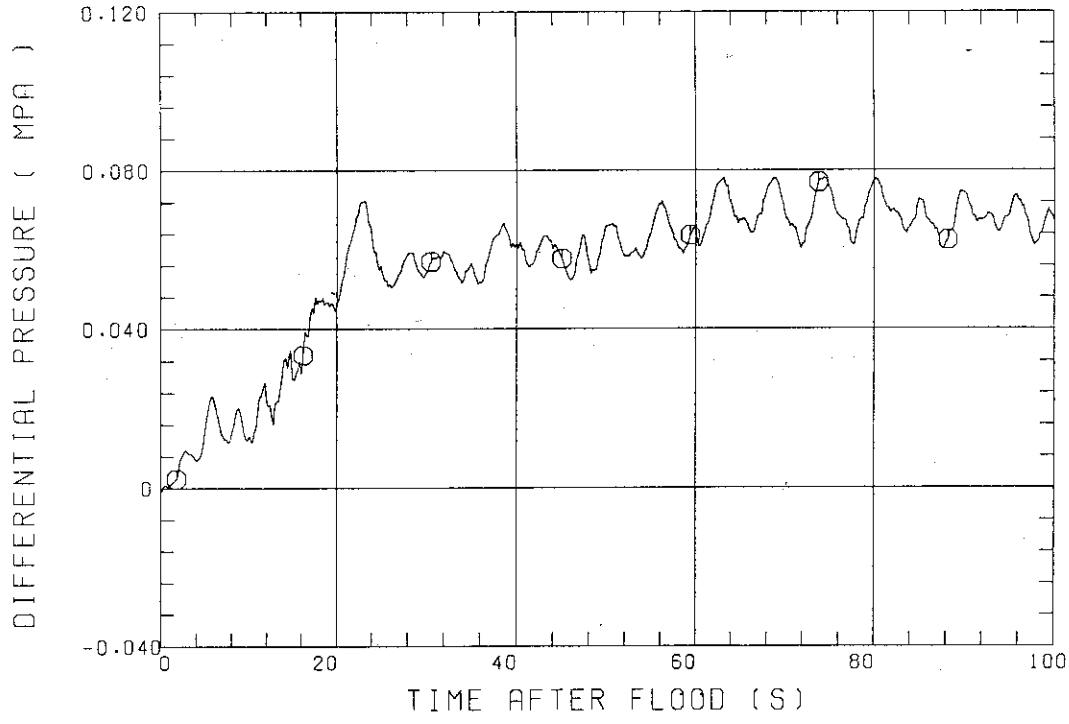

Fig. 3.24 Broken loop differential pressure

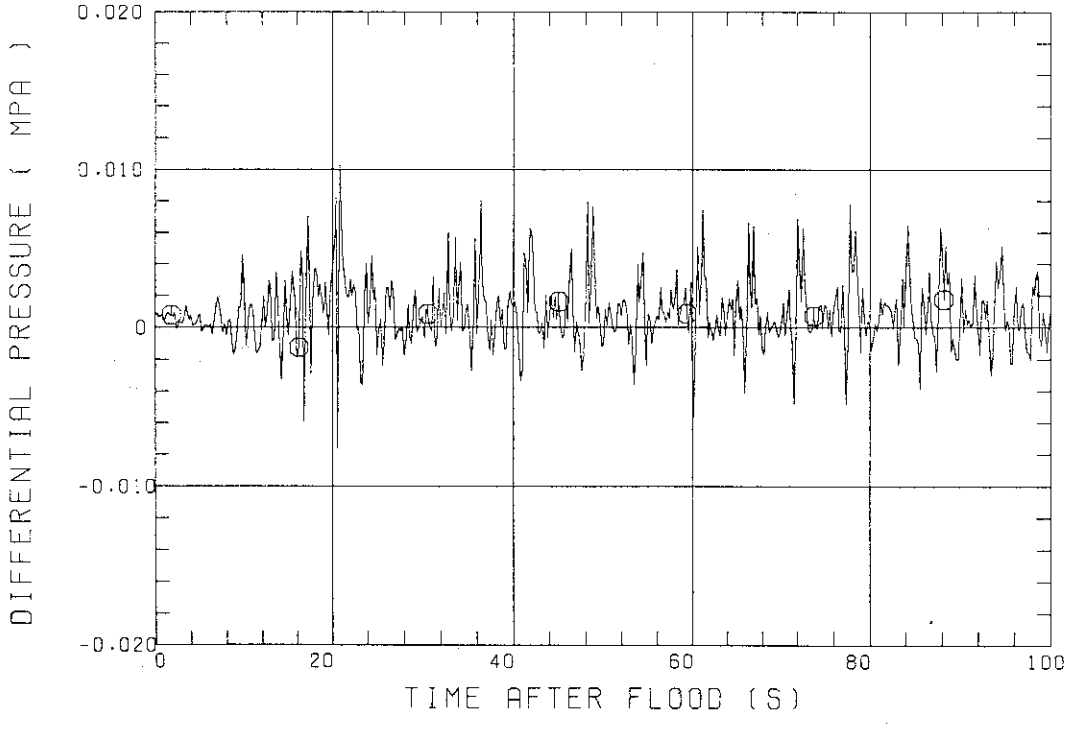

Fig. 3.25 Driving force for core flooding

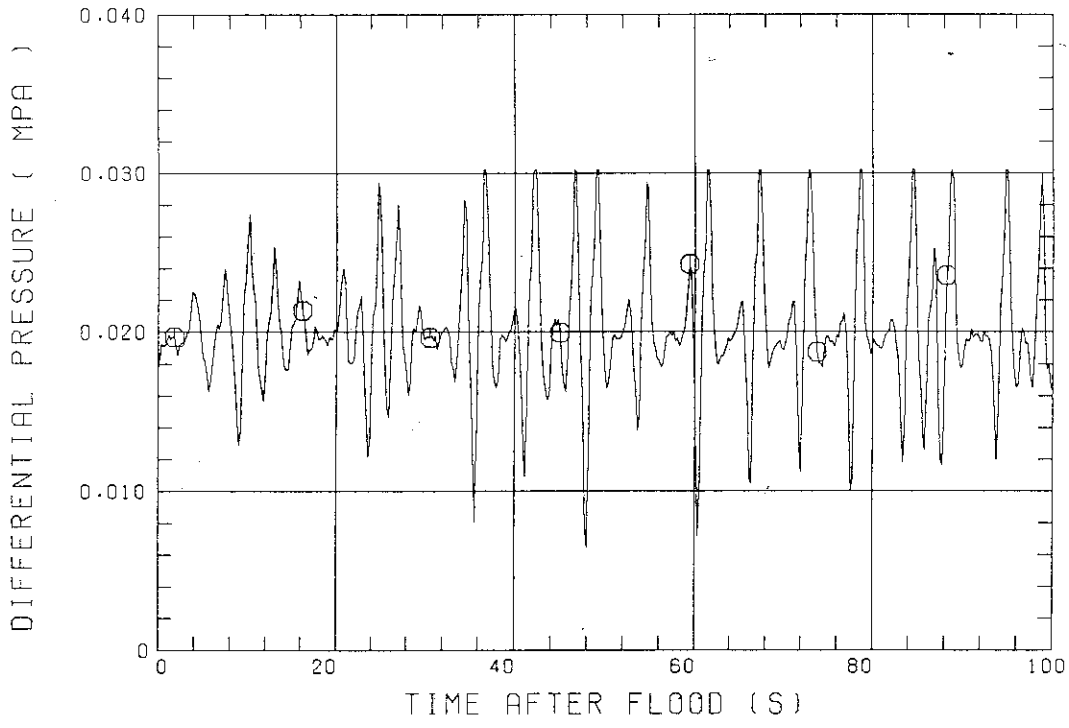

Fig. 3.26 Lower plenum differential pressure

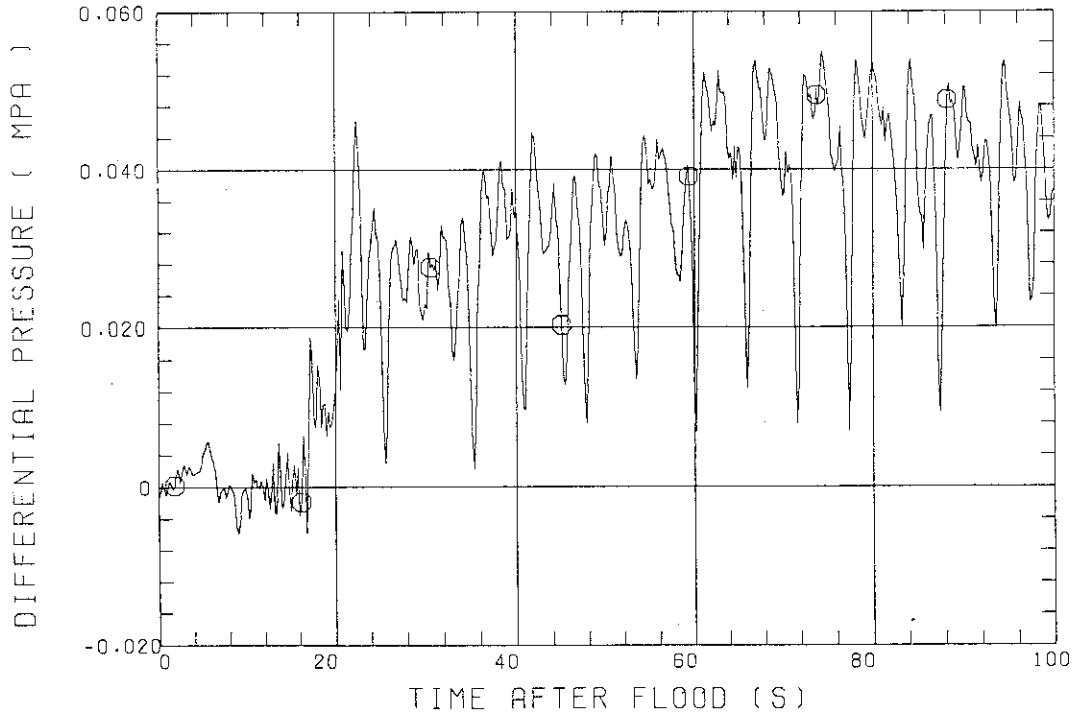

Fig. 3.27 Differential pressure through broken cold leg

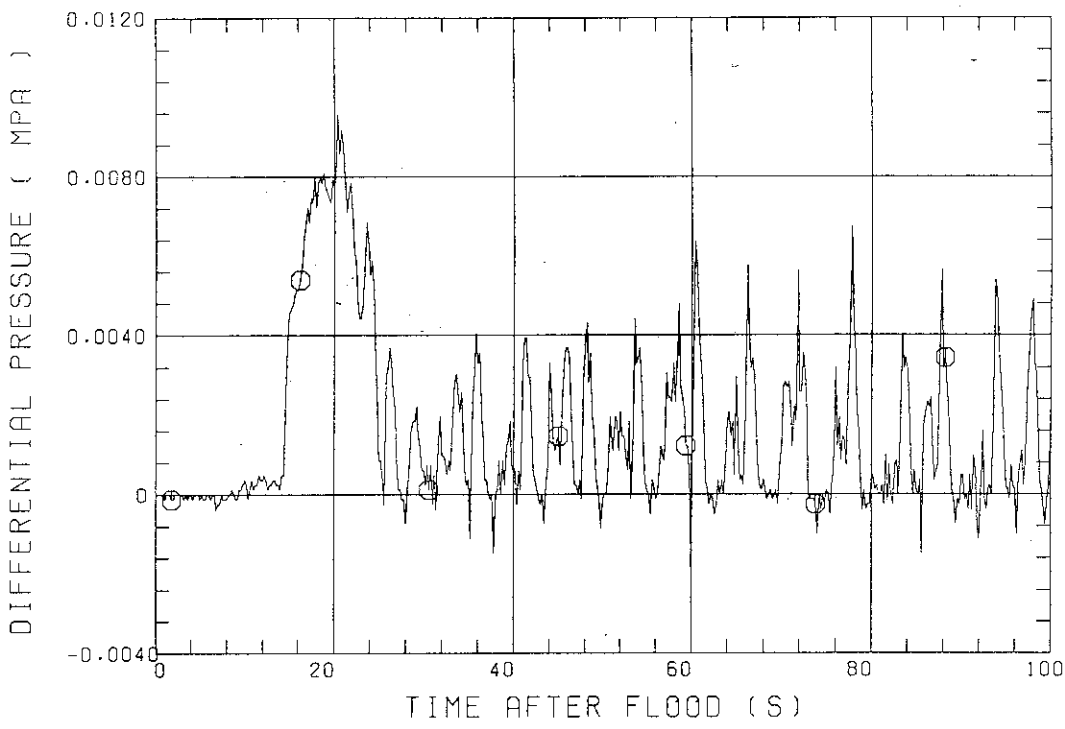

Fig. 3.28 Differential pressure in top section of downcomer (between 6.383 and 8.183 m elevations)

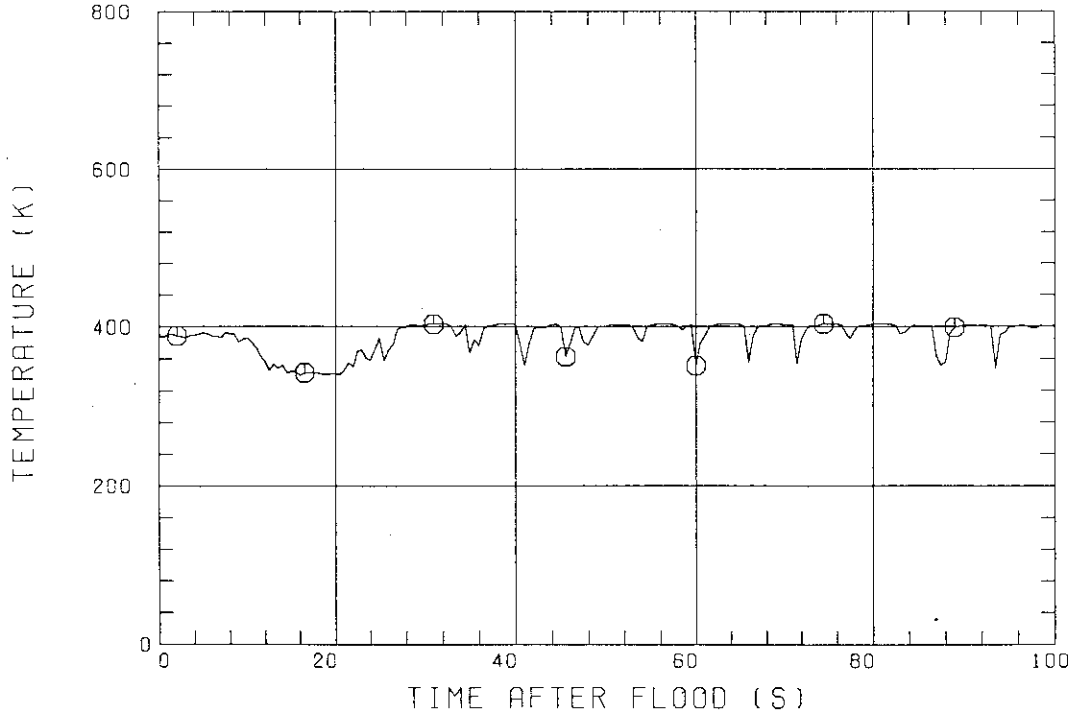

Fig. 3.29 Fluid temperature in downcomer at 6.743 m

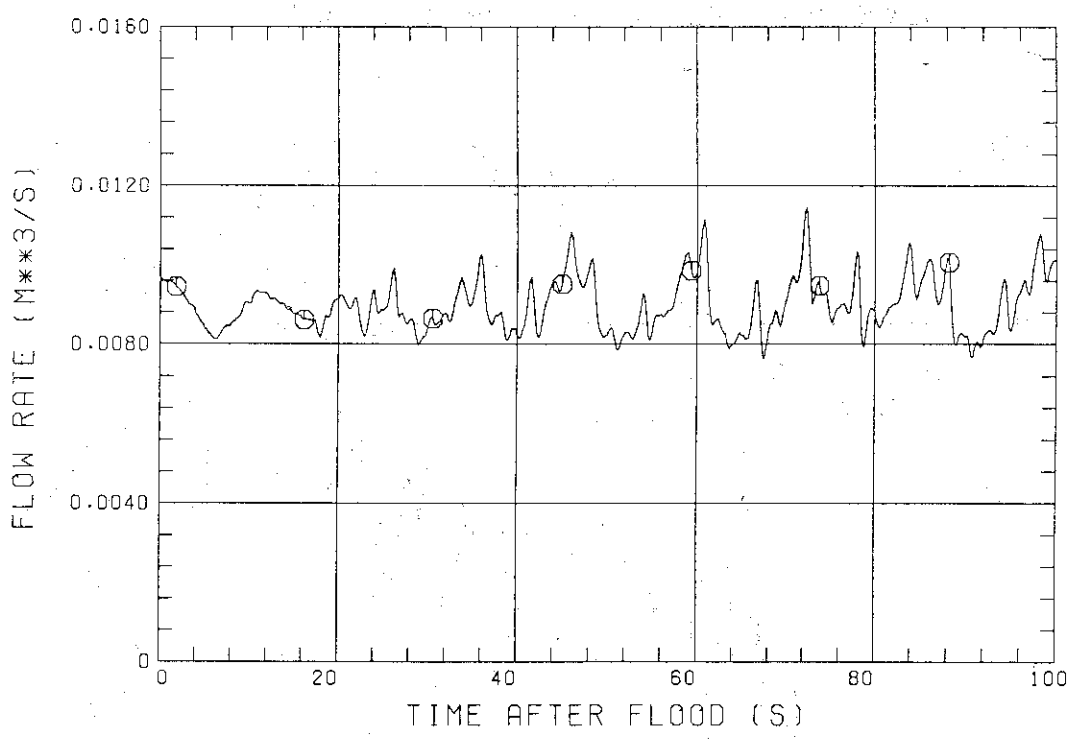

Fig. 3.30 Downcomer injection rate

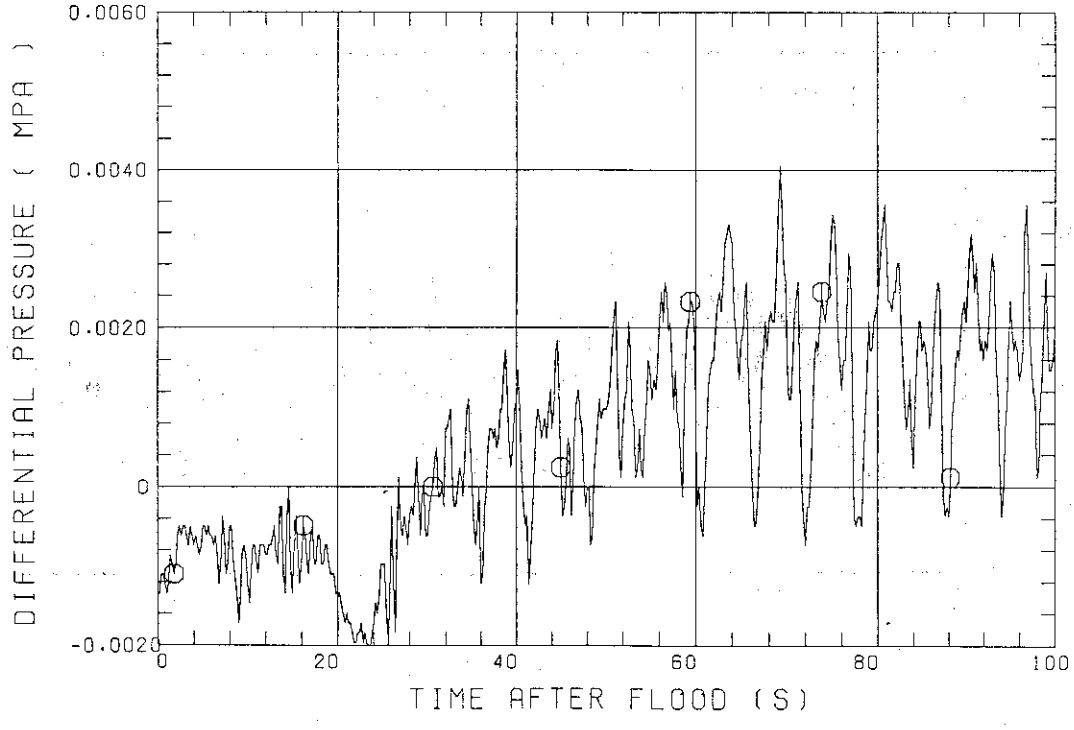

Fig. 3.31 Differential pressure between containment tank 1 and 2

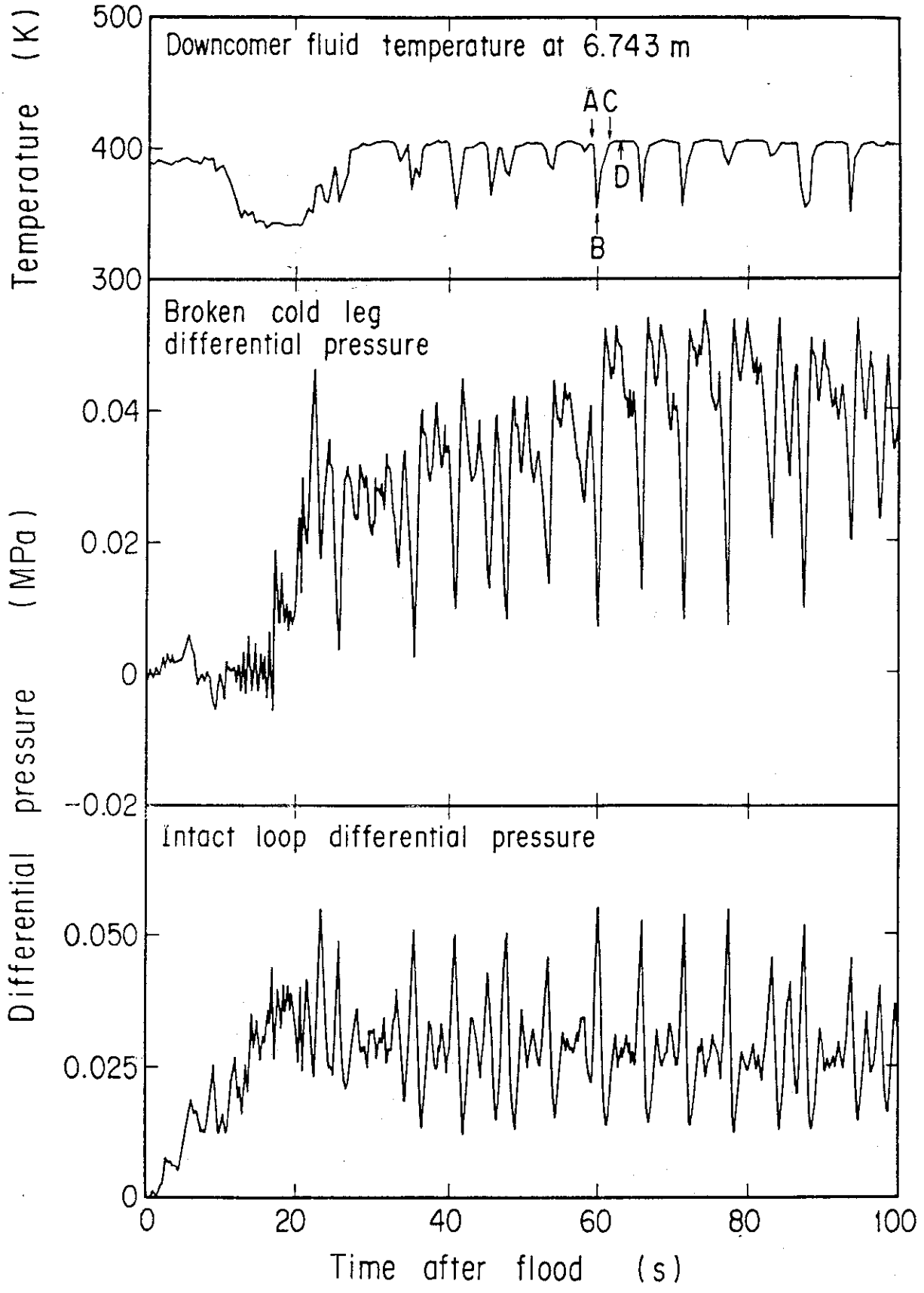

Fig. 3.32(a) Relation among downcomer fluid temperature at 6.743 m, broken cold leg differential pressure and intact loop differential pressure (between 0 and 100 s)

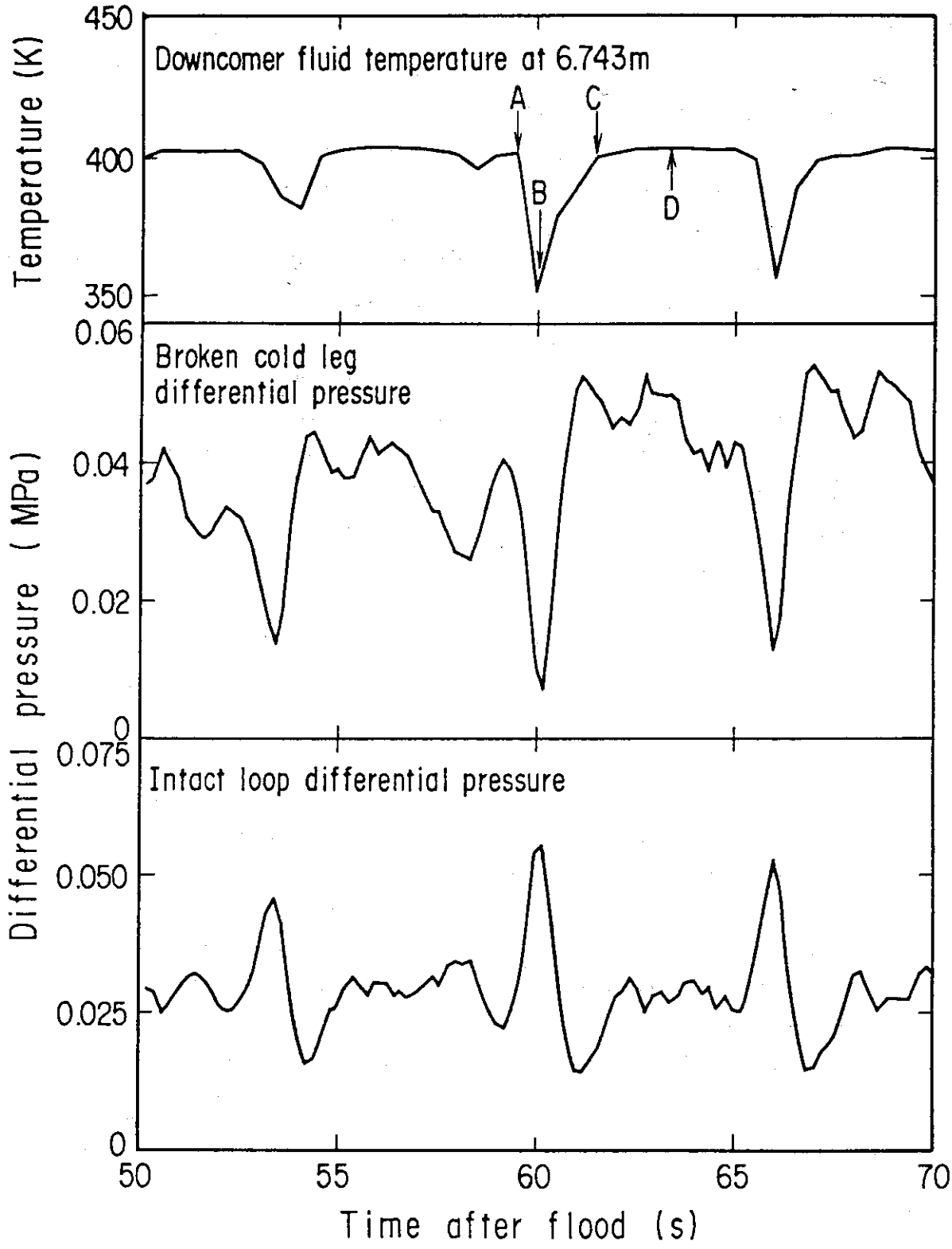

Fig. 3.32(b) Relation among downcomer fluid temperature at 6.743 m, broken cold leg differential pressure and intact loop differential pressure (between 50 and 70 s)

4. Conclusions

Comparing data of the present test with those of the base case test the following conclusions are obtained:

(1) The present test experienced a significant oscillation, which was not observed in the base case test (cold leg injection case). The oscillation was periodic and its period was 5.7 s. This type of oscillation is considered to occur in a PWR with the downcomer injection type ECCS under the "single-failure" assumption of the LPCI pumps.

(2) Thermal equilibrium by mixing of ECC water and steam flowing in the intact loops was not established at the downcomer in the present test, and hence, downcomer fluid temperature was observed to be subcooled and lower than in the base case test. This is considered to be the cause of the oscillation mentioned above.

(3) However, fluid temperature at the core inlet was higher than in the base case test. This is attributed to mixing of lower plenum fluid with core fluid due to the large oscillation. Quenching of heater rods were slightly later than in the base case test. This is attributed to the higher core inlet fluid temperature mentioned above. At the top part above 3 m elevation, however, the difference in quench time tended to get smaller.

(4) Although thermo-hydrodynamic behavior through the system was oscillatory in the present test, average values of the oscillatory data were nearly identical to those of the base case test except for the differences mentioned in items (2) and (3) above. This suggests, for analysis or prediction of core cooling for the downcomer injection case, it would be possible to use the same models, methods or computer codes as used for the cold leg injection case with adding a modification on predicting the fluid temperature at the core inlet.

Acknowledgments

The authors would like to express their appreciation to the member of their analysis group, especially Drs. H. Adachi and T. Iwamura, and Messrs. A. Ohnuki and Y. Abe, for valuable discussion. They are indebted to Dr. K. Okabe of Mitsubishi Atomic Power Industries, Inc. for his suggestions on the experiment. They also would like to express their thanks to the 2D/3D project members of USA and FRG, for valuable discussion.

They are deeply indebted to Messrs. Y. Fukaya, T. Ohyama, T. Wakabayashi, Y. Niitsuma, K. Nakajima, T. Chiba, J. Matsumoto, K. Komori, H. Sonobe and A. Owada for their contribution to the test conduction.

References

1. Hirano, K. and Murao, Y.: "Large Scale Reflood Test" (in Japanese), J. At. Energy Soc. Japan 22 [10], 681 (1980).
2. Murao, Y. *et al.*: "Analysis Report on CCTF Core-I Reflood Test", to be published as a JAERI-M report.
3. Hokkaido Electric Power Company: "Tomari (No. 1 and No. 2) Safety Analysis Report" (1982).
4. For instance, Okubo, T. *et al.*: "Evaluation of CCTF Core-II Second Acceptance Test C2-AC2 (Run 052)", JAERI-M 84-036 (1984).
5. Okubo, T. *et al.*: "Evaluation Report on CCTF Core-II Reflood Test C2-4 (Run 62) -- Investigation of Reproducibility --", JAERI-M 85-026 (1985).
6. Sudo, Y. *et al.*: "Experimental Results of the Effective Water Head in Downcomer during Reflood Phase of a PWR LOCA (2nd Report, 50 mm Gap Size)", JAERI-M 8978 (1980).
7. Akimoto, H. and Murao, Y.: "Evaluation Report on CCTF Core-I Reflood Tests C1-2 (Run 11) and C1-3 (Run 12) -- Effects of Initial Downcomer Wall Temperature --, JAERI-M 83-090 (1983).
8. Akimoto, H. *et al.*: "Pressure Drop through Broken Cold Leg during Reflood Phase of Loss-of-Coolant Accident of Pressurized Water Reactor", J. Nucl. Sci. Technol., 21[6],450 (1984).

Appendix A

Definitions of Tag IDs

Figure List

1. Definition of Tag. ID for clad surface temperatures and heat fransfer coefficients

Notation : TEnnYlm (temperature)

HTEmmYlm (heat transfer coefficient)

nn : Bundle number (see Fig. A.1)

m : Elevation number

	Elevation (m)	Axial power factor
3	0.38	0.651
5	1.015	1.147
7	1.83	1.40
9	2.44	1.256
A	3.05	0.854

2. Definition of power zone and boundle number

See Fig. A.1

3. Definition of Tag. ID for void fraction

See Fig. A.2

4. Definition of Tag. ID for average linear power of heater rod in each power unit zone

See Fig. A.3

5. Definition of Tag. ID for differential pressure through downcomer, upper plenum, core and lower plenum

See Fig. A.4

6. Definition of Tag. ID for differential pressure through intact and broken loop and broken cold leg nozzle

See Fig. A.5

7. Definition of Tag. ID for fluid temperature in inlet and outlet plenum and secondary side of steam generator

See Fig. A.6

8. Definition of Tag. ID for ECC water injection rate, ECC water temperature and vented steam flow rate

See **Fig. A.7**

9. Definition of initial temperature, turnaround temperature quench temperature, temperature rise, turnaround time and quench time. (See **Fig. A.8**)

T_i : Initial temperature (Clad surface temperature at reflood initiation)

T_t : Turnaround temperature (Maximum clad surface temperature in each temperature history)

ΔT_r : Temperature rise ($= T_t - T_i$)

T_q : Quench temperature (Clad surface temperature at quenching)

10. Definition of quenching

See **Fig. A.8**

Quench time t_t is determined as

$$t_t = i \times \Delta t - (\text{reflood initiation time})$$

In above equation, i is determined by the following criteria.

(1) Clad surface temperature is high, compared with the saturation temperature.

$$T_i > T_{sat} + \Delta T_1$$

(2) Decreasing rate of clad surface temperature is large.

$$\frac{T_{i+1} - T_i}{\Delta t} < - C_{st}$$

(3) Clad surface temperature falls around the saturation temperature.

$$T_i + k_1 \leq T_{sat} + \Delta T_1$$

(4) If the determined i is inadequate, the value i is manually re-determined.

Δt : Data sampling period (s)

T_i : Clad surface temperature (K)

T_{sat}: Saturation temperature at the pressure in upper plenum (K)

ΔT_1 : Temperature discrepancy (K)
Default value = 50.0

C_{st} : Decreasing rate of clad surface temperature (K/S)
Default value = 25.0

k_1 : Number of referred data (-)
Default value = 6

11. Definition of Tag. ID for core inlet mass flow rate, time-integral core inlet mass flow rate and carry-over rate fraction

(1) Core inlet mass flow rate : $\dot{m}_F$
Notation : MLCRI□ (□ = N, 1 or 11)

(2) Time-intefral core inlet mass flow rate : $\int \dot{m}_F dt$
Notation : IMLCRI□ (□ = N, 1 or 11)

(3) Carry-over rate fraction : $(\dot{m}_F - \dot{m}_{CR})/\dot{m}_F$
Natation : CRF□ (□ = N, 1 or 11)

where $\dot{m}_F$: Core inlet mass flow rat (See item 12)

$\dot{m}_{CR}$: Water accumulation rate in core

Suffix	$\dot{m}_F$ based on
N	Eq.(A.2)
1	Eq.(A.1) with K=15
11	Eq.(A.1) with K=20

12. Evaluation of core inlet mass flow rate

The reflood phenomena is a relatively slow transient and a steady state condition can be applied. In a steady state condition, based on the mass balance relations of the system, the core flooding mass flow rates $\dot{m}_F$s can be written as follows:

By using the data measured at the downstream of the core inlet, $\dot{m}_F$ is derived as,

$$\dot{m}_F = \dot{m}_C + \dot{m}_U + \dot{m}_B + \Sigma \dot{m}_I \quad , \qquad (A.1)$$

where $\dot{m}_C$ and $\dot{m}_U$ are the mass accumulation rates in the core and the upper plenum respectively. The $\dot{m}_B$ and $\dot{m}_I$ are the mass flow rates in the broken loop and the intact loop, respectively.

By using the data measured at the upstream of the core inlet, $\dot{m}_F$ is derived as,

$$\dot{m}_F = \Sigma \dot{m}_{DL} - \dot{m}_D - \dot{m}_O + \dot{m}_{ECC/LP} \quad , \tag{A.2}$$

where $\dot{m}_{DL}$ and $\dot{m}_O$ are the mass flow rates of the water flowing into and overflowing from the downcomer, $\dot{m}_{ECC/LP}$ and $\dot{m}_D$ are the mass flow rate of the ECC water injected into the lower plenum and the water accumulation rate in the dowmcomer respectively.

The $\dot{m}_I$s and $\dot{m}_B$ can be obtained from the pressure drops at the pump simulators with orifices by assuming the K-factor of the orifice is constant. The values of $\dot{m}_C$, $\dot{m}_D$ and $\dot{m}_U$ can be evaluated with the differential pressure ΔP_G, ΔP_D and ΔP_U, respectively, as follows:

$$\dot{m}_n = d(\Delta P_n S_n/g)/dt \quad (n : C, D, U) \quad , \tag{A.3}$$

where g is the gravitational acceleration and S_n is the cross sectional area. The value of $\dot{m}_O$ can be obtained from the liquid level X in the Containment tank 1 as,

$$\dot{m}_O = d(X\rho_\ell S_o)/dt \quad , \tag{A.4}$$

where ρ_ℓ is the liquid density and S_o is the cross sectional area of the containment tank 1.

The value of $\dot{m}_{DL}$, $\dot{m}_{DV}$ and h, which are liquid flow rate, steam flow rate and enthalpy of two phase mixture downstream each ECC port respectively, are obtained from the following mass and energy balance relations at each ECC port under the assumption of thermal equilibrium:

$$\dot{m}_{DV} + \dot{m}_{DL} = \dot{m}_{ECC} + \dot{m}_I \quad , \tag{A.5}$$

$$(\dot{m}_{DV} + \dot{m}_{DL})i = \dot{m}_{ECC} h_{ECC} + \dot{m}_I h_I \quad , \tag{A.6}$$

$$\text{if} \quad h_g \geq h \geq h_\ell \ , \ (\dot{m}_{DV} + \dot{m}_{DL})h = \dot{m}_{DV} h_g + \dot{m}_{DL} h_\ell$$

$$\text{if} \quad h \geq h_g \quad , \ \dot{m}_{DL} = 0 \quad , \tag{A.7}$$

$$\text{if} \quad h \geq h_\ell \quad , \ \dot{m}_{DV} = 0$$

where h is enthalpy of fluid and h_ℓ and h_g are enthalpies of liquid and steam at the saturation temperature, respectively.

The fluid temperatures can be measured with thermocouples immersed in the fluid and the enthalpies h_I and h_{ECC} can be estimated.

Mass balance calculations were performed with Eqs. (A.1) and (A.2). The K-factor of the orifice in the pump simulator was evaluated in the following two ways.

The K-factor of 20 was obtained with the steam and water single phase calibration tests using the flow meter and spool piece data. The K-factor of 15 was obtained with the Pitot tube measurement in a typical reflood condition assuming the flat velocity profile in the pipings. In the differentiation, higher frequency components of the data tends to be amplified more. Therefore, in the differentiation of the differential pressure data, the smoothing procedure was used to uppress the high frequency components of the data.

In the Acc injection period, the calculated $\dot{m}_F$s with Eqs. (A.1) and (A.2) are significantly different from each other. This discrepancy may be caused by inaccuracy of the mass flow rate injected into the system and by the unaccounting of the storage of water in the cold leg pipe. The former might be introduced from the slow time response of the flow meter (time constant 1 second) and the change of the gas volume in the injection line. In this period, especially before the steam generation from the core becomes noticeable, the mass flow rate, $\dot{m}_F$, calculated with Eq. (A.1) is probably reasonable, since the calculation uses the increasing rates of the masses in the core and the upper plenum and their accuracy is good enough for our estimation.

In the LPCI injection period, the calculated $\dot{m}_F$s are slightly different from each other. Judging from the time-integral values of both $\dot{m}_F$s, their average values are nearly proportional. The discrepancy was inferred to be caused by the disregard of the bypass of steam and liquid from the upper plenum without going through the hot legs in the calculation with Eq. (A.1). And additionally the discrepancy was caused by the disregard of the steam generation in the downcomer due to the hot wall of the pressure vessel in the calculation with Eq. (A.2). It was estimated that the disregard of the downcomer steam generation causes the error of 0.25 kg/s on predicted $\dot{m}_F$. The estimation was made by comparing the results of the tests with hot and cold downcomer conditions.

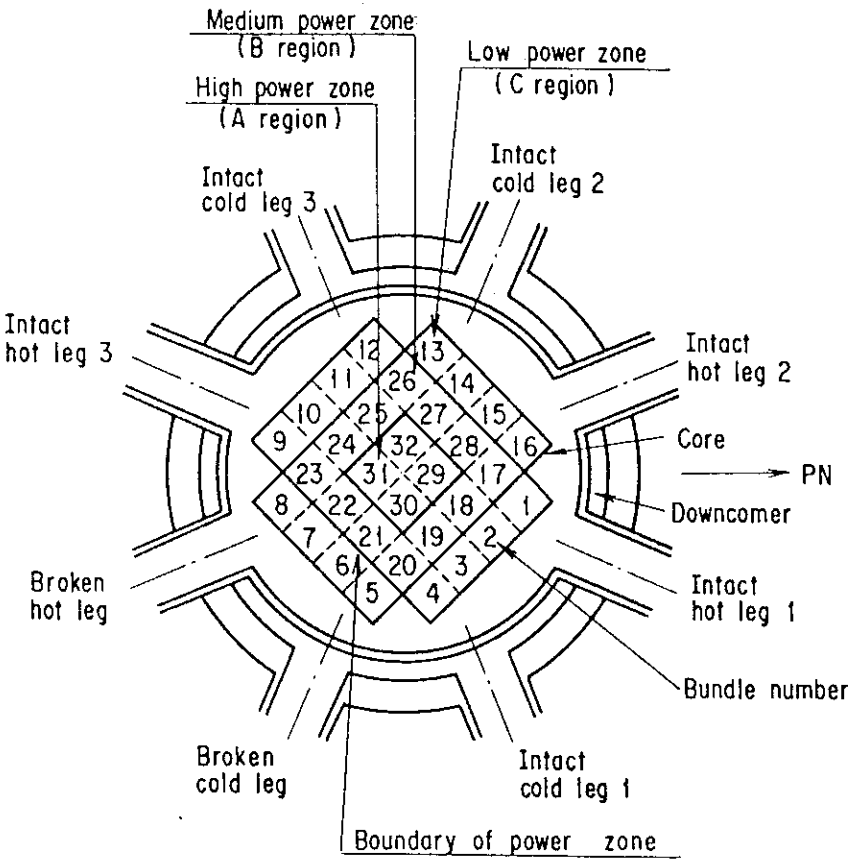

Fig. A.1 Definition of power zones and bundle numbers

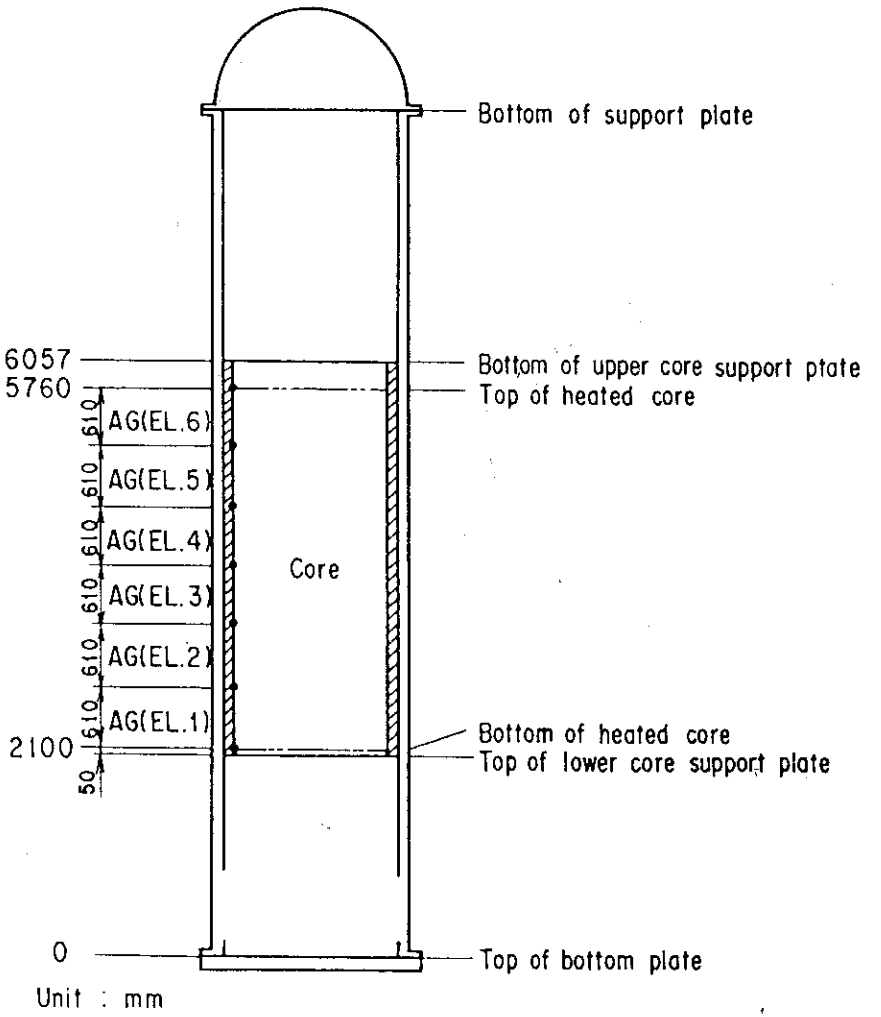

Fig. A.2 Definition of Tag. ID for void fraction (AG(EL.1) ~ AG(EL.6))

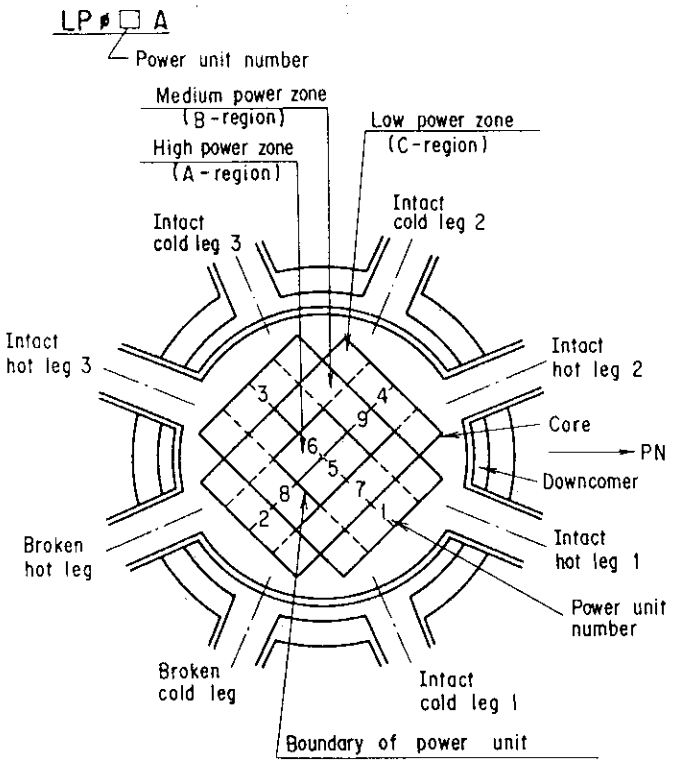

Fig. A.3 Definition of Tag. ID for average linear power of heater and in each power unit zone (LP01A ~ LP09A)

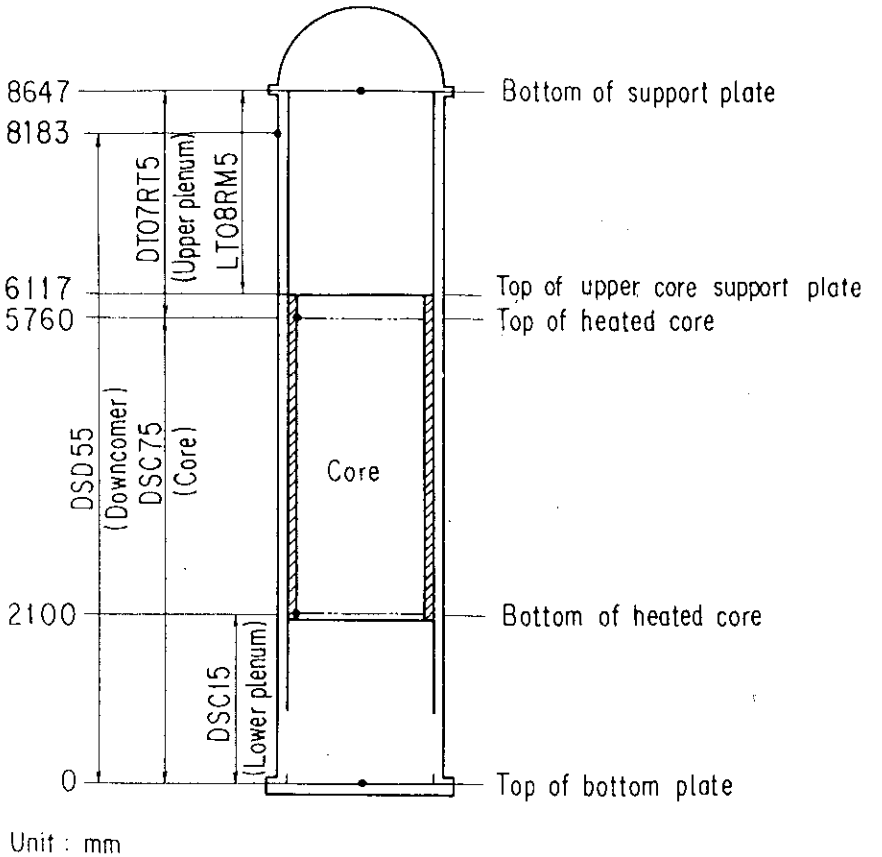

Fig. A.4 Definition of Tag. ID for differential pressure through downcomer, upper plenum, core, and lower plenum (DSD55, DT07RT5, LT08RM5, DSC75, DSC15)

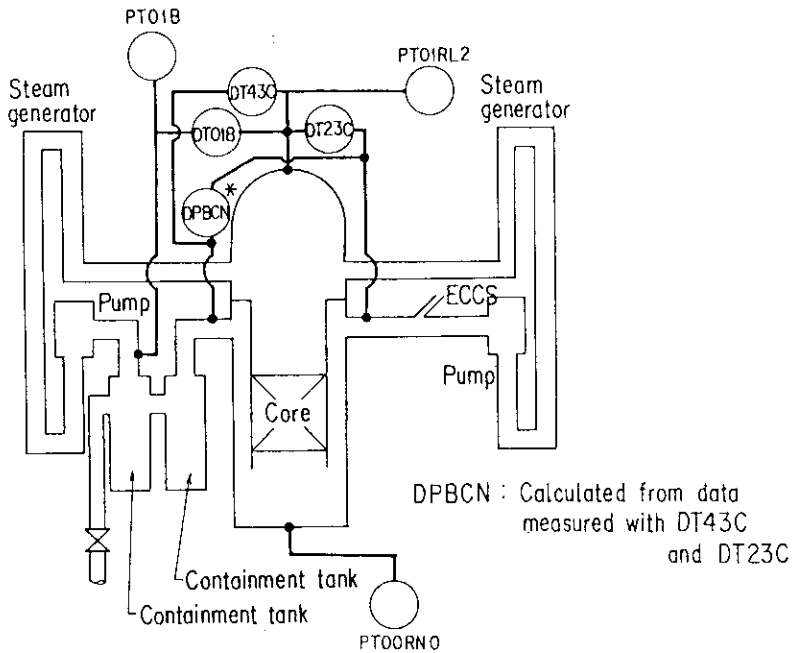

Fig. A.5 Definition of Tag. ID for differential pressure through intact and broken loop and broken cold leg nozzle (DT23C, DT01B, DPBCN)

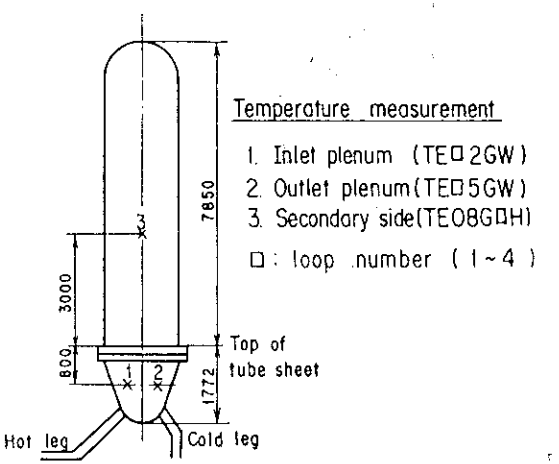

Fig. A.6 Definition of Tag. ID for fluid temperature in inlet and outlet plenum and secondary of steam genrator (TE□2GW, TE□5GW, TE08G□H)

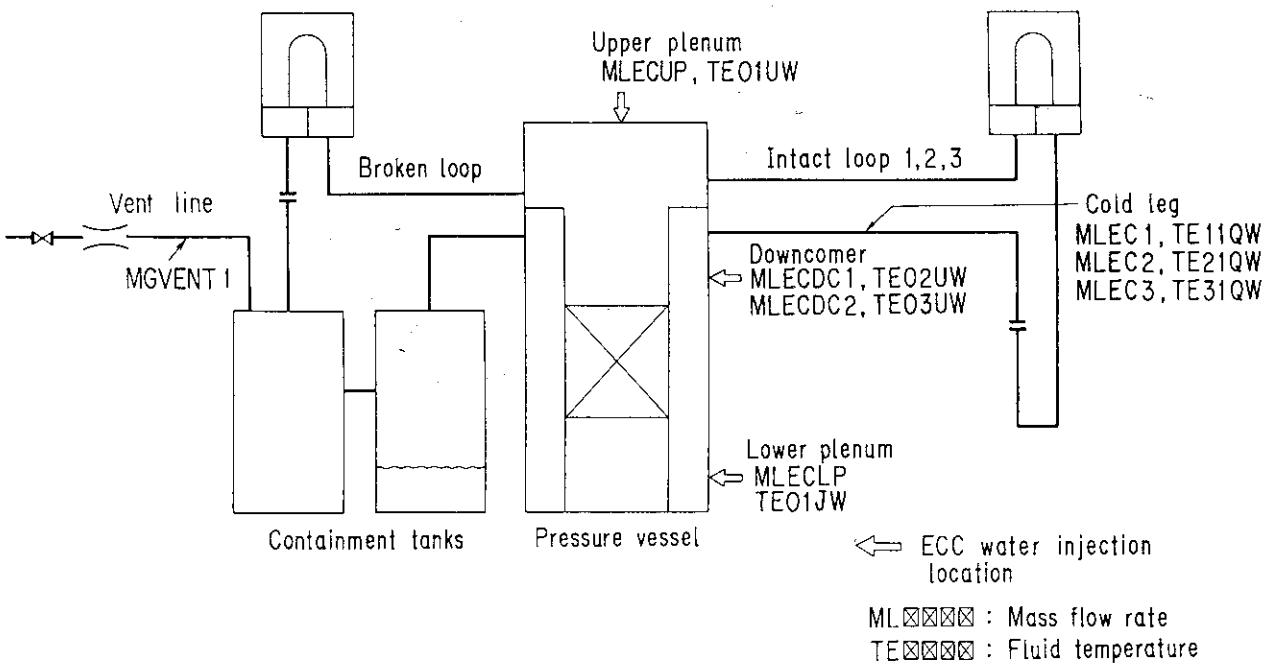

Fig. A.7 Definition of Tag. ID for ECC water injection rate, ECC water temperature and vented steam flow rate (MLEC1, MLEC2, MLEC3, MLECLP, MLECUP, MLECDC1, MLECDC2, TE11QW, TE21QW, TE01JW, TE01UW, TE02UW, TE03UW, MGVENT1)

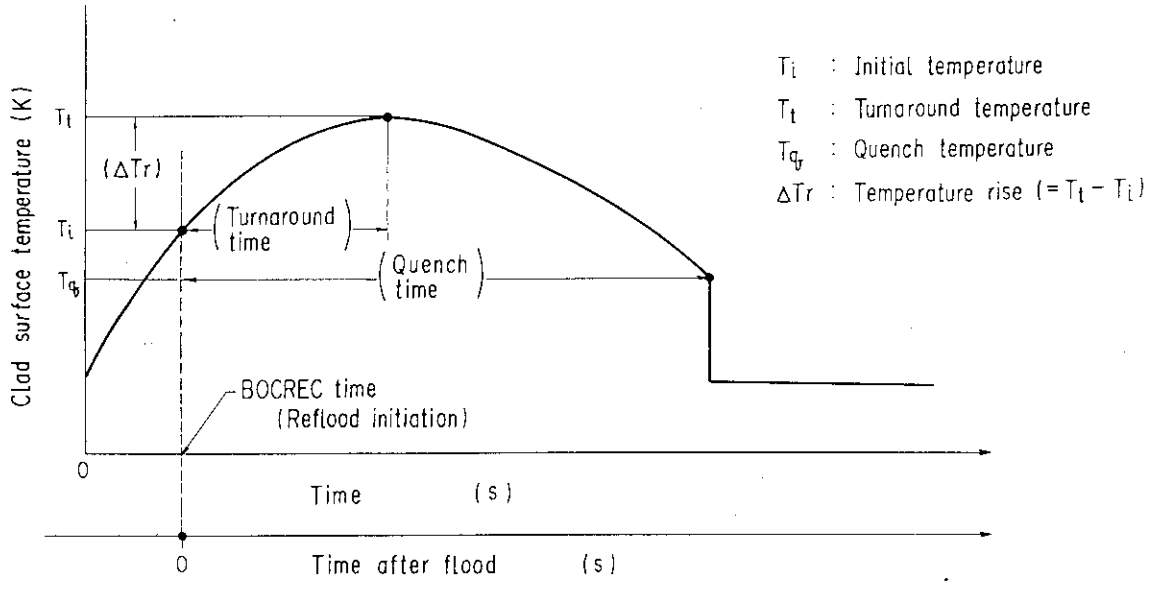

Fig. A.8 Definition of initial temperature, turnaround temperature, quench temperature, temperature rise, turnaround time and quench time

Appendix B

Selected data of CCTF Test C2-AA2 (Run 58)

Figure List

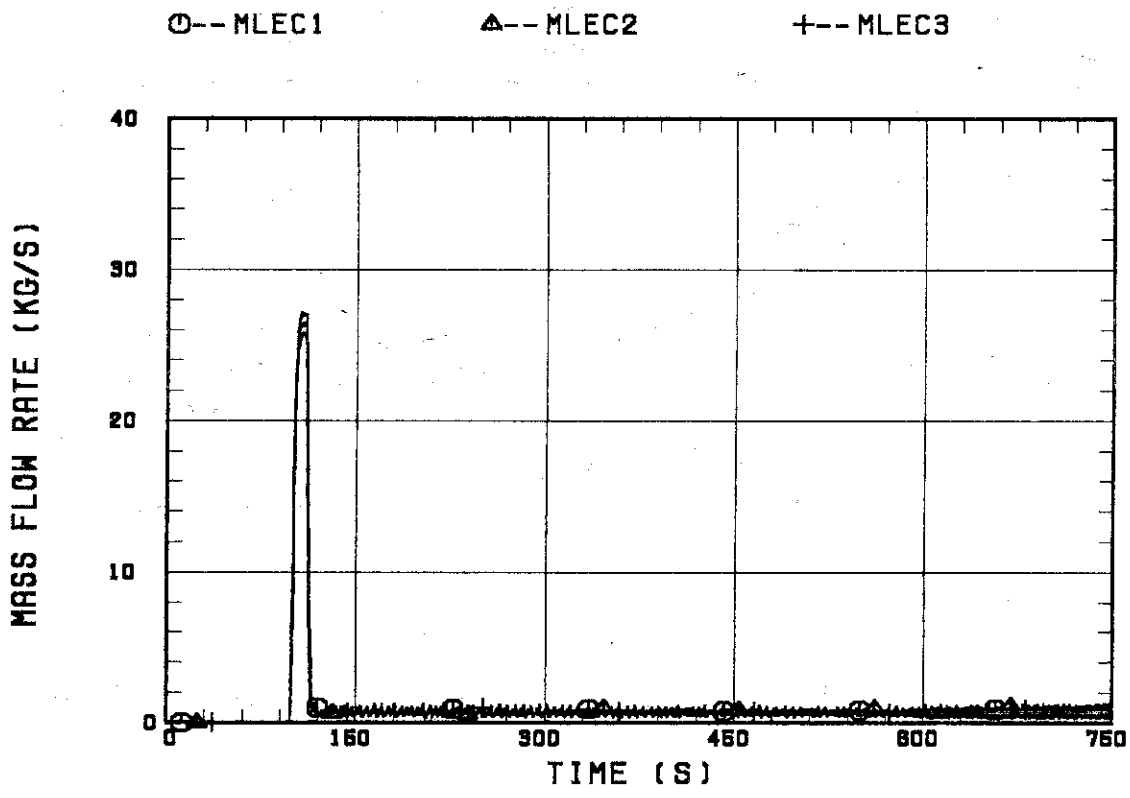

Fig. B.1 ECC water injection rates into the primary system

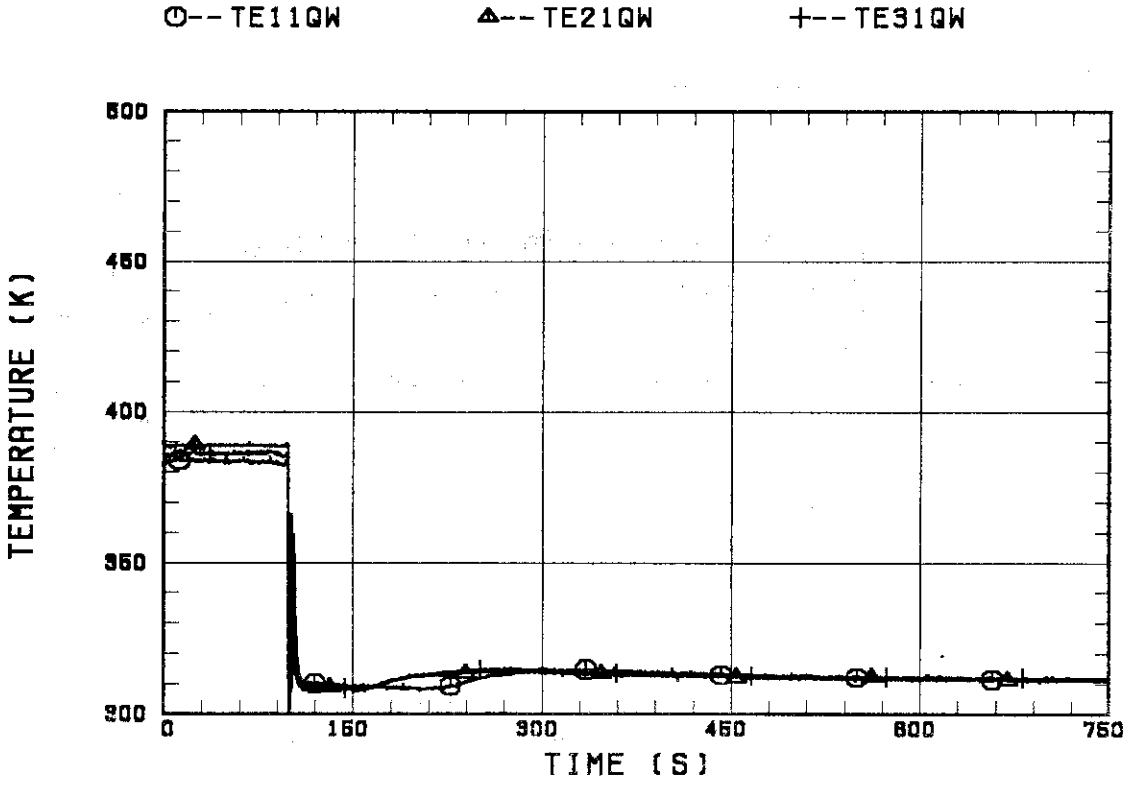

Fig. B.2 ECC water temperature

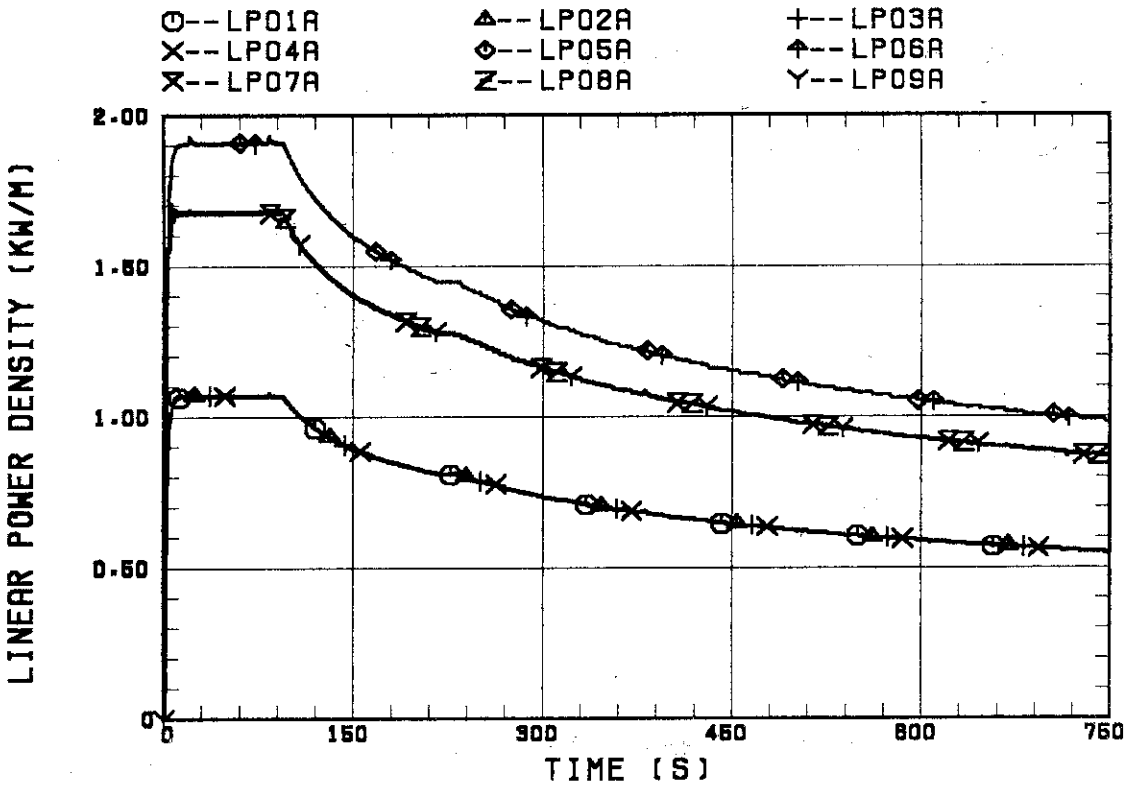

Fig. B.3 Average linear power of heater rod in each power unit zone

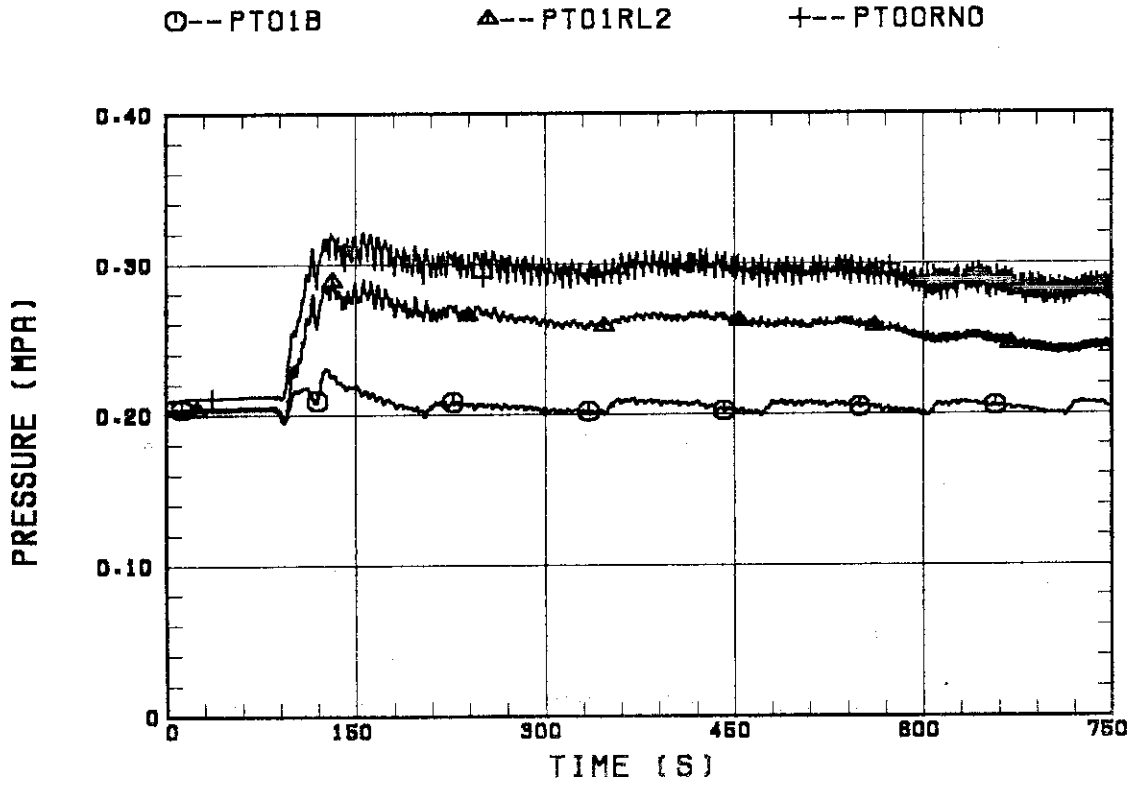

Fig. B.4 Pressure history in containment tank 2, upper plenum and lower plenum

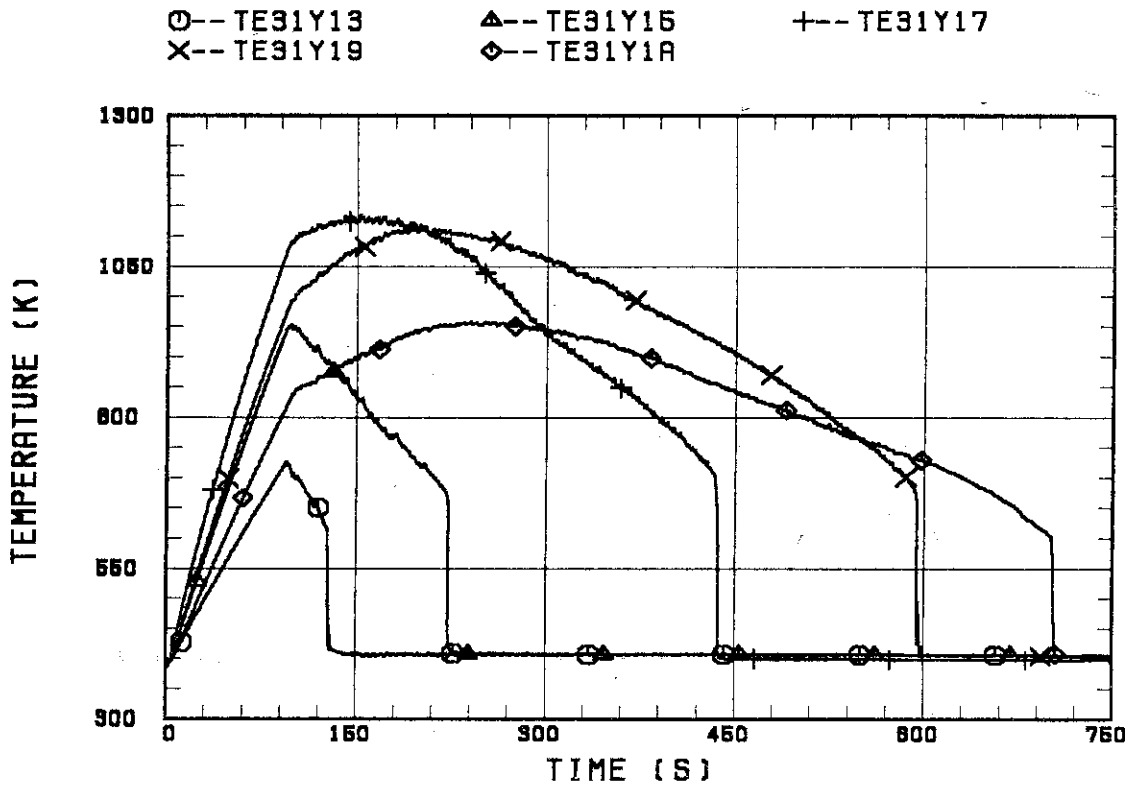

Fig. B.5 Clad surface temperature at various elevations along a heater rod in high power region (A region)

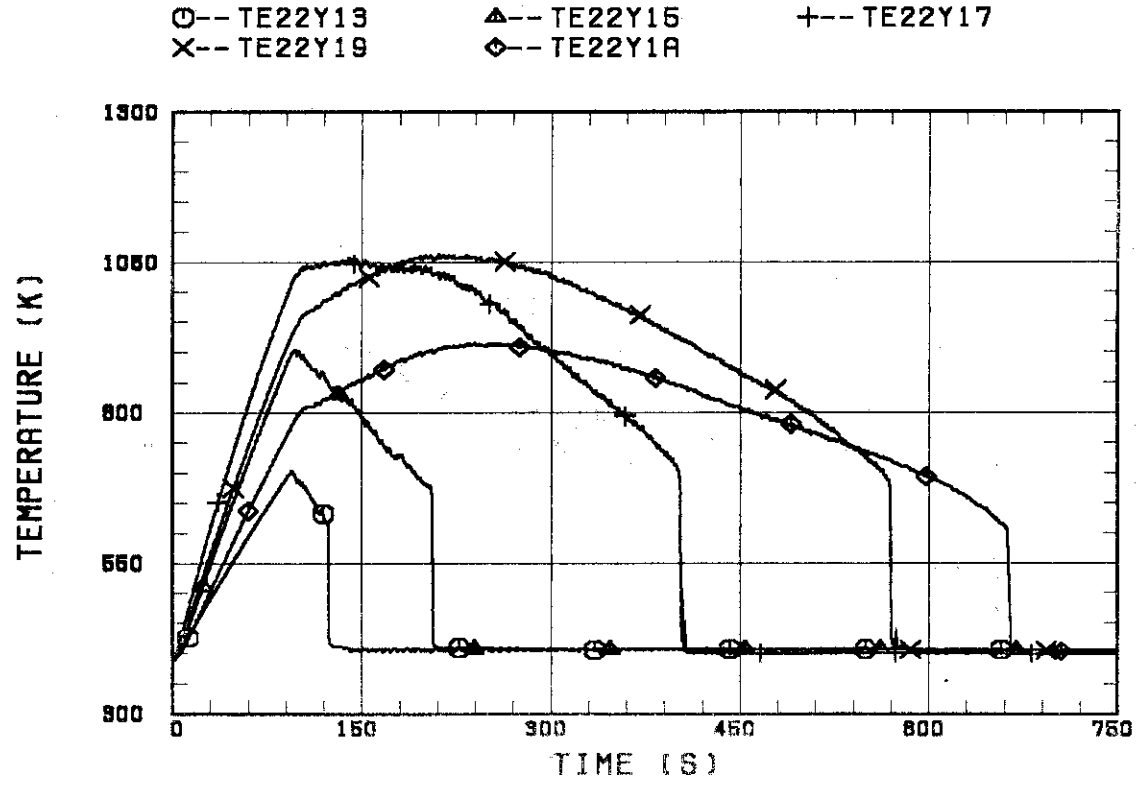

Fig. B.6 Clad surface temperature at various elevations along a heater rod in medium power region (B region)

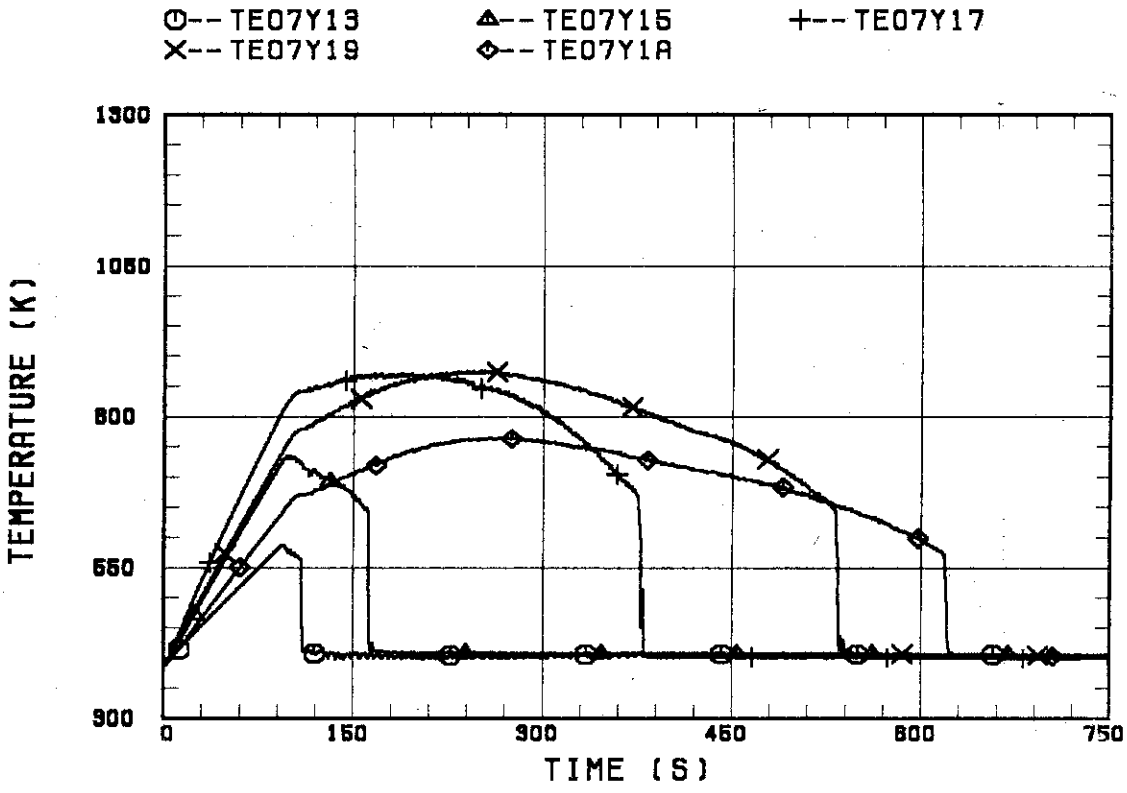

Fig. B.7 Clad surface temperature at various elevations along a heater rod in low power region (C region)

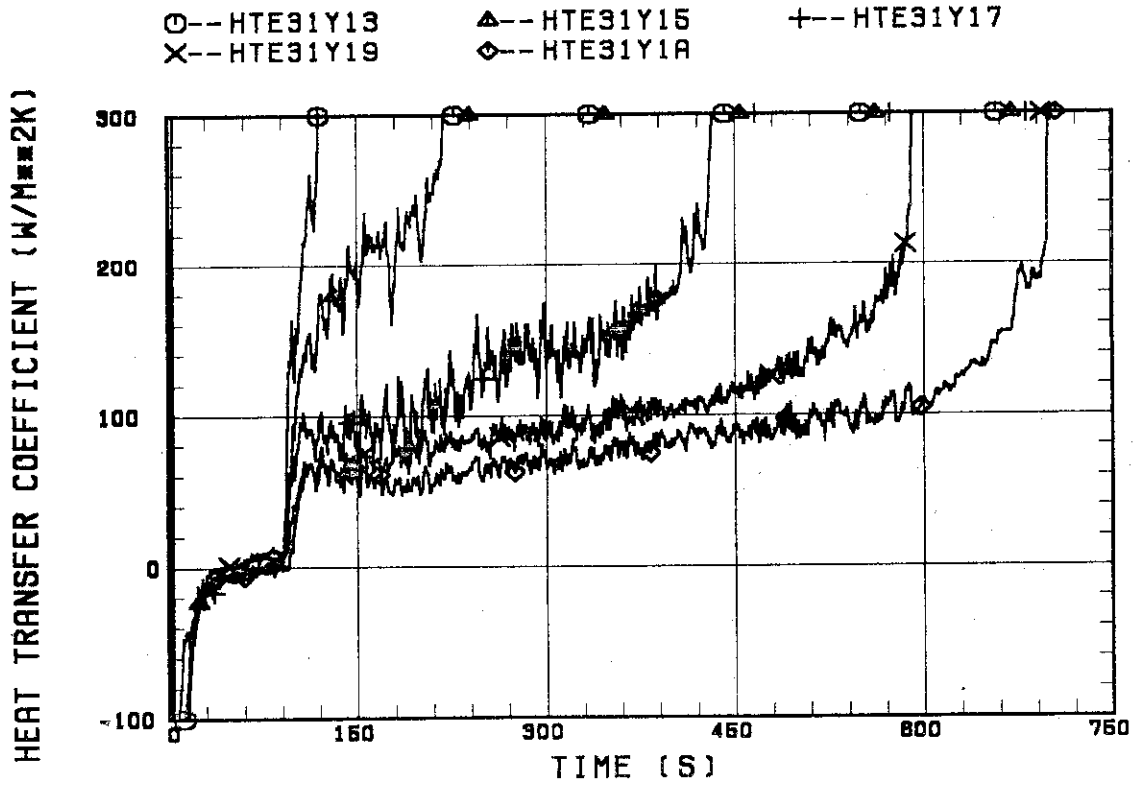

Fig. B.8 Heat transfer coefficient at various elevations along a heater rod in high power region (A region)

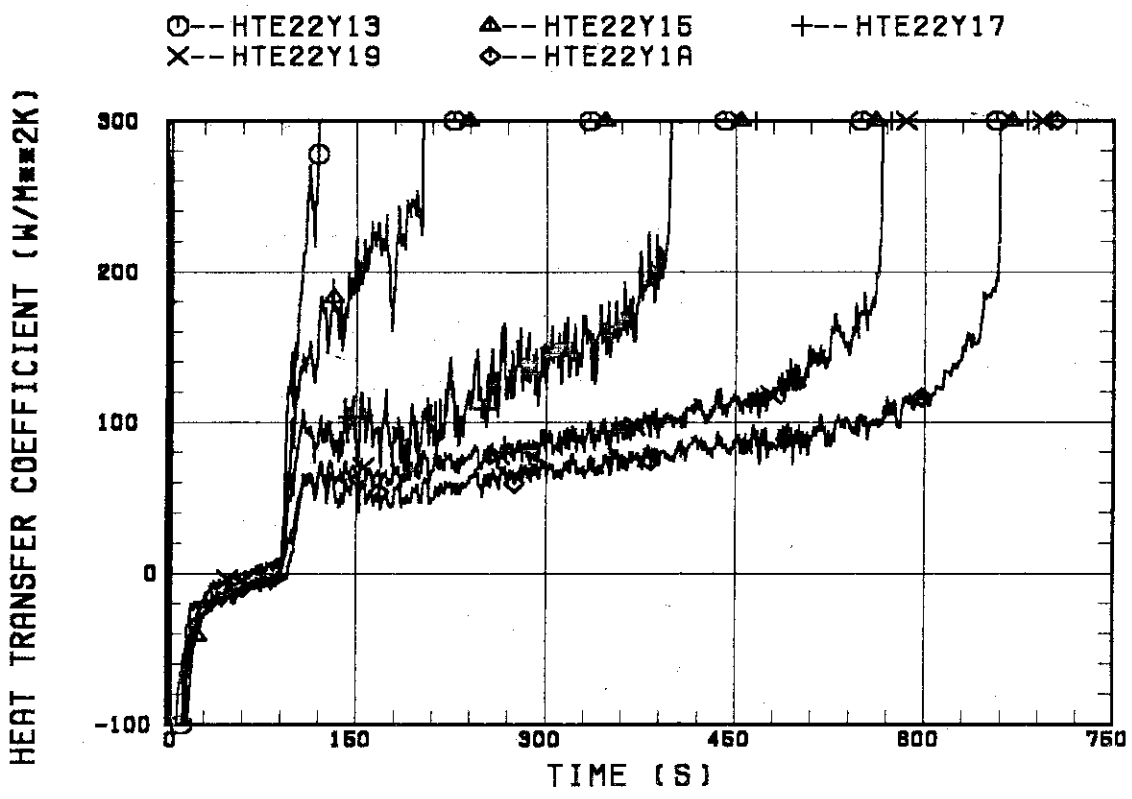

Fig. B.9 Heat transfer coefficient at various elevations along a heater rod in medium power region (B region)

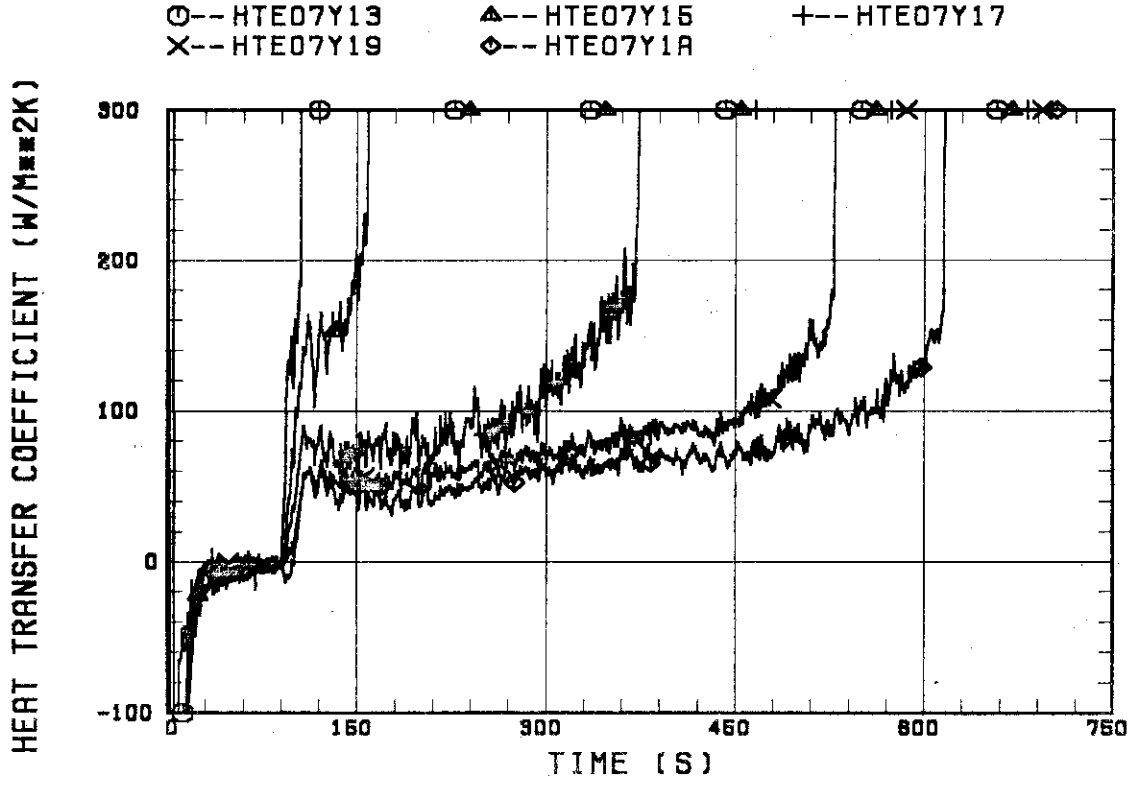

Fig. B.10 Heat transfer coefficient at various elevations along a heater rod in low power region (C region)

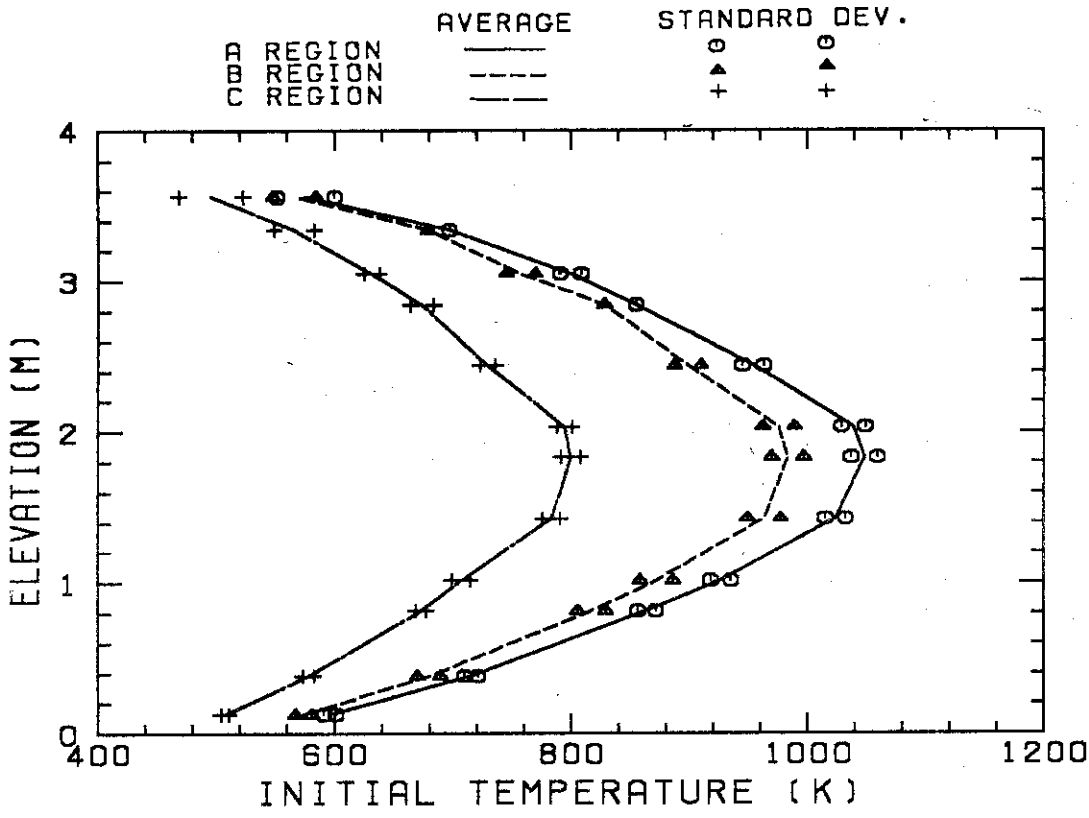

Fig. B.11 Initial clad surface temperature

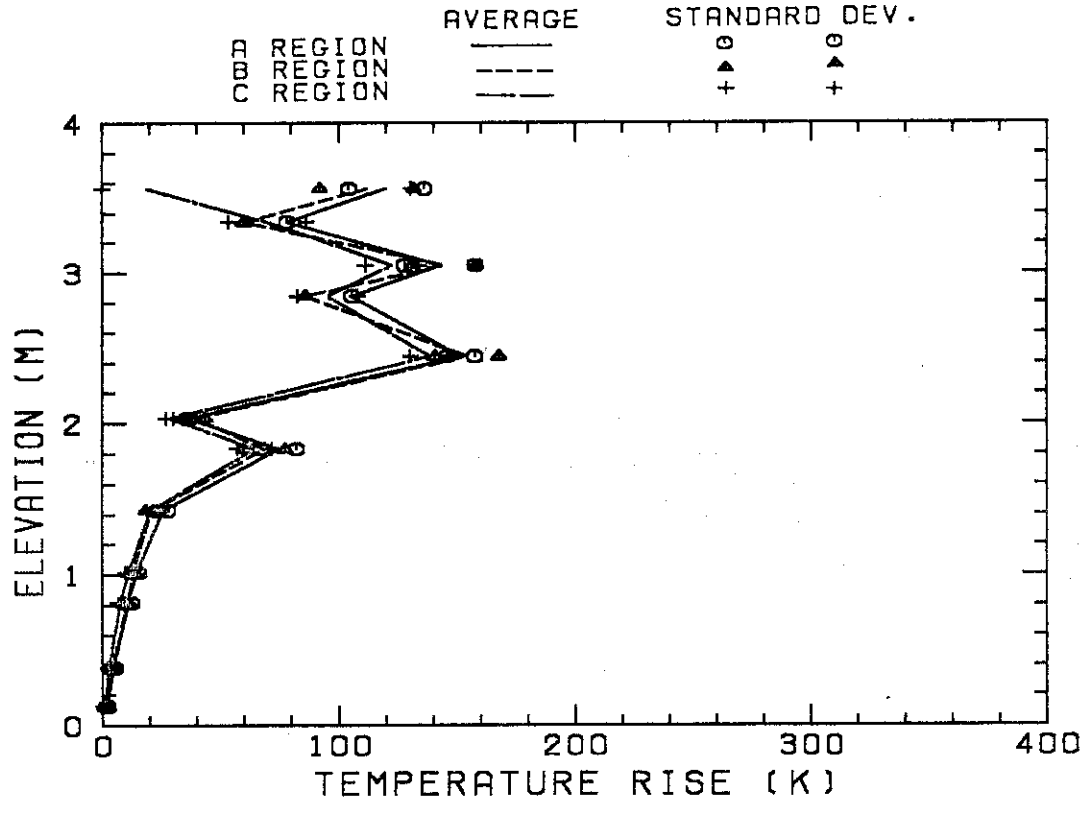

Fig. B.12 Temperature rise

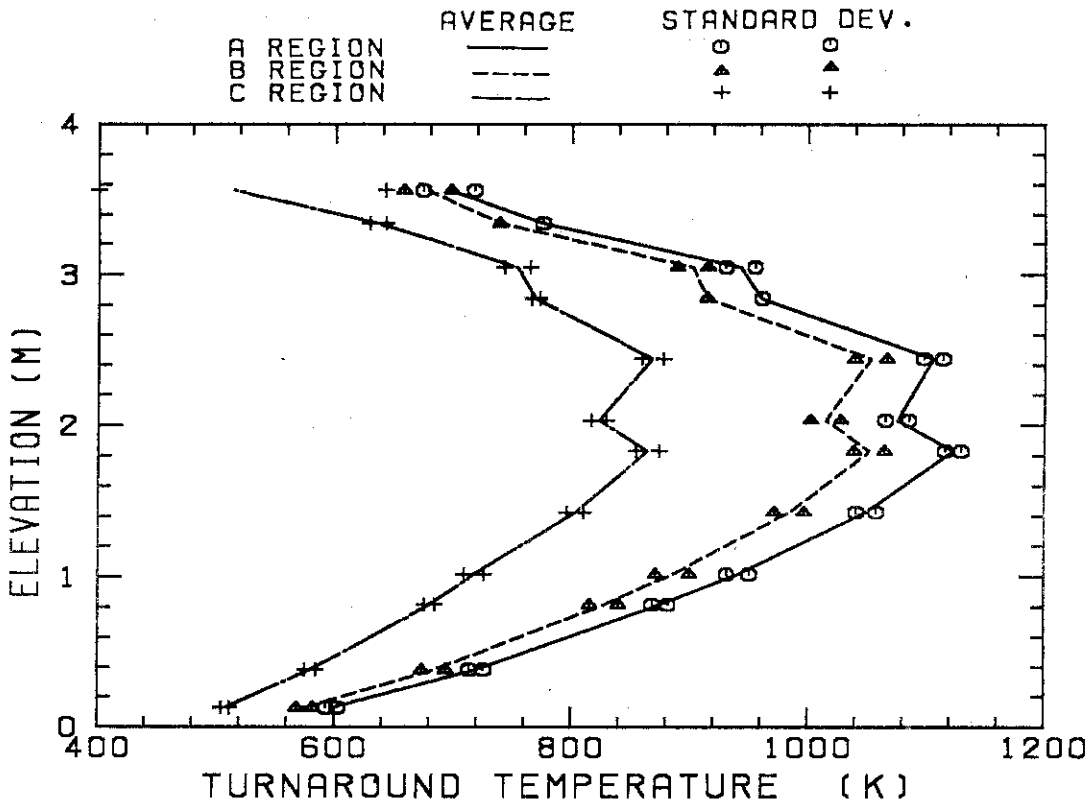

Fig. B.13 Turnaround temperature

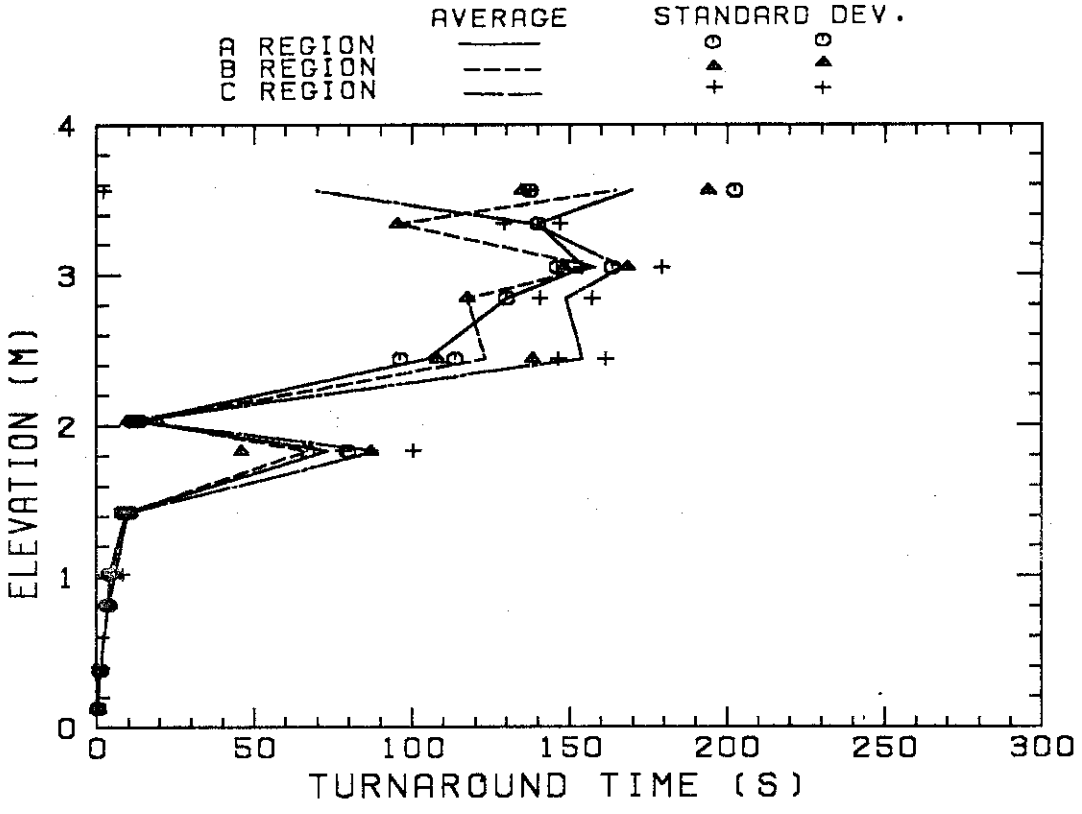

Fig. B.14 Turnaround time

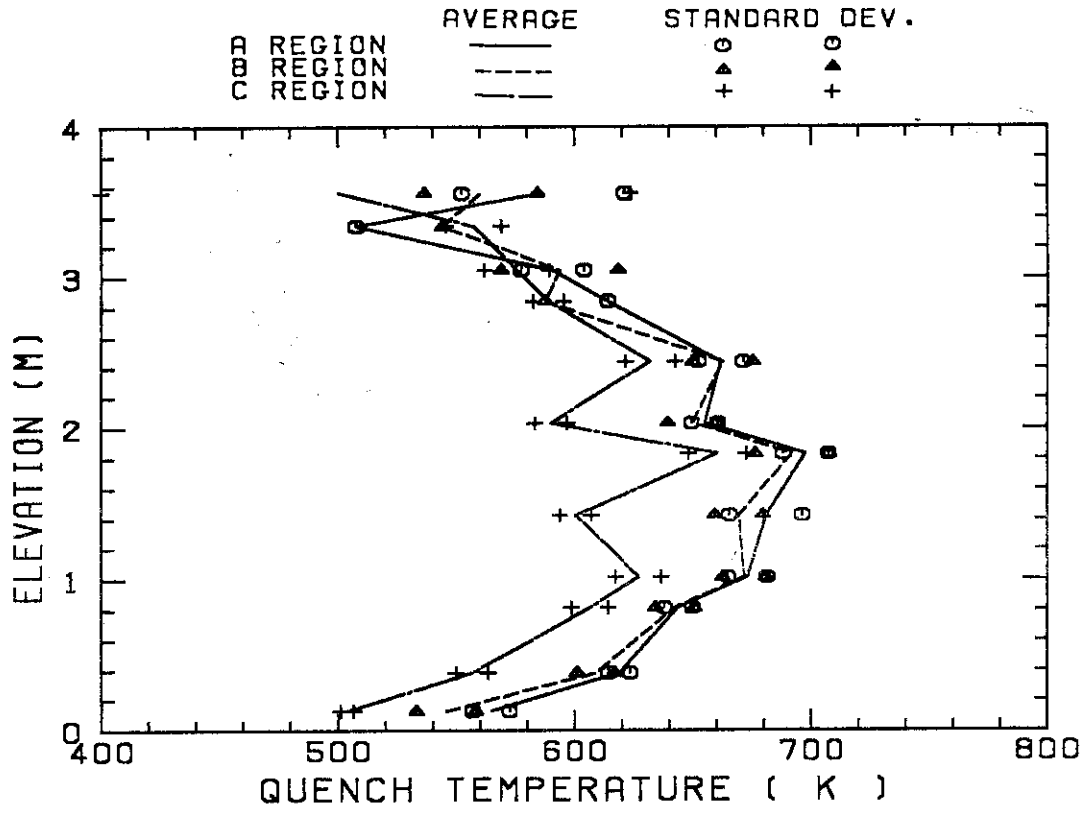

Fig. B.15 Quench temperature

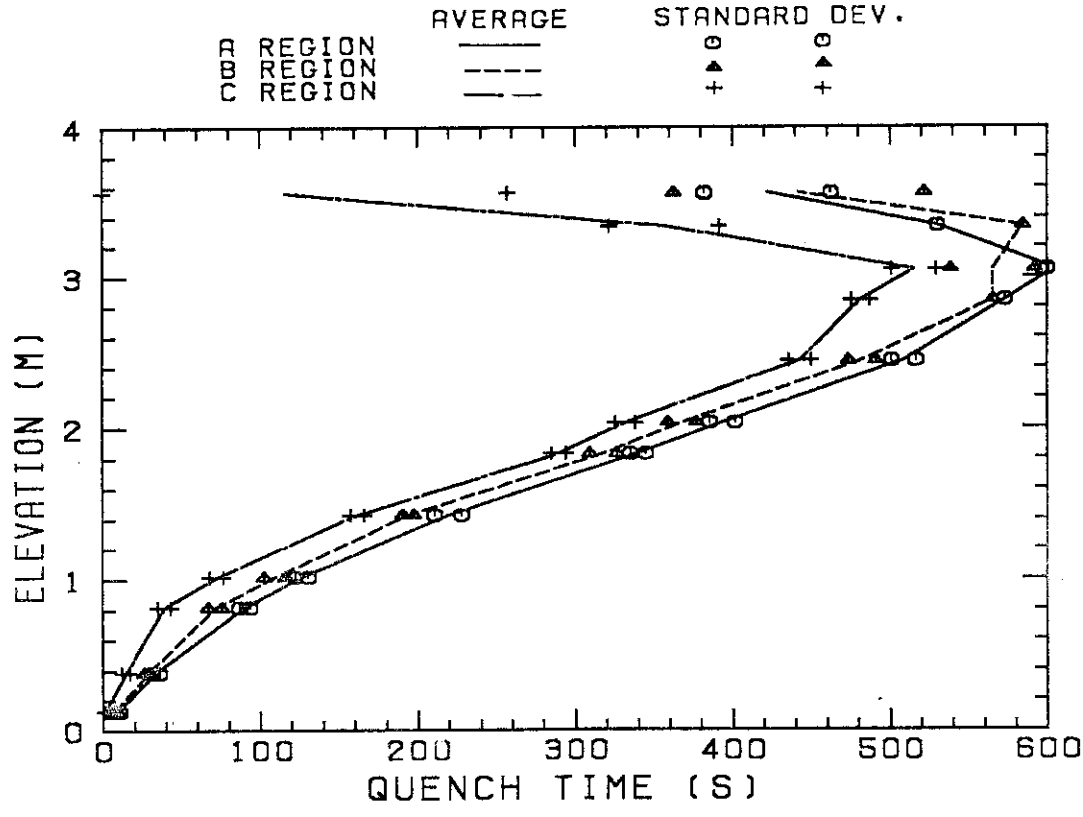

Fig. B.16 Quench time

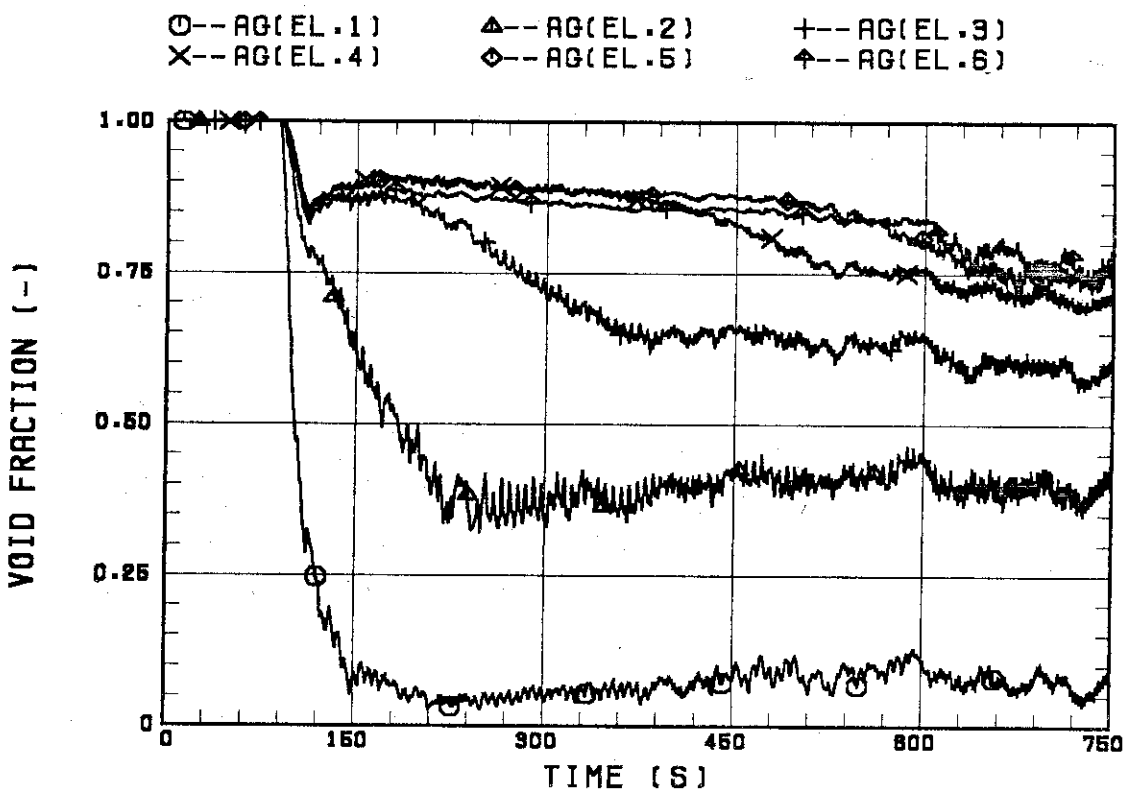

Fig. B.17 Void fraction in core

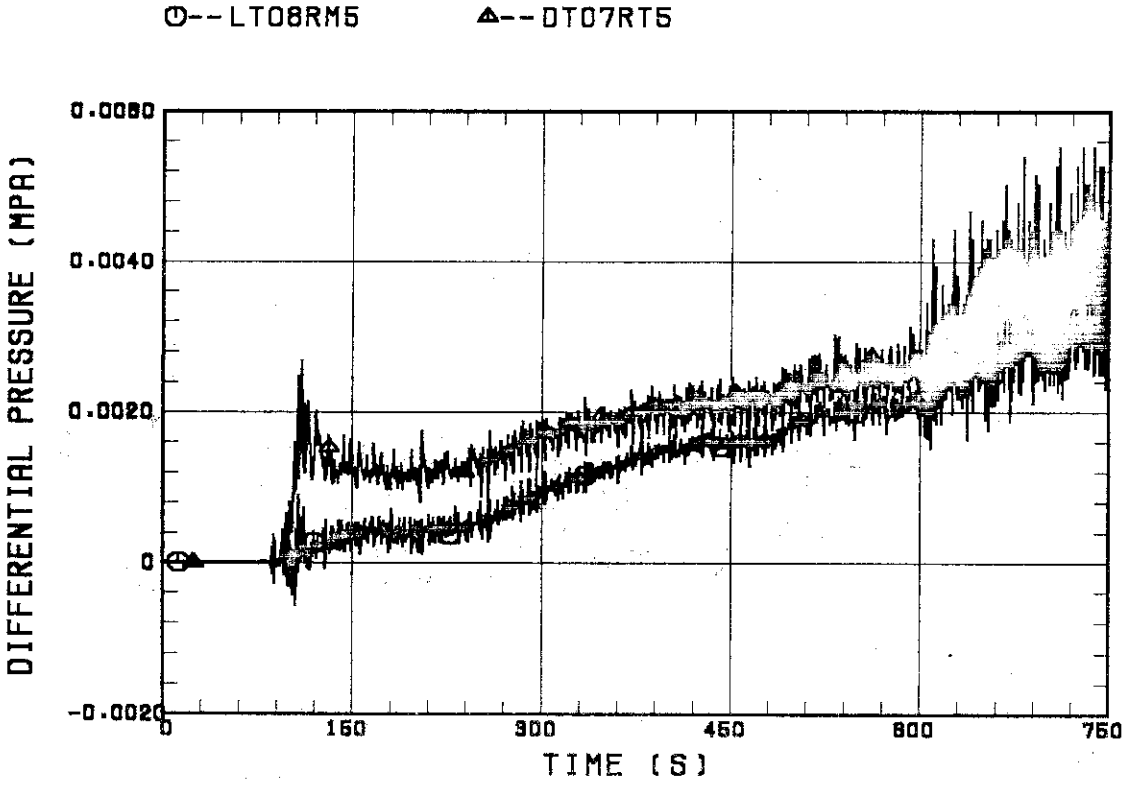

Fig. B.18 Differential pressure through upper plenum

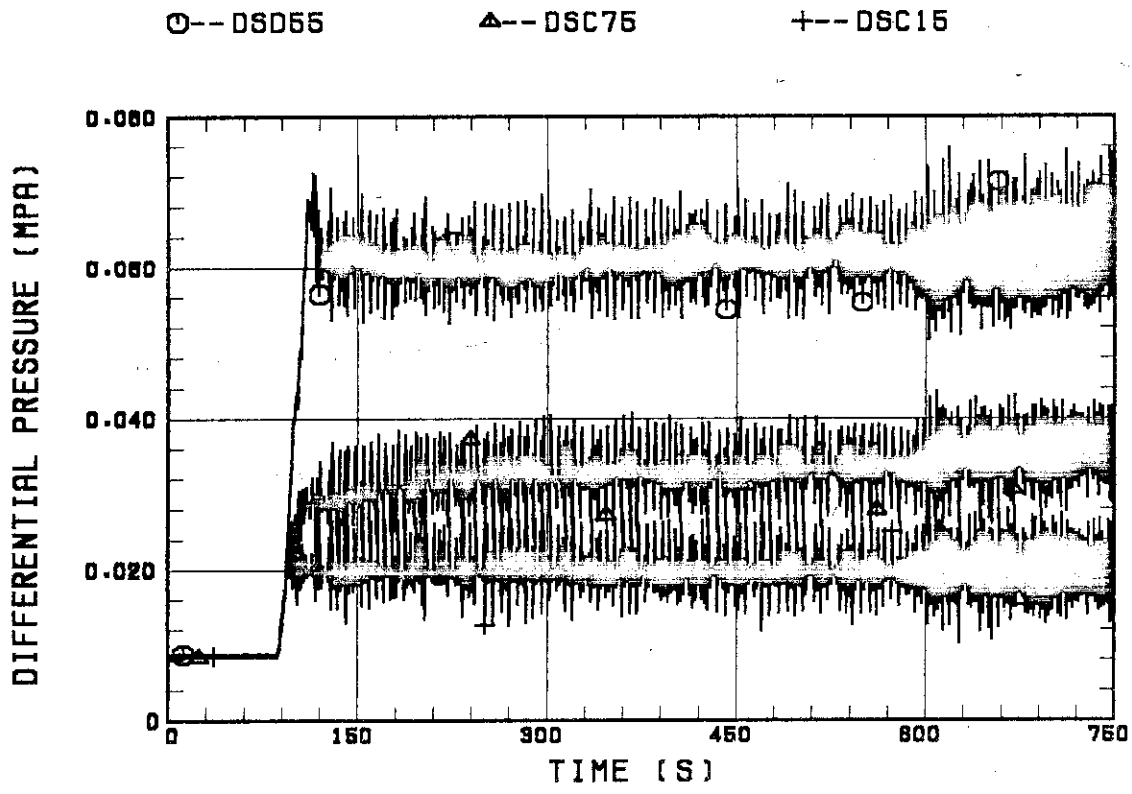

Fig. B.19 Differential pressure through downcomer, core, and lower plenum

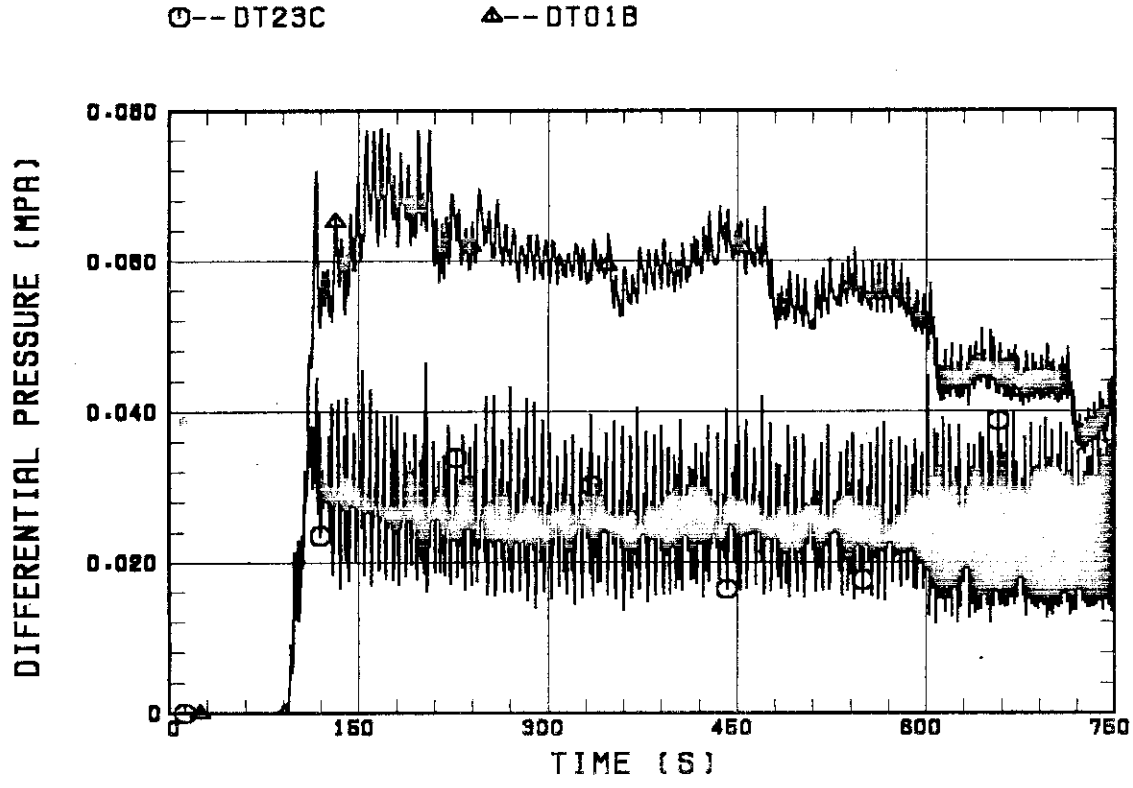

Fig. B.20 Differential pressure through intact and broken loops

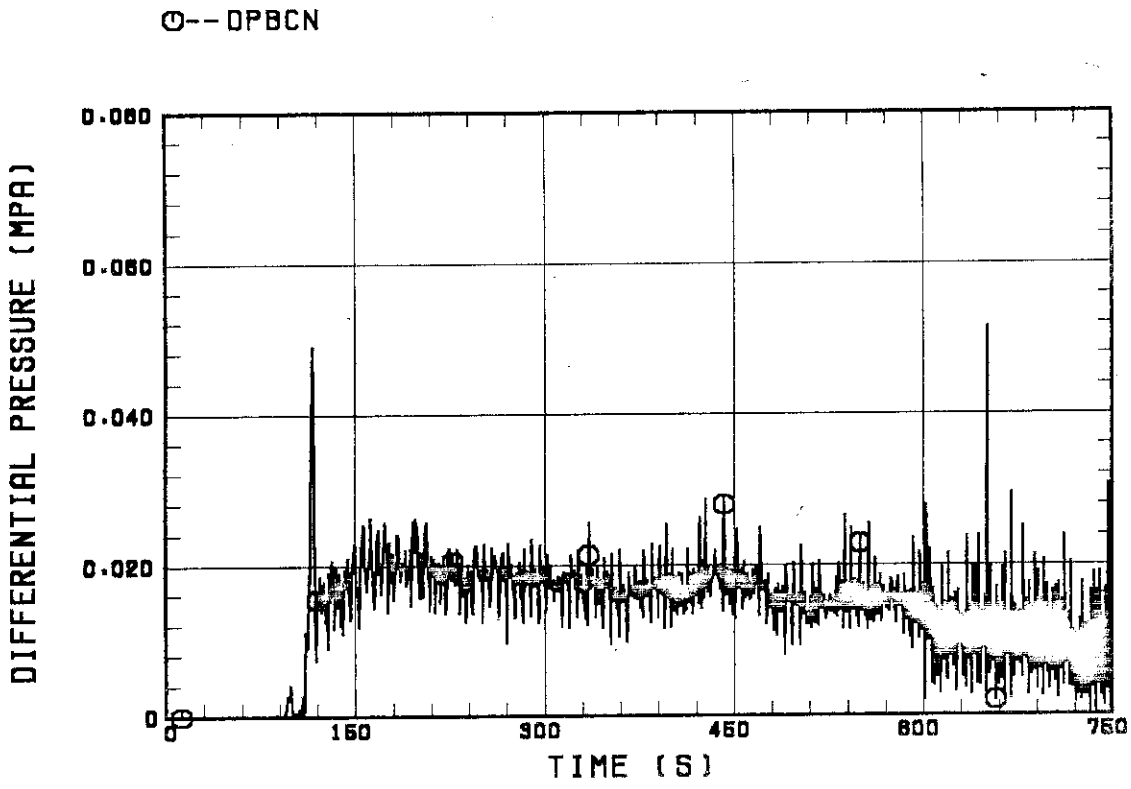

Fig. B.21 Differential pressure through broken cold leg nozzle

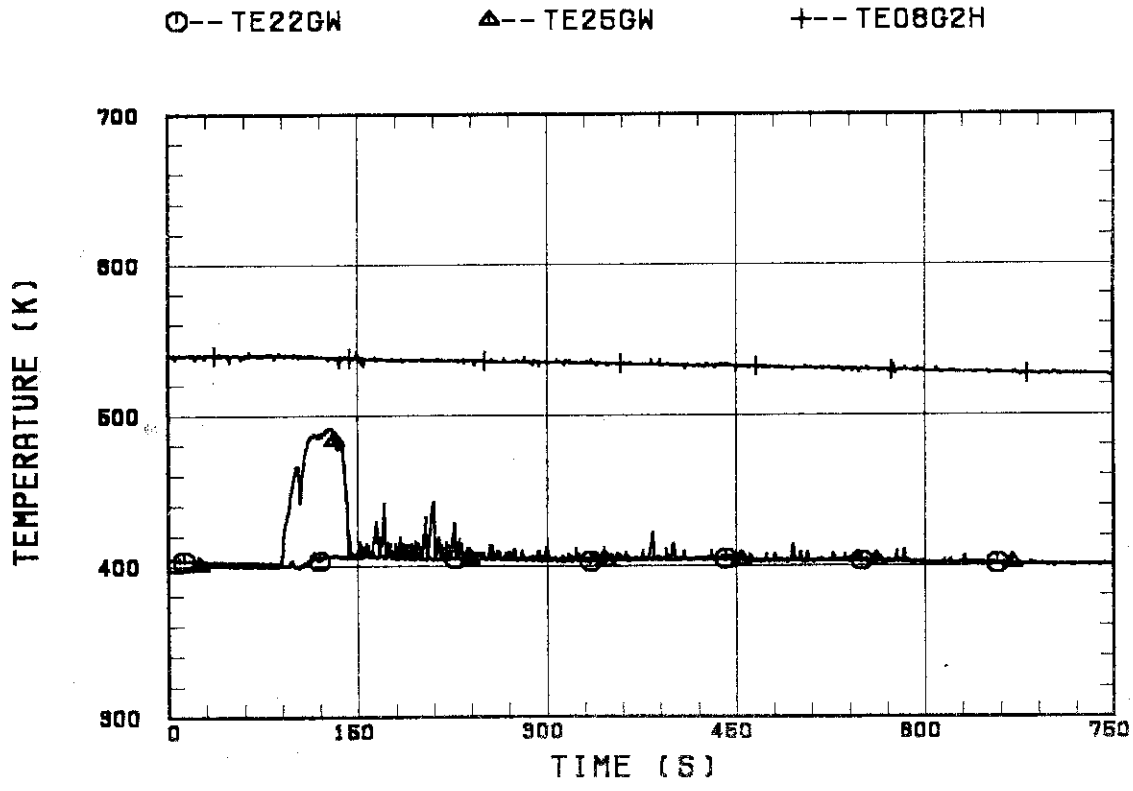

Fig. B.22 Fluid temperature in inlet plenum, outlet plenum, and secondary of steam generator 1

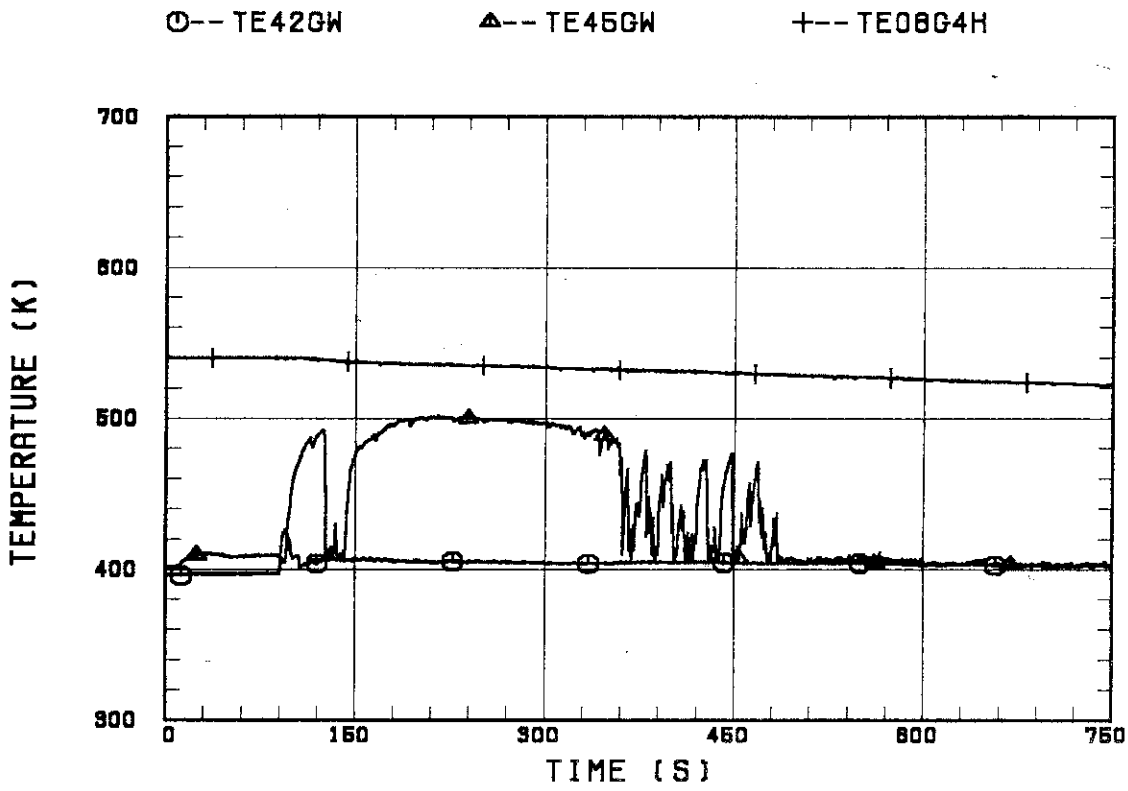

Fig. B.23 Fluid temperature in inlet plenum, outlet plenum, and secondary of steam generator 2

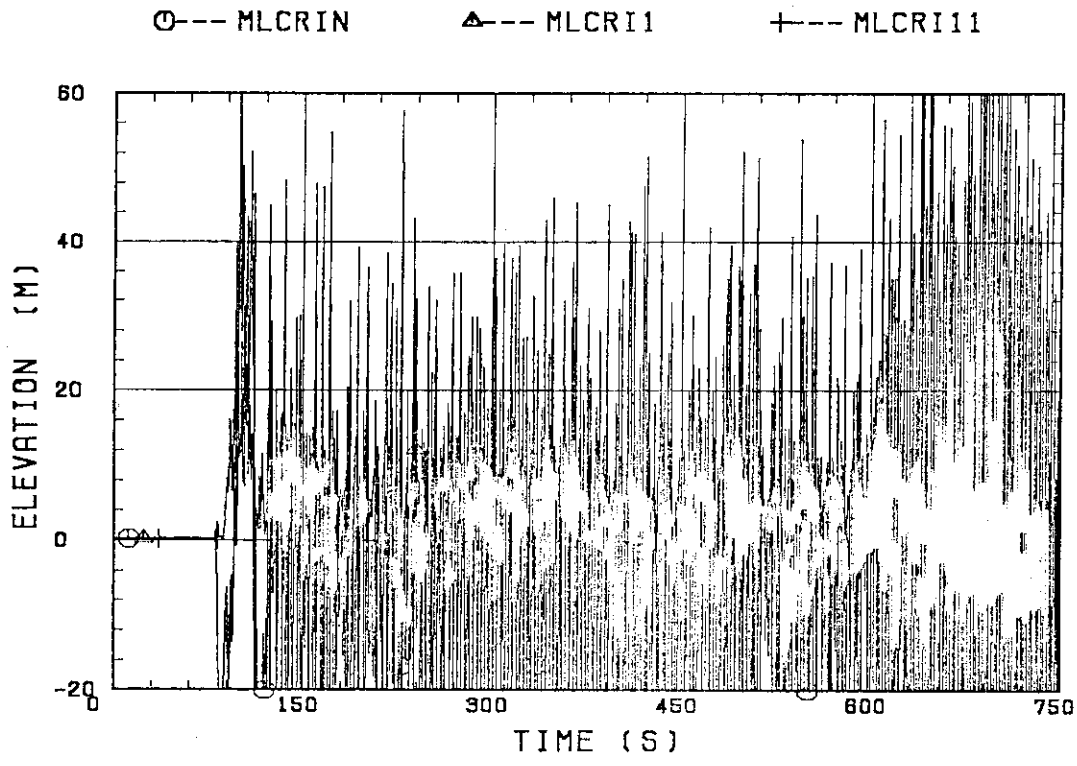

Fig. B.24 Core flooding mass flow rates evaluated with Eqs. (A.1) (A.2)

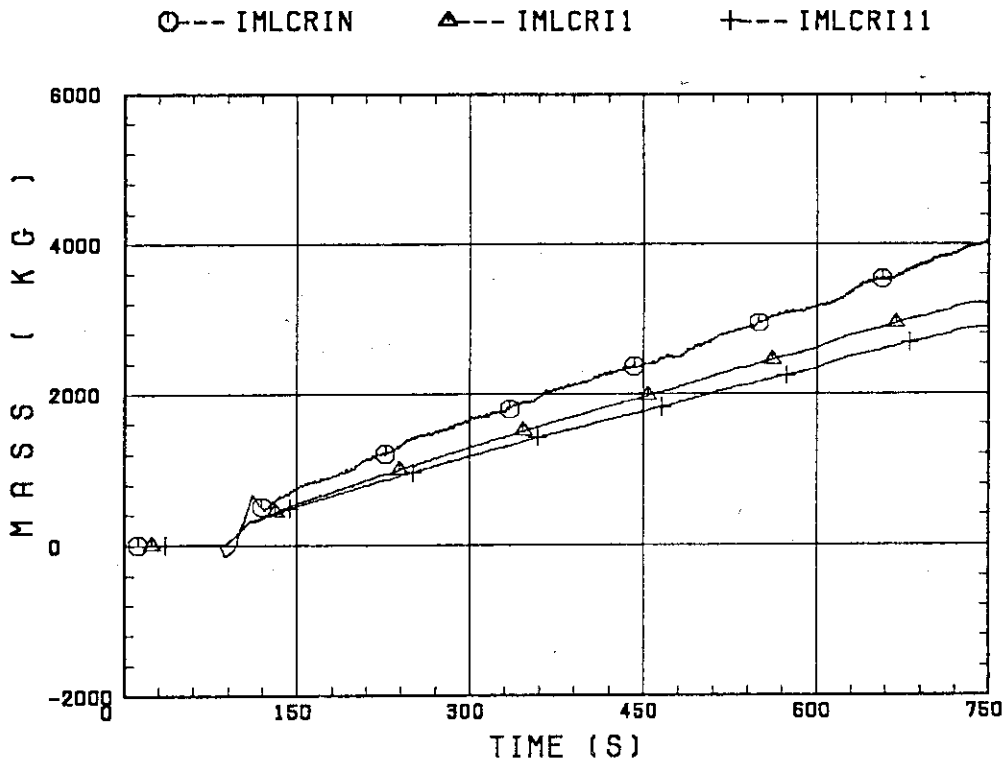

Fig. B.25 Time-integral mass flooded into core evaluated with Eqs. (A.1) and (A.2)

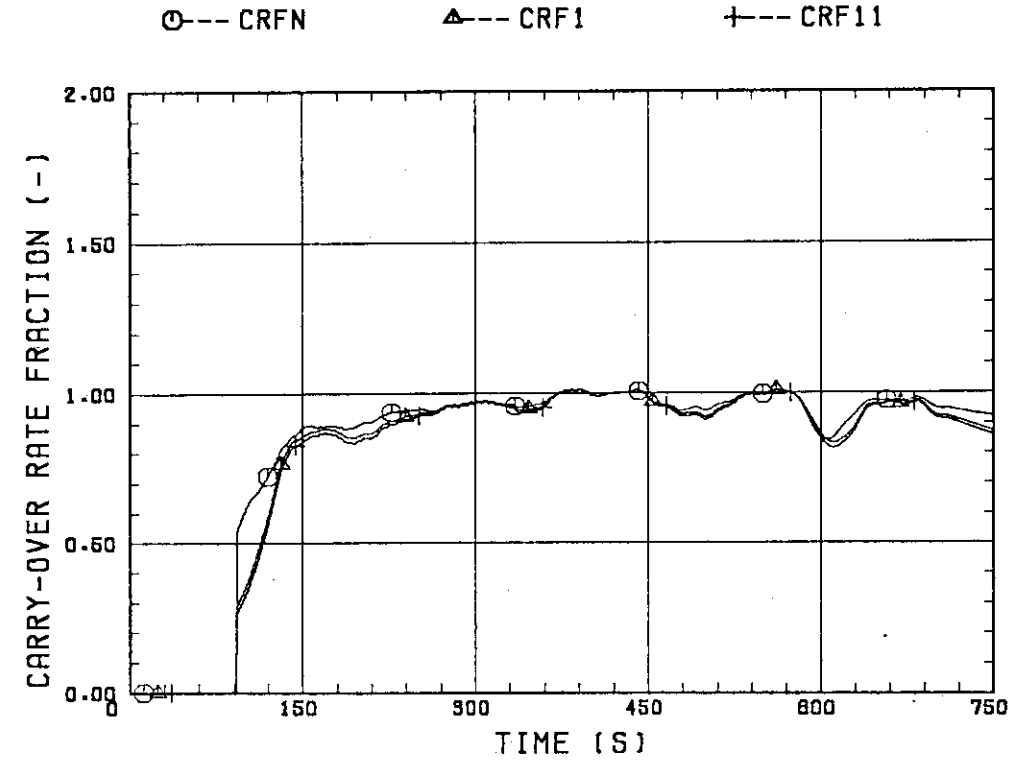

Fig. B.26 Carry-over rate fraction

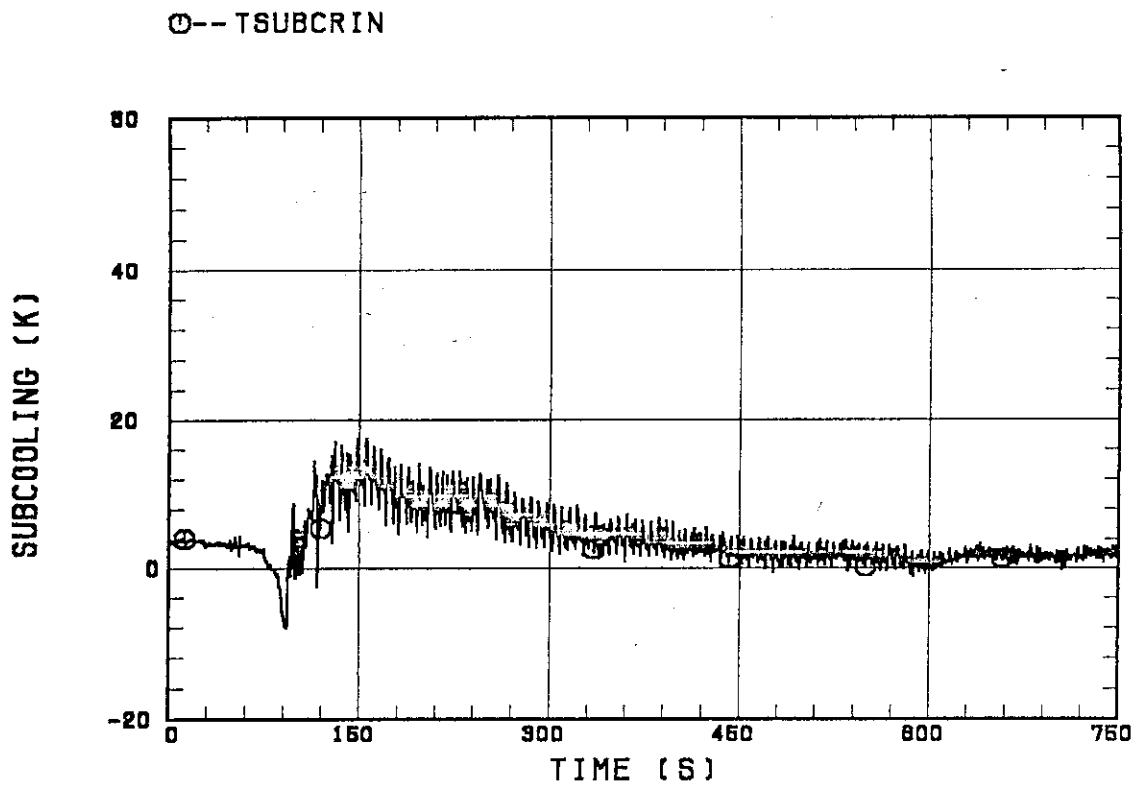

Fig. B.27 Core inlet subcooling

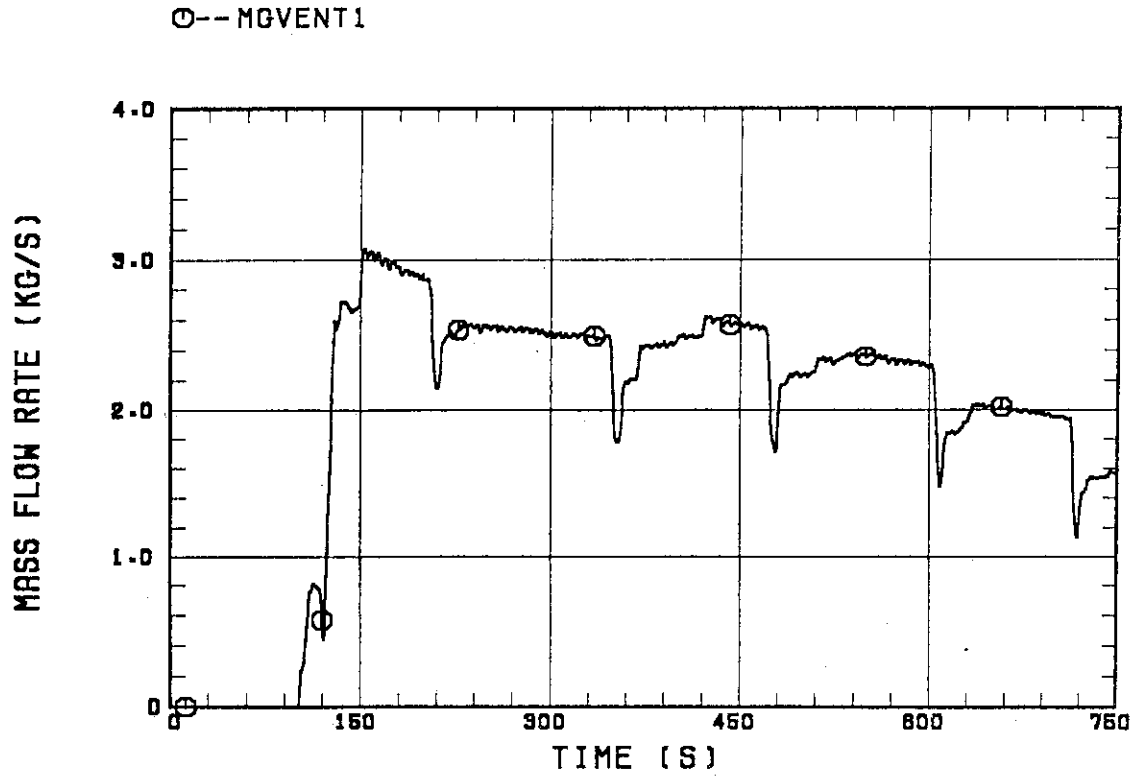

Fig. B.28 Exhausted mass flow rate from containment tank 2